# Momentum measurements of single-beam traps and quantitative holographic experiments: two sides of the same coin

Arnau Farré Flaquer

# Momentum measurements of single-beam traps and quantitative holographic experiments: two sides of the same coin


Cover design:
Ferran Marsà Samper

La recerca presentada en aquesta memòria de tesi ha estat possible gràcies a l'ajuda d'una beca doctoral FI de la Generalitat de Catalunya.

# Momentum measurements of single-beam traps and quantitative holographic experiments: two sides of the same coin

Arnau Farré Flaquer

Optical Trapping Lab - Grup de Biofotònica
Departament de Física Aplicada i Òptica
Universitat de Barcelona
Programa de doctorat de Física

Memòria de tesi per optar al títol de
*Doctor en Física*

Juliol 2012
Dirigida per Mario Montes Usategui i Estela Martín Badosa

# Resum

En aquesta memòria de tesis es presenta el projecte de recerca portat a terme durant el meu doctorat. Es fa primer una introducció a la temàtica, contextualitzant el projecte, i posteriorment es presenten els resultats principals i es discuteix la seva rellevància.

La recerca i els resultats que es descriuen a continuació han estat realitzats en el grup "Optical Trapping Lab – Grup de Biofotònica" del Departament de Física Aplicada i Òptica de la Universitat de Barcelona.

A llarg termini, l'objectiu principal de la recerca que he portat a terme en el grup està orientada a desenvolupar tecnologia de pinces òptiques per a la realització d'experiments en cèl·lules vives. En concret, per a l'estudi del transport intracellular responsable del bon funcionament d'una gran part de les funcions vitals de la cèl·lula. La principal aplicació de les pinces òptiques es troba, precisament, en la biologia molecular. No obstant, malgrat que l'estudi d'aquest tipus de sistemes, com ara els motors moleculars o les proteïnes de reparació de l'ADN, s'hauria de dur a terme en el seu entorn natural, és a dir, la cèl·lula, les limitacions de la tècnica fan molt difícil el seu ús en un entorn tan complex. És per això que, actualment, la majoria d'experiments es dissenyen *in vitro*, és a dir, en unes condicions controlades que intenten simular les condicions reals. La feina desenvolupada durant el doctorat, doncs, intenta superar aquestes restriccions i expandir el camp de les pinces a un terreny molt més ampli i ric. En aquest sentit, la contibució més important de la present tesi és el desenvolupament d'un mètode per mesurar les forces òptiques vàlid per mostres i entorns molt generals, en contrast amb els mètodes existents.

Les pinces òptiques, també anomenades trampes òptiques, són feixos de llum làser que quan són altament focalitzats permeten atrapar de forma estable mostres microscòpiques i manipular-les. Això s'aconsegueix mitjançant objectius de microscopi d'alta obertura numèrica, que permeten, alhora, observar les pròpies mostres. La captura estable de partícules és possible gràcies a l'efecte de les diferents components de la força òptica que actuen sobre la mostra. Aquest balanç de forces depèn, però, de varis paràmetres experimentals, com ara l'índex de refracció de la mostra, de la seva grandària, o de l'obertura numèrica del feix, que s'han de tenir en compte a l'hora de

dissenyar el sistema. En aquesta direcció, s'han publicat dos treballs en què s'analitzen els fonaments teòrics de les pinces. En un d'ells, a més, es va elaborar una aplicació gràfica que permet estudiar de forma interactiva totes aquestes dependències.

Un dels paràmetres importants que cal escollir és la longitud d'ona del làser utilitzat. En concret, l'eina es pot utilitzar per manipular mostres vives només si s'utilitza llum infraroja, ja que en aquest rang les cèl·lules gairebé no absorbeixen la radiació. Un altre dels paràmetres fonamentals és l'índex de refracció. Precisament, la captura d'estructures dins cèllules és més complexa que la de microesferes *in vitro* degut a la semblança dels índexs de refracció de la partícula i del medi que l'envolta. Un dels treballs que es presenten aquí versa sobre l'ús de la tècnica en cèl·lules NG-108, de tipus neuronal, que nosaltres mateixos cultivem.

A part de la manipulació, hi ha una altra característica fonamental que fa les pinces tan atractives per la biologia: la possibilitat de mesurar de forma acurada forces de pocs piconewtons (0.1-100 pN), que és, precisament, el rang de forces propi del domini molecular. Per exemple, les proteïnes motores responsables del transport de material dins la cèl·lula generen forces de 1-7 pN, o la ruptura de parells de bases d'una molècula d'ADN es produeix a 15 pN. Així doncs, no sols es poden moure estructures dins cèl·lules, sinó que també es podrien mesurar, en principi, les forces que les molècules exerceixen sobre elles. No obstant, sorgeixen dos problemes importants quan s'intenten obtenir mesures en aquest cas. El primer respon a la dificultat d'aconseguir informació individualitzada sobre el sistema, donat que el trànsit intracel·lular o vesicular es porta a terme mitjançant la coordinació d'un gran nombre de proteïnes diferents que interactuen entre si. Això comporta experiments complexos en què diferents components tenen un paper destacat i, per tant, els resultats no tenen una interpretació clara. Aquest és un problema comú de tots els possibles sistemes de mesura de forces que existeixen. El segon, en canvi, és un problema específic del mètode que s'utilitza normalment per fer aquestes mesures: la manera estàndard de calibratge de les pinces òptiques, necessària per mesurar forces, falla quan s'intenta utilitzar en condicions poc controlades, com per exemple dins cèl·lules. Han aparegut durant els últims anys algunes poques alternatives. No obstant, totes les possibilitats presenten una o altra mancança, ja sigui deguda a l'alt grau de complexitat experimental, o bé perquè els resultats són poc acurats. Això, lligat amb la necessitat de realitzar primer estudis dels sistemes *in vitro*, en condicions

més controlades, ha provocat que es deixessin de costat els experiments en cèl·lules vives.

L′objectiu principal de la present tesis doctoral ha estat emplenar aquest buit fonamental que roman poc explorat, consistent en el desenvolupament d′una tècnica de mesura de forces capaç de treballar en entorns molt generals i, en particular, en l′interior de cèl·lules vives. El mètode principal de mesura que s′utilitza actualment requereix l′ús de mostres esfèriques, normalment microesferes de poliestirè o silici, que s′utilitzen com a sondes de manera activa, per aplicar forces conegudes sobre la mostra i veure la seva resposta, o, de forma passiva, per determinar la força que genera el sistema estudiat. En qualsevol cas, la força, $F$, produïda per la llum de la trampa òptica és proporcional a la posició relativa, $x$, entre el feix làser i la partícula. És a dir, la pinça esdevé un petit dinamòmetre que es regeix per la llei de Hooke ($F = -\kappa x$). De manera que, calibrant el sistema (obtenint un valor experimental de $\kappa$), podem determinar les forces a partir de la mesura de la posició de la mostra. En els últims anys s′han desenvolupat diferents tècniques per mesurar $\kappa$ i $x$, però l′estructura bàsica del sistema de mesura ha romàs igual.

De totes formes, malgrat la seva extraordinària precisió i flexibilitat, el mètode presenta un problema greu: la constant $\kappa$ de la pinça depèn de les variables experimentals, tals com la mida de la mostra, el seu índex de refracció o el del medi on es troba, entre daltres, i és necessari conèixer el valor d′alguns d′aquests paràmetres. Quan aquesta informació no està disponible, o quan les condicions són canviants, no es pot realitzar una mesura fiable de la força. En canvi, el mètode que s′ha desenvolupat en aquesta tesi no presenta cap d′aquestes limitacions, sols requereix algunes restriccions experimentals per funcionar degudament. El sistema es basa en la mesura del canvi del moment dels fotons del feix de llum que interaccionen amb la mostra. Aquest canvi de moment està relacionat amb la força que produeixen, a través de la segona i tercera lleis de Newton, de manera que, mesurant el moment de la llum abans i després de passar per la mostra, podem determinar la força que aquesta exerceix. La detecció del canvi de moment no depèn de les propietats òptiques o mecàniques del sistema estudiat. Sols requereix un calibratge previ en condicions conegudes; un cop realitzat, l′aparell determina les forces sigui quin sigui el sistema que analitzem. En concret, reduiria considerablement els problemes que sorgeixen en les mesures dins cèl·lules i possibilitaria experiments nous.

Malgrat que l′aplicació del mètode es segueix desenvolupant a dia d′avui, els primers resultats confirmen que podria funcionar en experiments de transport intracellular *in vivo*. A més, per un altre costat, els avantatges que presenta la tècnica i, en concret, la possibilitat d′utilitzar el mètode sense tenir coneixements de pinces òptiques, ja que no requereix cap tipus de calibratge, fa que sigui comercialment valuós. En aquest sentit, s′ha portat a terme un procés de valorització mitjançant una sèrie de projectes amb l′Àrea de Valorització i Llicències de la Fundació Bosch i Gimpera de la Universitat de Barcelona i amb ACC1Ó de la Generalitat de Catalunya, que ens ha portat a la sol·licitud de patents a Europa, Japó i Estat Units. A més, s′ha realitzat un estudi de mercat en colaboració amb l′escola de negocis EADA per començar a comercialitzar l′aparell a través de l′empresa *Impetux*, que constituïrem en breu.

Simultàniament, durant la tesi, s′ha portat a terme també un altre treball enfocat a fer compatibles les mesures de forces amb l′ús de pinces òptiques hologràfiques. La introducció de tecnologia hologràfica permet multiplicar les prestacions de la tècnica. El control de la propagació del feix làser mitjançant un modulador espacial de llum fa possible, entre altres opcions, la creació simultània de múltiples trampes o l′ús de trampes amb propietats especials. No obstant, en aquest cas la mesura de forces esdevé més complicada. De fet, existeixen pocs treballs en què s′utilitzi aquest tipus de pinces en experiments quantitatius precisos. Un d′ells és el que es va presentar com a resultat de la recerca que vaig fer durant la meva estada a la Universitat Simon Fraser de Vancouver, Canadà.

En aquest projecte, vàrem explorar la possibilitat d′exercir forces altes amb sistemes hologràfics. Els moduladors presenten fluctuacions degudes al refresc de la pantalla de cristall líquid, a l′escriptura dels hologrames que realitza l′electrònica a altes freqüències i al propi canvi d′holograma quan es mou la trampa. Quan s′apliquen forces altes, les partícules poden escapar degut a aquests efectes. No obstant, els experiments d′estirament de molècules individuals d′ADN que realitzàrem mostraren que no hi ha problemes rellevants en el rang de forces que vàrem generar amb aquest tipus de trampes.

Per un altre costat, també s′ha analitzat quines conseqüències té l′us de diferents tipus d′electròniques de direccionament dels moduladors. L′escriptura dels hologrames depèn de si l′electrònica és digital o analògica. Les primeres són més econòmiques i, per tant, molt comuns, però la naturalesa binària del senyal que s′envia a la pantalla de

cristall líquid és, en principi, incompatible amb la variació contínua que es necessita per canviar la fase del feix de llum. Això es soluciona típicament mitjançant la "modulació per amplària d'impuls" ("pulse-width modulation"), que és un mètode molt extès per imitar el direccionament analògic. No obstant, això introdueix més soroll en el feix i, per tant, més inestabilitats. Es varen estudiar les fluctuacions en la fase del feix làser després de reflectir-se en el modulador, així com també el seu efecte en l'estabilitat en la posició de la trampa. Es va concloure que, pels moduladors analògics, era semblant a les trampes convencionals i, pels digitals, malgrat ser pitjor, era propera als valors comuns.

Tot aquest treball hauria de permetre apropar la potència de l'holografia als experiments de mesura de posició i força de precisió. Malgrat tot, la recerca continua i encara queden alguns aspectes important per adreçar.

# Overview

In this dissertation I present the research project that I carried out during my PhD. First, I make an introduction to the subject, giving the context of the research and, later, I present the main results and I discuss their relevance.

The research detailed below has been done at the "Optical Trapping Lab - Grup de Biofotònica" from the Departament de Física Aplicada i Òptica at the Universitat de Barcelona, Spain.

In the long run, the main goal of the research carried out in the group is oriented to the development of optical trapping technology for experiments inside living cells. In particular, for the study of the intracellular transport responsible for the proper development of essential functions of the cell. The main application of this tool is indeed in molecular biology. However, although the study of these biological systems, such as molecular motors or DNA-associated proteins, should be carried out in their natural environment, that is, inside the cell, the limitations of optical traps make its use difficult for such complex conditions. It is because of this that most of the current experiments are designed *in vitro*, under controlled conditions that simulate the interior of the cell. The work developed during this thesis tries to overcome such restrictions and expand optical tweezers to richer and wider fields. In that sense, the most important contribution of this thesis is the development of a method for measuring the optical force valid for general samples and environments, in contrast to the existing methods.

Optical tweezers, also called optical traps, are highly-focused laser beams that allow trapping and manipulation of micron-sized particles. This is achieved by means of high-numerical aperture objectives, which are simultaneously used to observe the samples. The stable trapping of particles is possible due to the effect of different components of the optical force that act on the sample. This balance depends on several experimental parameters, such as the refractive index of the object, its size or the numerical aperture of the beam, which must be considered for the design of the system. In this direction, we have published two works on the theoretical principles of optical traps. Moreover, in one of them, we developed a graphic application to interactively study all these dependencies.

One of the important parameters to be chosen is the laser wavelength. In particular, the tool can be used to manipulate living samples only if it is implemented with infrared light, since in this range cells absorb a small fraction of the radiation. A second fundamental parameter is the refractive index of the sample (relative to that of the surrounding medium). The capture of membranous structures within cells is indeed more complex than that of microspheres *in vitro* because of the small refractive index mismatch between the particle and the medium. One of the works presented here deals with the use of optical traps in living NG108 cells (neuron-like) that we culture in our facilities.

Besides the manipulation, one of the fundamental features that makes optical traps so appropriate for biology is the possibility to accurately measure forces of some piconewtons (0.1-100 pN), which is, indeed, the range where the typical molecular processes take place. For example, the stall forces of motor proteins responsible for the transport of material within the cell are 1-7 pN, or the unzipping of DNA takes place at 15 pN. Thus, one can move structures inside cells, but also measure the forces that molecules exert on them. Unfortunately, two problems arise when forces are to be measured inside a complex environment such as the cell. The first corresponds to the lack of specificity. Processes within the cell are typically carried out by many different molecules working simultaneously, so it becomes difficult to extract force information of only one of these molecules. Results do not usually have a clear interpretation. This is a problem that affects all the existing systems to measure forces. The second issue is, however, specific of the method typically used in the measurements: the standard calibration, which is a necessary step, fails when the conditions of the experiment are not controlled, as it happens in cells. A few alternatives have arisen during the last years. Nonetheless, all the options exhibit different drawbacks, either because of the high degree of complexity or because results are not accurate enough. This, together with the need of carrying out the more controlled and specific *in vitro* experiments first, have left experiments with living cells lagging behind.

The main goal of my thesis is to fill this fundamental gap, which has remained barely explored so far, regarding the development of a technique for measuring forces within living cells. The method most currently used requires spherical particles (usually latex or glass microspheres) that can apply known forces on the sample to observe its response or, acting as passive probes, determine the force generated by the analyzed

system. In any case, the force produced by the light in the trap is proportional to the displacement of the trapped particle from the origin, $x$. That is, the tweezers become a small tensiometer that is governed by Hooke's law ($F = -\kappa x$). Thus, the calibration of the trap (the determination of $\kappa$) allows measuring dynamic forces out of the sample positions. In the last years, different groups have proposed techniques to measure $\kappa$ and $x$, but the essence of the measurement has remained intact.

Despite its extraordinary precision and flexibility, the method presents a strong limitation: the constant $\kappa$ depends on the experimental conditions, such as the sample size, its refractive index or that of the surrounding medium, and it is necessary to know them. When the information is not available, or when the conditions change, it is not possible to carry out a reliable measurement of the force. By contrast, the method developed in this thesis does not show any of these restrictions. The system relies upon the determination of the momentum change of the trapping beam due to the interaction with the sample. This change is related to the force through Newton's second and third laws, so measuring the light momentum before and after trapping the sample immediately provides the force applied on it. The detection of this momentum does not depend on the optical or mechanical properties of the object. It only requires a previous calibration under controlled conditions; then, the instrument measure the forces regardless of the sample properties. As a consequence, it should considerably reduce the issues found in living cells and should enable new experiments.

Despite the application of the method is still currently in progress, the first results confirm that it works in *in vivo* experiments of intracellular transport. Furthermore, on the other hand, the possibility to use the instrument without a previous knowledge on optical tweezers, makes the method commercially valuable. In this direction, we worked in the valorization of the results through different grants together with the Valorization and Licensing area of the "Fundació Bosch i Gimpera" from the University of Barcelona and with the agency ACC1Ó from the Generalitat de Catalunya, which have led us to the application for patents in Europe, Japan and USA. In addition, we have carried out a market research in collaboration with the Business School EADA to start commercializing a system based on this technology, through the spin-off company *Impetux* that we will soon start.

In parallel, during the thesis, I have carried out a second line of work focused on making holographic tweezers compatible with force and position measurements. The

introduction of the holographic technology multiplies the performance of the trapping technique. The control of light propagation by means of a spatial light modulator allows, for example, the creation of multiple traps or complex intensity profiles with special properties. Nevertheless, in this case, the measurement of forces is more complicated. In fact, there are few works in which holographic tweezers are used in precise, quantitative experiments. One of them is the research that I did during my stay at the Simon Fraser University in Vancouver, Canada.

In that project, we explored the possibility to exert large forces with holographic systems. Modulators exhibit fluctuations due to the liquid crystal refresh signals, to the high-frequency addressing of the electronics and to the hologram change during trap steering. This can perturb the trapping of particles when high forces are applied. However, the DNA stretching experiments that we carried out showed that there are not relevant issues associated with these fluctuations.

On the other hand, I also analyzed the consequences of these effects on the positional stability of the generated traps. In particular, the use of different electronics for the control of the liquid crystal display. Digital and analog SLMs use different strategies to imprint the holograms on the display. The former have a lower cost and are, therefore, very common, but the binary nature of the electronic signal sent to the liquid crystal is, in principle, incompatible with the continuous variation needed to change the phase of the light. This is typically solved by means of "pulse width modulation", which is a popular method to emulate an analog addressing in these situations. Nonetheless, this option introduces more noise to the beam and, hence, more instabilities. We studied the fluctuations of the beam phase after being reflected at the modulator, as well as their effect on the positional stability of the trap, and concluded that for analog-addressed SLMs the results were similar to conventional traps and, for the digital addressing, although worse, were close to common values.

All this work represents a step toward the combination of the power of holography and precise experiments of position and force measurements.

# Contents

# Chapter 1

# Introduction

In this first chapter, we make a historical introduction to optical trapping. As the field is extensive and its applications are very different, we only review the most important milestones, especially focusing in the main subject of this thesis: the measurement of forces, that is, in the use of this technique as a *picotensiometer*. At the end, and in a lesser degree (proportional to its relevance to the whole thesis, see Chapter 2), we also explain the advances in trapping multiple particles, in particular, with holographic optical traps, as well as its combination with force and position measurements.

## 1.1 First years of optical trapping

Although optical trapping has finally found in biology its best ally to grow and mature in a sort of scientific symbiosis, the technique was originally developed in a different context, in close connection with atomic physics.

By the early 1970s, Arthur Ashkin was working at the Bell Labs in the application of the recently discovered laser to the manipulation of particles with light. Laser was in vogue and seemed the key to open the door to new experiments that could clarify old questions about the nature of light and its interaction with matter. One of these questions was radiation pressure.

This property of light had been theoretically proposed by Maxwell and observed by others decades earlier, but the larger radiometric forces found in the experiments made more precise studies difficult. Ashkin was the first to show that glass microspheres suspended in air or water could be trapped and manipulated by means of a focused laser

beam taking advantage of the radiation pressure (1). Laser trapping became rapidly a test bench for theoretical physicists in the fields of optics and quantum physics, and old debates, such as the so-called Abraham-Minkowski controversy, came immediately to the fore. Ashkin himself, for example, motivated by the recent work of Burt and Peierls, published three years later new results on this controversy, showing that a laser hitting an air-liquid interface pushes the surface outwards, being compatible with Minkowski′s option (2).

As Gordon proved immediately afterwards (3), the experiment was not conclusive. However, optical trapping was finding an increasing acceptance in a variety of fields. During the following decade, optical traps expanded, especially to the trapping and cooling of atoms, which finally led, among other important milestones, to the experimental observation of the Bose-Einstein condensate.

## 1.2 Late 1980s and the birth of optical tweezers

Despite the successful advances achieved by optical traps, the technique did not find its greatest splendor until Ashkin again proposed the so-called optical tweezers in 1986 (4) and used them to manipulate biological samples one year later (5).

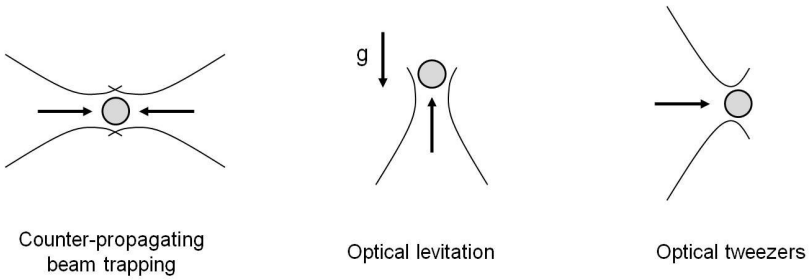


**Figure 1.1:** - Trapping schemes.

Ashkin had come up with different trapping configurations during the first decade before proposing the optical tweezers. The initial scheme was based on two counter-propagating beams (Fig. 1.1) (1). Two lasers were focused by low-numerical aperture lenses inside a flow chamber where microspheres were suspended in a fluid. Due to the Gaussian profile of the intensity, beads were dragged towards the optical axis and pushed forward because of the scattering (Fig. 1.2). The laser propagating in the

opposite direction operated similarly so particles could be stably trapped in the middle point.

Soon after that, he proposed using gravity as an alternative to compensate for the scattering force that pushed beads downstream (Fig. 1.1) (6). However, none of these schemes had the versatility and power to turn optical trapping into a full-fledged experimental technique. This came with the discovery of optical tweezers (4).

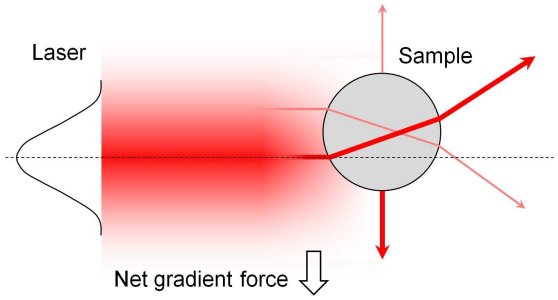


**Figure 1.2:** - Ray diagram.

Ashkin realized that when the same laser beam was focused by a high-NA lens, the sample could be stably trapped without any further element. The same force that tended to push particles to the maximum intensity in the transverse direction could also be used to confine particles axially if the intensity gradient was strong enough in that direction. This conferred a great simplicity and robustness to the instrument. The optical trap was easily aligned and could be retrofitted into a microscope, taking advantage of the imaging system (Fig. 1.3).

## 1.3 Gradient force: the attractive component

The decomposition into scattering and gradient force (initially called "ponderomotive") does not have, in general, a practical application, since one cannot distinguish their contributions. The only possible separation is that of transverse and axial forces, the two simultaneously containing both components. Still, the division is important to understand the different forces acting on a trapped particle. The decomposition is also interesting from a theoretical perspective, since they have different origins and properties. Using an intuitive example, the gradient would be a bumpy pool table in a pocket billiard, where the collision between balls were due to scattering.

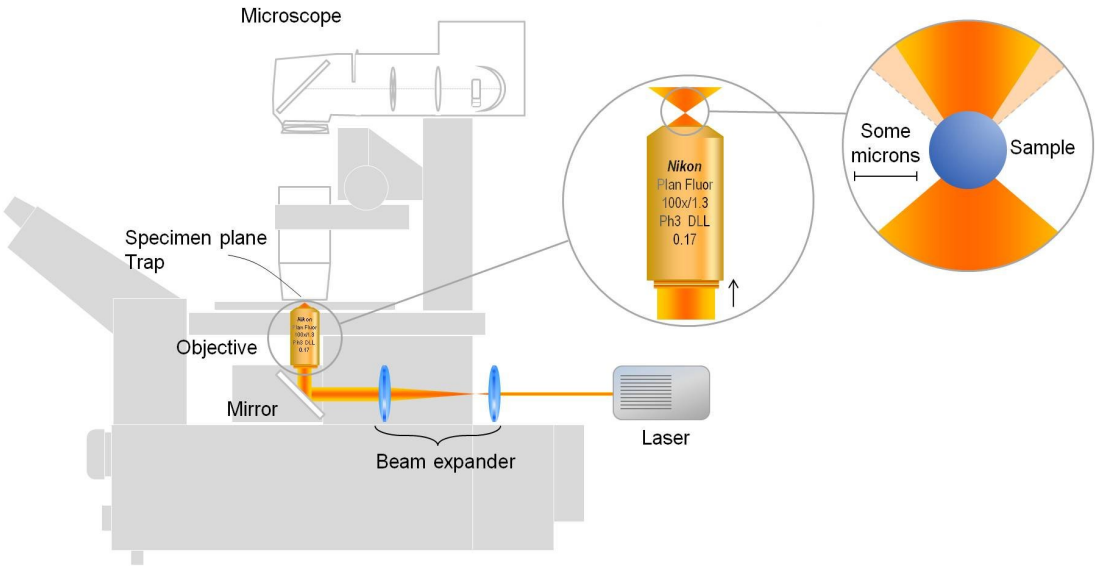


**Figure 1.3:** - Layout of an optical tweezers system.

The existence of the restoring term had been shown in 1978 for atoms (7). The results from the 1986 paper, however, "covered the full spectrum of Mie and Rayleigh particles", as noticed by the authors, which was the range where optical tweezers were to find its major success. For these sizes, from tens of nanometers to tens of micrometers, the range of attainable forces with optical tweezers (0.1-100 pN) was indeed the same that governs particles at this length scale (brownian, molecular, etc.). This rapidly turned the technique into a perfect tool for the study of mesoscopic objects, such as macromolecules and cells.

## 1.4 Optical tweezers in biology: two milestones down the road

By the late 1980s, two important biological discoveries related to optical tweezers were made. The two had an important impact on the subsequent evolution of optical trapping. The first was due to Ashkin *et al.* In 1987, they found that infrared lasers could be used for trapping living samples by reducing the damage caused to them (5). They observed normal division of yeast cells (Saccharomyces cerevisiae) and bacteria (Escherichia coli) after 5 hours in a trap with 80 mW of laser power and a wavelength of

1064 nm, which indicated a correct growth of the cells. Previous results with argon lasers (515 nm) had shown damage for shorter expositions.

The second discovery was the identification of kinesin. In a work published in 1985 (8), Vale *et al.* presented a new force-generating molecule (different from myosin and dynein) capable of translocating along microtubules by means of the hydrolization of ATP. They called this new protein kinesin. The molecule is responsible for the transport of material within the cell, such as mRNA, organelles, synaptic vesicles, etc.

The application of optical tweezers to the study of the recently found kinesin gave a definitive boost to the technique and, with it, to single-molecule experiments. Soon, biophysicists realized that optical traps had the potential to study the physical and chemical properties of single molecules, replacing more cumbersome alternatives such as microneedles or atomic force microscopes, obtaining unprecedented information about biological systems. The features of the technique (range of forces, versatility and absence of harm or contact) were crucial for its quick development. A major driving force in this period was Steven Block's lab in Stanford University (USA). They were one of the promoters of the technique, especially turning it into a quantitative tool to measure positions and, more importantly, forces.

## 1.5 Optical tweezers as "picotensiometers"

The development of optical tweezers as force transducers relied on prior work by Ashkin (9). In 1992, he showed that, close to the origin, the force applied onto a micron-sized sphere exhibited a linear dependence with the particle displacement. The position of the sample could then be used as a dynamic measurement of the force, if the constant of proportionality was previously determined. This enabled the use of traps as *picotensiometers* (10).

Kuo and Sheetz were the first to implement this idea and obtained the first results of forces produced by single kinesins (11). They experimentally proved the linear relation predicted by Ashkin and proposed a method to determine the proportionality factor. They were soon followed by Svoboda *et al.* who, using the optical trap to precisely track a moving bead, resolved the stepping behavior of the enzyme (12).

Ashkin obtained his results on the basis of ray optics. He derived analytical expressions for the force exerted by single rays, but the model was only an approximation

valid for objects several times larger than the laser wavelength.

It was not until some years later that more complex descriptions for other sizes appeared. Mathematical models such as the Generalized Lorenz-Mie Theory or the T-matrix formulation started being applied to the development of computational simulations. The fundamental point was that the results found with these more complex and comprehensive theories were qualitatively similar. The message was essentially the same.

In general, when the laser beam interacts with a sample, the refractive index mismatch leads to a change in the direction of propagation of the beam, which ultimately produces a net force onto the particle. This force is given by the divergence of the Maxwell stress tensor, $\mathbf{T}$:

$$\frac{\partial(\mathbf{p}_{mech} + \mathbf{p}_{em})}{\partial t} = \nabla \cdot \mathbf{T} \tag{1.1}$$

where $\mathbf{p}_{mech}$ and $\mathbf{p}_{em}$ are the mechanical and electromagnetic components of the light momentum, respectively. The radial component $\mathbf{T}_{rr}$ of the tensor is related to the light intensity, so the angular distribution of light scattered by the sample contains the information of the force:

$$\langle \mathbf{F} \rangle = \int_V \langle \mathbf{f} \rangle dv = \int_V \langle \nabla \cdot \mathbf{T} - \frac{\partial \mathbf{p}_{em}}{\partial t} \rangle dv = \oint \frac{n}{c} I(\hat{\mathbf{s}}) \hat{\mathbf{s}} da \,. \tag{1.2}$$

Here, the brackets indicate time average, $\hat{\mathbf{s}}$ is a unit vector normal to the surface, $da$ and $dv$ are elements of area and volume, respectively, and the term $\langle \partial \mathbf{p}_{em}/\partial t \rangle$ vanishes for optical frequencies.

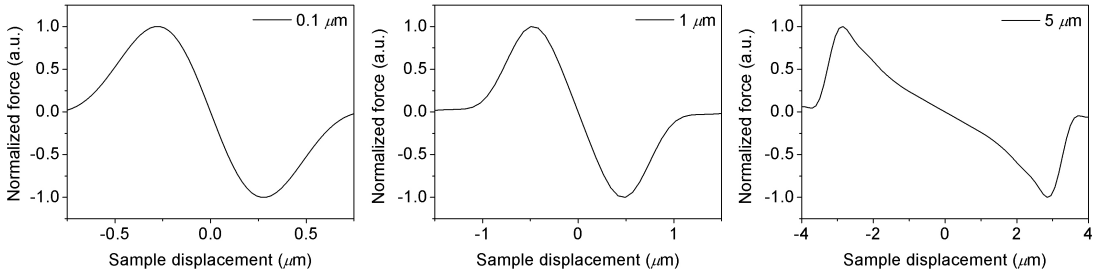


**Figure 1.4:** - T-matrix simulation of the force-displacement curve for polystyrene (n=1.57) microspheres of different sizes. Regardless of the size of the sample, there is always a linear region close to the origin.

Generally, the form of $I(\hat{\mathbf{s}})$ is rather complex so the integral cannot be solved analytically. However, as shown in Fig. 1.4, if one simulates the force for different displacements along the transverse direction for particles with various physical properties (13), a region close to the origin where:

$$F = -\kappa r \qquad\qquad r \ll \lambda\,, \tag{1.3}$$

is always found. The proportionality factor is called *trap stiffness*, $\kappa$, and $r$ is the radial distance. This constant strongly depends on different experimental variables, especially, the bead radius, $a$, and its refractive index, $n$ (Fig. 1.5). Typically, the stiffness increases with the value of $n$, whereas the dependence with $a$ is more complex. The latter is by far the most relevant parameter because of its large variability in different experiments (from hundreds of nanometers to several microns) and its impact on the different mathematical theories about optical forces. Depending on the size, the description of the interaction between light and sample changes and so the models of the force.

We can distinguish three regimes:

- For large objects ($> 5\lambda$), the trap stiffness, computed according to ray optics, is inversely proportional to the bead radius (Fig. 1.5). As explained earlier, the mathematical description of the force in this regime was first obtained by Ashkin in 1992 (9).

- For small particles ($\lesssim \lambda/20$), the interaction between the beam and the sample is that of a wave and an induced dipole. For this, the Rayleigh theory predicts a cubic relationship with size. Similarly, the first formulations were developed by Ashkin (4) and Gordon (3), but a more extensive development was due to Harada and Asakura (14).

- Finally, for the intermediate region, where neither approximation is valid, only computer simulations can give accurate information on the dependence of $\kappa$ with the experimental parameters. In this region, the stiffness takes its largest values, being maximum for $a \sim \lambda/2$. An important feature for these sizes is the existence of resonances that produce local maxima both for $n$ and $a$ (Fig. 1.5).

More information on the theory of optical forces can be found in any of the available original manuscripts or in later reviews (15).

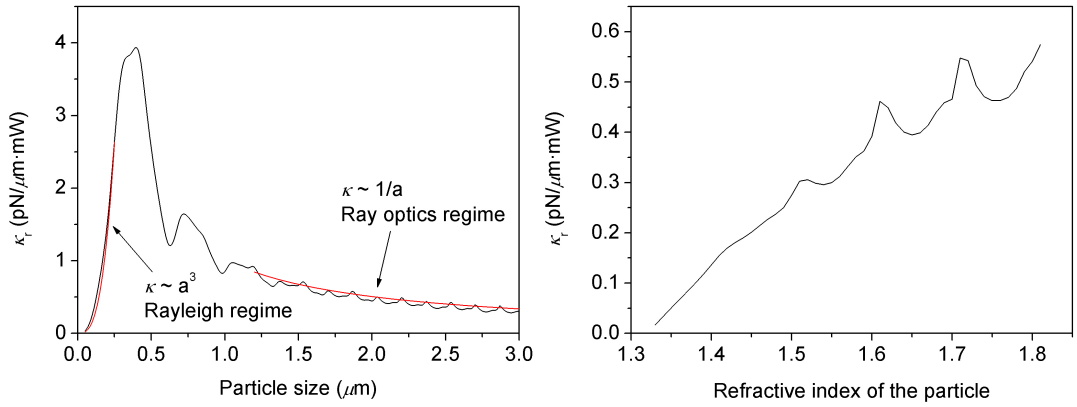


**Figure 1.5:** - T-matrix simulation of the variation of the stiffness for different conditions (size and refractive index). The laser wavelength is 1064 nm.

## 1.6 Determination of sample positions

The first step to measure forces is to find a method to determine positions with high accuracy and large bandwidth. Sample positions directly provide information about the coordinate $r$ in Eq. 1.3, but also indirectly about $\kappa$, through the analysis of the motion of the sample confined in the optical potential and subjected to a certain external force due, for example, to thermal energy.

The first solution was video microscopy (11) (Fig. 1.6(a)). However, both the spatial and temporal resolutions were too poor to detect the events typically involved at the molecular scale. This rapidly changed. The limits were pushed down from 10 nm to 1 nm and the frequency bandwidth increased from $\sim$ 30 Hz to 4 kHz by the use of the trapping laser itself to image the sample onto a quadrant photodiode (Fig. 1.6(b)). This solution was first employed in optical trapping by Finer *et al.* in 1994 in an experiment with myosins (16) based on prior work from Kamimura and Kamiya (17). Unfortunately, the system required a delicate and frequent alignment to correctly image the sample onto the center of the detector. This was solved by the use of non-imaging techniques.

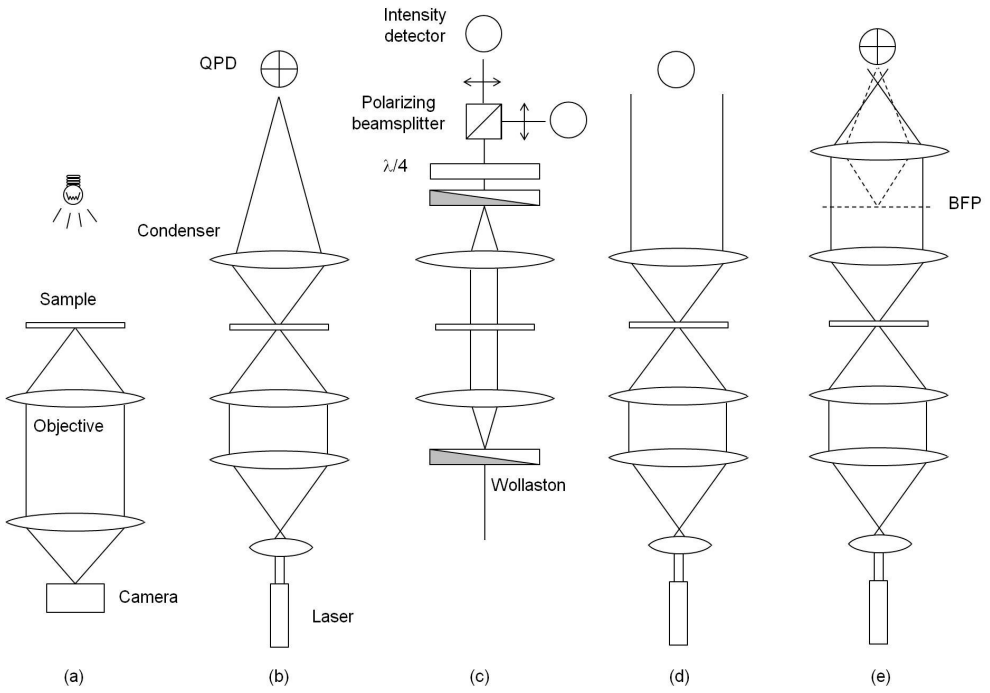


**Figure 1.6:** - Position detection schemes. Not to scale.

Svoboda *et al.* (12) implemented the laser differential interferometer of Denk and Webb (18) in a trapping system, simultaneously using the laser for imaging and trapping (Fig. 1.6(c)). In this technique, related to DIC microscopy, a laser was split into two overlapping spots after going through a Wollaston prism. The signal from a trapped object was found to be linear with position so that it could be used to measure once the calibration between both had been determined.

Nonetheless, soon after this work, Webb again came up with a more powerful method, which was to have a great impact on the development of the field (19, 20). He realized that an optical trap could be used similarly to a scanning-force microscope, where the trapped object played the role of the cantilever. Following this scheme, the light scattered by the sample was collected by a second lens and the mean deflection angle of the radiant intensity distribution measured by an intensity photodetector located in a non-imaging plane (Fig. 1.6(d)). The instrument could determine the sample position with high precision in all three dimensions.

Finally, only a couple of years later, Visscher *et al.*, based on the ideas of Ghislain and Webb, put forward the measurement of positions through back-focal-plane

interferometry (BFPI) (21). The main differences with the scanning-force microscope proposed by Webb three years earlier were the positioning of the detector at the back focal plane of the collecting lens and the use of a quadrant photodiode (Fig. 1.6(e)). This configuration was particularly sensitive to sample motion but insensitive to both the displacements of the trap across the sample plane and to noise in the detection arm. The theoretical principles were explained by Gittes and Schmidt two years later (22) and extended to three dimensions soon after that (23). The technique rapidly became a standard method and more profound studies (24) and improvements regarding the detection range appeared (25, 26).

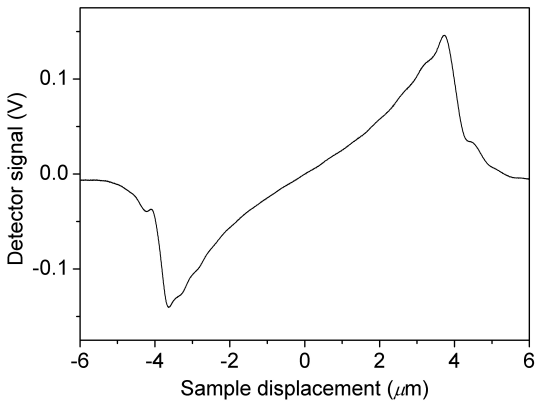


**Figure 1.7:** - Detector signal vs. sample position in a BFPI setup. The curve was obtained by moving an 8 $\mu m$-polymethacrylate bead across the laser beam in the transverse direction.

In BFPI, as in previous methods, there is a region in which the detector signal is proportional to sample displacements (Fig. 1.7). Thus, if the calibration factor (typically called $\beta$) is determined, volts can be directly converted into nanometers.

There are several options to calibrate the position. The first was due to Svoboda *et al.* (12). They attached a bead to a glass slide and made a scan across the laser beam in the transverse direction. The calibration factor $\beta$ was determined from the slope at the origin in the curve obtained.

Unfortunately, this method has some serious drawbacks. The bead used to calibrate the sensor and that used in the experiments are necessarily different, so differences in their properties translate into errors in the measurements. The positioning of the bead

relative to the laser, especially in the axial direction, is difficult and critical. Finally, the presence of the glass surface can alter the interaction between the light and the particle (27). As a result, this technique has been progressively replaced by others. For example, the position of a trapped sample can be simultaneously recorded with the detector and a camera when the chamber is moved back and forth with a piezoelectric stage.

However, the easiest and most reliable calibration of the position sensitivity is obtained together with the stiffness, as we will show next. Currently, this is likely the most popular option.

## 1.7 Trap calibration

The determination of the stiffness is the second pillar of force measurement. Its development was concomitant to the advances in the determination of sample position. However, the first attempts at measuring forces with an optical trap followed a different path.

In 1989, Block *et al.* (28) used the optical tweezers as a force sensor taking advantage of the linear relation between laser power and the maximum attainable force. The measurement of the force was not dynamic, but allowed them to determine the compliance of bacterial flagella.

At low Reynolds numbers, the viscous force for a microsphere of diameter $d$ moving at a constant speed $v$ in an incompressible fluid of viscosity $\eta$ has a simple analytic expression, $F = 3\pi d\eta v$. Using this principle, they measured the escape force of the trap for different laser powers. A fluid flow around a trapped particle was generated while the laser power was reduced, until the bead jumped off the trap. The relationship between the fluid velocity and the minimum laser power enabled the measurement of the force. Only one year later, Ashkin *et al.* (29) used this approach in an experiment with dyneins in living *Reticulomyxa* cells.

A slight modification was the basis of the first calibration of a trap as an optical spring (11): Kuo and Sheetz determined the force for different displacements of a trapped particle by moving a piezoelectric stage back and forth. The linear relationship with the sample position was used to measure forces on the molecular motor kinesin.

Svoboda *et al.* (12), using a variant where the microchamber was displaced following a sinusoidal function (see example in Fig. 1.8), explored the high-force regime. The real change, however, came with a new method introduced by them to explore the center of the trap with high precision, which soon became the standard procedure. The short excursions of a sample in the trap due to thermal energy were recorded with a high-speed photodetector and its power spectrum analyzed to obtain the value of $\kappa$.

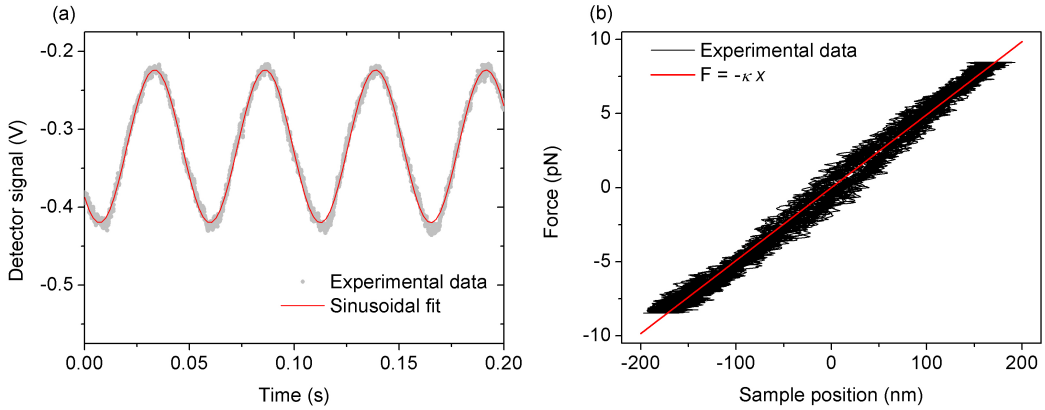


**Figure 1.8:** - (a) Detector signal recorded when a 1.16 $\mu m$ bead is dragged by the surrounding fluid with a flow generated by a piezoelectric stage moving at 19 Hz with an amplitude of 15 $\mu m$. The force exerted by the fluid is given by the Stokes' equation, $F = 3\pi d\eta v(t)$. (b) For small displacements, the applied force is proportional to the sample position.

The calibration through viscous forces is still used but discrepancies with the results of the power spectrum analysis have cast doubt upon its accuracy (see Table 1.1). The problems arise mainly due to uncertainties in the medium viscosity, whose value is very sensitive to sample size, changes in temperature and distance of the microsphere to the walls of the experimental chamber. The main advantage, on the other hand, is that it allows the reconstruction of the potential well created by the trap to thus determine the extent to which the force is proportional to the position (Fig. 1.8).

The power spectrum analysis has definitely become the preferred method to calibrate optical traps. Curiously enough, the method should be affected by the same uncertainties in the medium viscosity, $\eta$, since the value of the drag coefficient, $\gamma = 3\pi\eta d$, is needed for computing $\kappa$ (where $d$ is the sample size). It is generally accepted, however, that the results from this method are accurate and, therefore, they are typically used as a benchmark for the others.

In the power spectrum analysis, the thermal motion of a trapped sample is recorded and the two-sided power spectrum is calculated and fitted to the theoretical model:

$$P(f) = \frac{D}{2\pi^2(f^2 + f_c^2)}, \tag{1.4}$$

where $f_c = \kappa/2\pi\gamma$ is the characteristic corner frequency and $D = k_B T/\gamma$ is the particle diffusion constant.

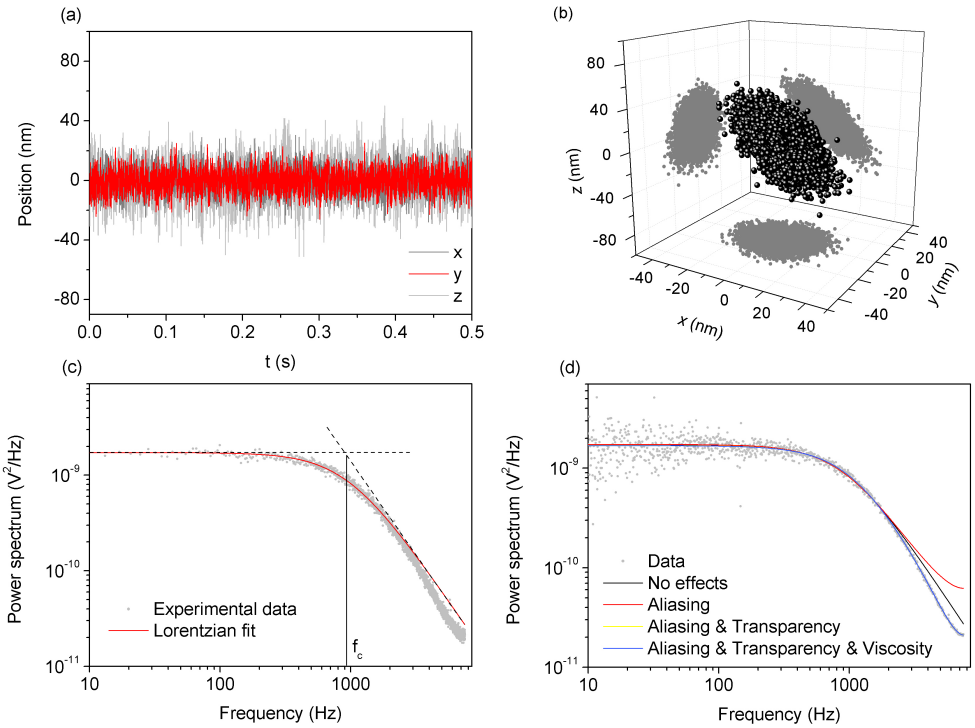


**Figure 1.9:** - (a) Temporal series of the positions $x$, $y$ and $z$ of the brownian motion of a 1.16 $\mu m$ trapped microsphere. The laser power at the sample was 36 $mW$. Position was recorded through BFPI at 15 kHz. (b) Volume of positions visited by the sample during a 50 s record. (c) Illustrative two-sided power spectrum of the trapped particle: experimental data (dots) and fit to the Lorentzian curve given in Eq. 1.4 (solid line). The vertical line indicates the value of the corner frequency $f_c = 960$ Hz that can be estimated visually from the crossing of the two dashed lines. (d) Fitting to a corrected Lorentzian taking into account the effects explained in the text.

Figure 1.9 shows an example of a power spectrum of a 1.16 $\mu$m polystyrene bead. The first fitted parameter ($f_c$) gives a value of the stiffness ($\kappa$) if $\gamma$ is known. On the other hand, as mentioned in the previous section, the value of $D$, obtained in units of

volts, can be used to extract the second constant, the position calibration, $\beta$, of the BFPI instrument.

Typical values of $f_c$ are in the kHz range so video cameras are not fast enough to sample the Brownian motion appropriately and are therefore generally discarded. The slower recording translates into modifications of the Lorentzian shape given in Eq. 1.4. Blurring due to the integration time of the camera and the tracking error (typically larger than in BFPI, where this effect can be neglected) are the main contributions. In a recent work, Van der Horst and Forde (30) found good agreement between the calibrations obtained with BFPI and high-speed video tracking when these effects were included in the theoretical model. Nevertheless, there are still other important limitations compared to BFPI, such as the necessity to calibrate off-line, the large data files generated, or the outcome being the absolute position of the sample (in contrast to the relative separation from the trap obtained in BFPI).

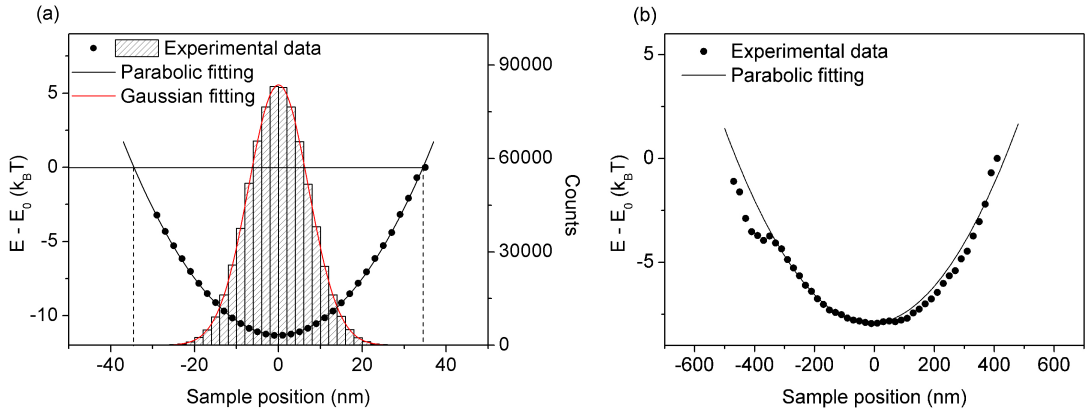


**Figure 1.10:** - (a) Harmonic potential for a trapped microsphere reconstructed from the Gaussian distribution of sample positions. Given the total energy of the system determined by the laser power and the temperature of the bath, the particle is confined to a region of less than 80 nm (dashed lines). (b) When the trap is aberrated or has a more complex profile, this method can be used to analyze the perturbations on the harmonic potential, in this case, due to the presence of a second close trap.

Thermal calibration of optical traps has been finally consolidated by the work of Berg-Sørensen and Flyvbjerg (31), who made a thorough analysis of different effects that modify the Lorentzian shape of the power spectrum with BFPI. In particular, they took into account the aliasing due to the detector finite bandwidth, the low-pass filter effect due to the transparency of silicon photodiodes at infrared wavelengths (32) and

the dependence of the viscosity with frequency (33). With all these changes, the fitting reproduces accurately the data up to the Nyquist frequency (Fig. 1.9(d)).

Alternatives to this method have appeared throughout these decades, especially during the 1990s. In 1993, Ghislain and Webb presented their scanning-force microscope based on an optical trap (19). In the same work, they suggested the use of the equipartition theorem to calibrate the system, using the expression:

$$\frac{1}{2}\kappa\langle x^2\rangle = \frac{1}{2}k_B T\,, \tag{1.5}$$

which relates the thermal and potential energies of the sample per degree of freedom. In this case, no previous knowledge about the medium or the particle is required, only the temperature of the bath. A similar performance is obtained when the analysis is based on the distribution of sample positions. As explained by Florin *et al.* (34), the particle moves in a bath in thermal equilibrium so the Maxwell-Boltzmann statistics relates the confining potential and the probability function of positions, $p(x)$, according to:

$$E - E_0 = -k_B T \ln p(x) = \frac{1}{2}\kappa\langle x^2\rangle\,. \tag{1.6}$$

Thus, the measurement of $p(x)$ allows reconstructing the potential well (Fig. 1.10). This may be useful when the trap is not harmonic, although the range of positions typically visited by a trapped particle is small, so only the center of the trap is explored.

The last two methods are likely the most simple ones but also the less precise. They are largely affected by low-frequency noise that can be inadvertently assimilated to thermal fluctuations and result in an underestimation of the stiffness. This effect can be clearly observed in the Allan variance of a typical position trace. Allan variance is typically used to determine long-term instabilities, such as mechanical drifts, in a regime where the power spectrum is under sampled (35). When we compute the Allan variance, $\sigma$, of the position of a trapped microsphere (Fig. 1.11), we observe that the signal starts deviating from the thermal limit for temporal windows of some seconds, indicating the presence of sources of error that can change the value of $\kappa$, if this is determined from the standard deviation of the whole measurement. A better estimation of the stiffness can be obtained if we use the region where the sample motion is limited by Brownian noise (see Fig. 1.11).

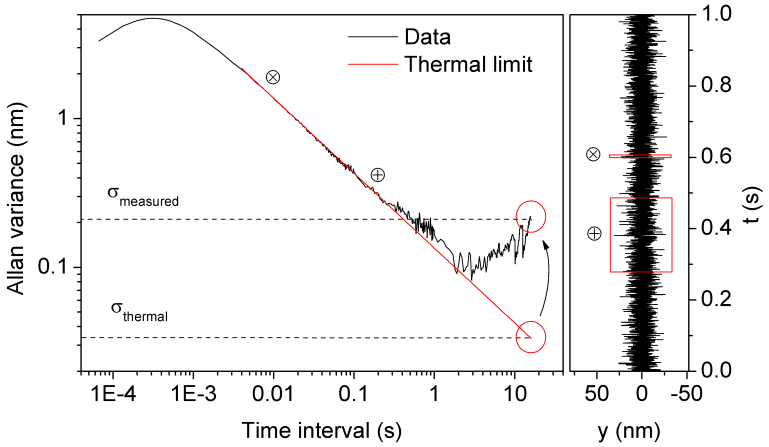


**Figure 1.11:** - Allan variance for a 1.16 $\mu m$ trapped microsphere. The value of $\sigma$ is computed for temporal windows of increasing length, which provides information about the sources of noise at different time scales. Two examples at 0.01 and 0.2 seconds (indicated by $\otimes$ and $\oplus$, respectively) are shown. For small intervals, $\tau$, the curve follows the expression $\sqrt{2k_BT\gamma/\kappa^2\tau}$, which can be used to determine the stiffness. Beyond 2-3 seconds, the measurement is no longer limited by thermal noise and $\sigma$ starts to increase. Then, the value of $\kappa$ obtained with the $\sigma$ of the whole measurement would be misleading.

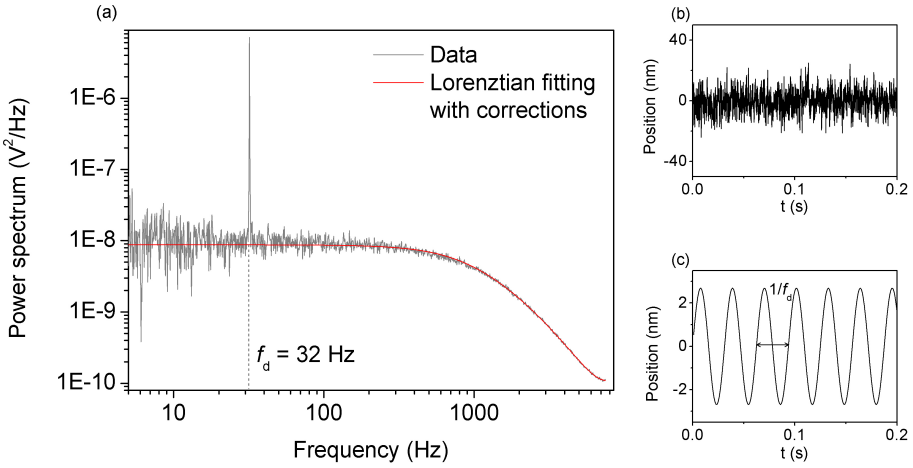


**Figure 1.12:** - (a) Power spectrum of a 1.16 $\mu m$ trapped particle subjected to a sinusoidal perturbation with a driving frequency of 32 Hz. The resulting motion is the sum of the thermal contribution (b) and the pure oscillation (c).

Finally, in 2006, Tolić-Nørrelykke *et al.* (36) developed an improved version of the power spectrum analysis. A similar idea had been proposed a couple of years earlier by Buosciolo *et al.* (37). The calibration was based on integrating two complementary procedures in one single step: a bead was trapped and its motion was recorded as a small perturbation was generated by the fluid in the microchamber, which was moved by a piezoelectric stage with a sine wave. Its main advantage is that it retains the key properties of the original method but, in addition, it does not require prior knowledge of the fluid viscosity or the sample size, which are always the main sources of error. The power spectrum of a typical signal with this method is shown in Fig. 1.12.

The combined analysis of the peak in the power spectrum and the Lorentzian fitting provides the three parameters: the position sensitivity, $\beta$, the trap stiffness, $\kappa$, and the drag coefficient, $\gamma$.

Because of its generality, an extension of this idea is being currently applied to calibrate traps inside non-homogeneous and non-viscous media (38). The method has been shown to be applicable in a viscoelastic medium consisting in a network of actin filaments (39).

| | Lorentzian | Equipart. | Boltzmann | Corrected Lorentzian | Allan | Stokes + spectrum |
|---|---|---|---|---|---|---|
| $\kappa\,(pN/\mu m)$ | 65.3 | 79.0 | 76.4 | 69.2 | 67.5 | 69.2 |
| Non-spherical | | X | X | | | X |
| Non-gaussian | | X | X | | | X |
| Provides $\beta$ | X | | | X | | X |
| Non-viscous | | X | X | | | X |

**Table 1.1:** Comparison of the stiffness obtained through the different calibration methods, and typical properties: whether the method provides $\beta$ and is applicable to non-spherical samples, non-gaussian beams or non-viscous environments.

Table 1.1 compares the values of $\kappa$ obtained through each of these calibration methods, and summarizes their most relevant features. Although the more recent developments typically give the better results, the combination of several of them often provides a wider picture of the system and is, hence, desirable. The power spectrum analysis, for example, enables the identification of high-frequency noise. On the contrary, long-term drifts are usually better observed with the Allan variance. Similarly, the method based

on the Maxwell-Boltzmann statistics is affected by low-frequency noise, but provides information on the potential shape by direct inspection.

## 1.8 Measurement of forces through the determination of light momentum

Despite all the improvements, calibration is still one of the limiting features of measurements with optical traps. The approximation of the system as an optical spring requires, in general, the use of Gaussian beams coupled with the use of spherical particles. Other objects or illumination beams can lead to non-linearities in the potential and make the calibration difficult, or even impossible.

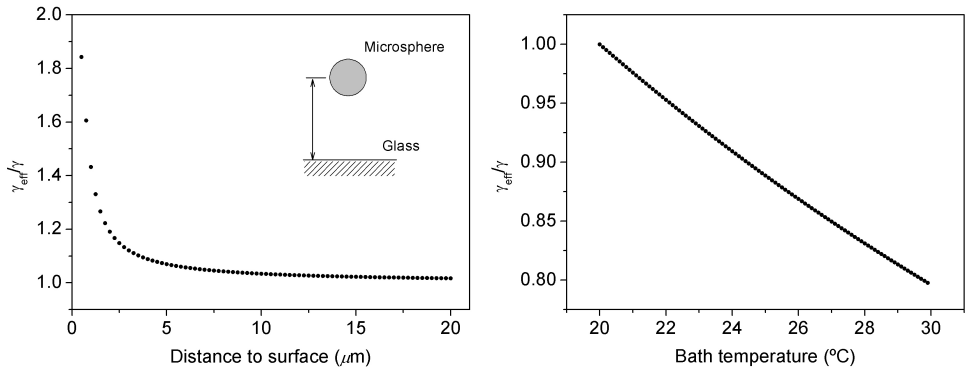


**Figure 1.13:** - Simulations of the dependence of water viscosity with temperature and distance to a surface. The viscosity is used to determine both $\beta$ and $\kappa$ so small variations in these parameters can have a strong impact on the calibration, even in *in vitro* experiments. Curves were computed for a $1.16\,\mu m$ bead.

Furthermore, the process is delicate because of the strong dependence of $\kappa$ and $\beta$ on the experimental parameters, so any small change in the experimental conditions can give significant errors in the measurements (Fig. 1.13). Consequently, the optical trap needs to be recalibrated before each experiment. In addition, its use in more complex environments like the cytoplasm of a cell has been very scarce as the determination of the two constants, $\kappa$ and $\beta$, generally requires viscous, homogeneous buffers. The recent attempts to bring the calibration of forces over into media with more sophisticated mechanical properties are still under discussion. As mentioned earlier, the validation in a viscoelastic solution of actin filaments has been possible but its transfer into the

cell has still to be proved. Even for simple environments, calibration always requires a physical model of the trap and sample and is, therefore, subjected to the approximations included in the model and all the inaccuracies thereof. This always leads, to a variable degree, to errors in the measurements of the force and explains the variability of $\kappa$ observed in Table 1.1.

The different modifications of the calibration procedure have tried to overcome these drawbacks, yet without modifying the root of the problem. Only Smith *et al.*, in 1996, proposed a radical change to address these questions (40).

They noticed that measurements with the system developed by Ghislain and Webb (19) inherently contained information about the momentum structure of the beam, so they were directly related to the force exerted by the light (41, 42, 43). Several modifications of the experimental setup allowed them to directly measure the force without any previous calibration. A position detector located between the condenser lens and the image plane provided an electric signal, $S$, that was proportional to the force, $F$, through a constant, $1/\alpha$, that depended only on the features of the measuring instrument (Fig. 1.14).

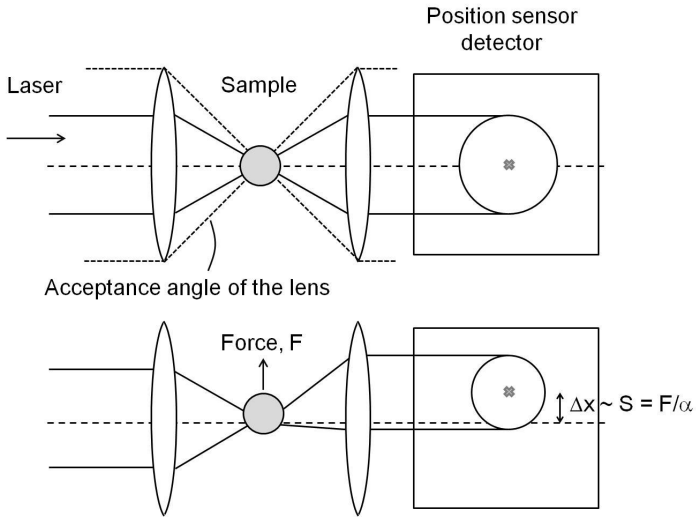


**Figure 1.14:** - Force detection through the measurement of the light momentum change in a counter-propagating beam system. Only one laser is shown for the sake of simplicity.

The main limitation is that the method developed by Smith requires the use of counter-propagating beams (see 1.2). This is necessary to collect all the light leaving

the trap whose momentum has changed. Otherwise, the loss of relevant information leads to errors in the measurements.

Despite the apparent conceptual differences with BFPI, the two methods are intimately connected as pointed out by Smith himself and, more briefly, by Gittes and Schmidt in their theoretical model (22). We have recently proved experimentally that when the light is collected and analyzed only partially, the force signal is degraded and the far-field distribution can only measure positions, losing the characteristic permanent and robust calibration of the method based on light momentum.

Unfortunately, the setup required for directly measuring forces is less flexible than that for BFPI, experimentally more complex due to the requirement of a precise alignment of the two lasers and not compatible with other microscopy techniques. As a result, the method has never been generally adopted. Different optical trapping reviews (21, 44) included this method but its actual acceptance has remained low.

## 1.9 Multiple traps

The second distinctive aspect of optical trapping is the translocation and manipulation of samples. Since the early 1990s, and in parallel to the development of the measurement of forces, the technique has experienced a growing sophistication in the capacity to manipulate particles. Optical tweezers have been combined with different beam-shaping technologies to enable the simultaneous trapping of many objects (as many as some hundreds) or to create traps with complex intensity profiles to, for example, rotate particles, move samples through long distances or achieve selective trapping according to size.

A strong motivation was the study of colloidal systems, although biological experiments, where the measurement of forces often need to be supported by a method equally powerful to manipulate samples (especially, to create multiple steerable traps (16)), are a perfect target for these technologies.

The most direct, but also expensive strategy to generate several trapping points is the use of more than one laser. However, in many experiments, only two traps are needed. In this case, a simpler option is to split a single laser by polarization. This scheme was introduced by Misawa *et al.* in 1992 (46) and applied to study the properties of myosin shortly afterwards (16). One year later, Visscher *et al.* (47)

presented an alternative method based on a fast switching of the beam throughout all the trapping positions. If the laser refresh rate is above the roll-off frequency of the trap, the laser does not perturb the sample motion, and the time-shared beam is equivalent to multiple permanent traps. Several different technologies can be used to steer the beam at high rates. The original idea (47) was based on galvanometric scan mirrors, but acousto-optic or electro-optic deflectors (AODs or EODs) can also be employed.

More recently, in 1999, Hayasaki *et al.* (48) showed the manipulation of multiple samples using digital holography, which has become since then a strong contender against the time-shared approach. A spatial light modulator (SLM) was used to modify the wavefront of the trapping beam to generate multiple holographic traps. The static holograms initially used by Dufresne and Grier (49) could be thus changed in real-time, providing a dynamic control. The main potential advantage for high precision experiments, compared to galvanometric mirrors or AODs, is that traps are permanent.

Different works have appeared during this decade related to holographic optical tweezers (HOTs) and their use in position and force measurement experiments. Monneret *et al.* determined that the potential wells of holographic traps are harmonic within a range of a few hundred nanometers (52), and the associated stiffness was found to vary only a 4% over a range of 20 $\mu$m across the sample plane (53). On the other hand, the minimum step size attainable with modulators was obtained theoretically and experimentally ($\sim$2 nm) (53, 54) and the intensity changes during trap steering, which is one of the distinctive drawbacks of HOTs, were thoroughly analyzed and minimized by the use of the restricted phase change algorithm (55). Similarly, other algorithms with very high efficiency (up to 99%) have also been designed (56) and their implementation in real time has been possible both with CPUs (57) and GPUs (58).

However, the use of SLMs in position and force measurements has been rather limited (50) and HOTs have been mainly employed to manipulate samples. Generally, when precision is needed, a dual-trap system is built with one single laser split into two polarizations. As pointed out in (45), this has been primarily motivated by the lack of an alternative method for position and force detection with a performance comparable to that of back-focal-plane interferometry (BFPI) (22) and compatible with multiple permanent traps. High-speed tracking with a video camera still exhibits some serious drawbacks (absolute measurement of position, low frequency acquisition, blurring (30),

calibration off-line, large data files). In addition, holographic traps also show "blinking" due to the refreshing of the hologram displayed on the liquid crystal SLM. Although it has never been specifically studied, this casts doubt upon their reliability for precise experiments.

As we will explain in the next chapter, our work has been oriented to assess some of these questions to couple together HOTs and precision experiments; in particular, we have studied the possibility to exert high forces and have determined the positional stability of traps created with SLMs.

# Chapter 2

# Results

In this chapter, we present a summary of the most relevant results obtained in this thesis. The scientific publications related to these works are included at the end of the dissertation. In the papers, one can find the technical details, as well as all the results and a deeper analysis of each subject. Here, by contrast, we focus on the motivation of the work, its relevance and its relation with the global picture. We present only the most significant works, those that deserve a special attention, either because of their length or their impact in the whole thesis. The five papers that represent the nucleus of this thesis are briefly summarized and interrelated in separated subsections.

The research can be divided into two lines, which can be seen as two sides of the same coin, my attempt to make optical trapping a bit more general and useful:

- The main project (probably more than 80% of my time) has revolved around the integration of single-beam optical traps and the method developed by Smith *et al.* (42) based on the determination of the light momentum change.

  As explained in the previous chapter, the standard approach to measure forces relies on the harmonic approximation of the force. Its use has stringent requirements such as the necessity of a previous calibration, the use of Gaussian beams and spherical particles and the necessity of doing the experiments inside a viscous medium; all of them important limitations for the development of optical trapping.

  In contrast, measurements of the light momentum are not affected by all these problems. However, they could not be used with optical tweezers, which are much

more flexible, simple and popular than counter-propagating traps.

In this thesis, we have shown how to integrate them and combine the strengths of both.

- On the other hand, I have also worked on the most elemental aspect of optical trapping: the manipulation; specifically, by holographic optical traps. Optical tweezers have the potential to generate many trapping points or beams with sophisticated profiles for complex manipulations. The possibilities that light offers make this technique unique. We have a strong control on the propagation and on the properties of a laser beam, and we can use this versatility to move objects in three dimensions.

  One of the most powerful technologies for the control of light propagation is digital holography. However, as explained earlier, spatial light modulators still pose some restrictions, particularly for precision experiments.

  My work in this field has been the evaluation of holography as a technology to manipulate samples in quantitative experiments. I have studied different aspects of holographic optical trapping that are important for its implementation in high-precision force and position detection experiments.

## 2.1 Early work. Intracellular transport: touchstone of optical trapping

A. Farré, C. López-Quesada, J. Andilla, E. Martín-Badosa, and M. Montes-Usategui, *Holographic optical manipulation of motor-driven membranous structures in living NG-108 cells*, **Opt. Eng.** 49, 085801(2010).

The first work that we present was also the first in time. It is important because it naturally introduces the two questions that we have just explained. It is the prelude to the subsequent work about measurement of forces and manipulation with HOTs and started as my MSc thesis in Biophysics.

Vesicles and organelles were trapped inside living cells with our holographic optical tweezers system. As explained earlier, the study of motor protein activity has become a paradigm in optical trapping and a perfect example of its potential in high-impact

scientific fields. However, its analysis *in vivo* has remained rather limited, likely motivated by the difficulty to obtain relevant data from particles moving in the crowded and noisy interior of the cell. The variability of conditions in the cytoplasm make these studies more complex. For example, the transport of cargos *in vivo* is often carried out by several motors of different polarities simultaneously pulling from the same organelle, cooperating or competing through highly regulated mechanisms still not well understood. Sometimes, these proteins even correspond to different families, so combinations of actin-based and microtubule-based motors are found switching on and off, their coordination being again a problem whose surface has only been barely scratched. All this activity ultimately makes the interpretation of the results difficult.

Nevertheless, our knowledge about these biological systems has evolved quickly during the last years, and the necessity to make a step forward and bring inside the cells the experiments typically performed *in vitro* has increased. A growing trend toward more complex *in vitro* experiments and into the cell interior is clearly discernible, but a lot of development along these lines is still needed.

Our work was motivated by one of the first issues found in these complex environments, the lack of a method to measure forces. In the experiments, we tried to estimate the escape forces of the motors pulling the structures within the cells using the approach developed by Block *et al.* (28) and used by Ashkin *et al.* with dyneins (29). We realized, however, that a different solution was needed if forces were to be measured with higher precision and larger bandwidth.

By that time, we were already working in the implementation of BFPI. It was then when we came in contact with the method based on the measurement of light momentum changes proposed and developed by Smith *et al.* (42). This was the seed of my first line of research.

The work with the NG108 cells brought up a second important question: the manipulation of samples. We assessed the possibility of using holographic traps to manipulate both freely-floating and motor-driven subcellular structures. The rapid and intermittent movement exhibited by some cargos in the cell required the ability to steer the laser beam automatically or, at least, fast enough to stop them, which we achieved with holography and SLMs.

However, during that year, Van der Horst and Forde published a work about the instabilities introduced by SLMs on trapped microspheres (53). We then started asking

ourselves whether this technology could have fundamental flaws when carrying experiments involving force measurements.

## 2.2 Measuring forces through the detection of light momentum changes in optical tweezers

A. Farré and M. Montes-Usategui, *A force detection technique for single-beam optical traps based on direct measurement of light momentum changes*, **Opt. Express** 18, 11955-11968 (2010).

The literature about BFPI has been always somewhat unclear and scarce, at least for people starting in the field. We were particularly interested in really understanding the light patterns recorded by the photodetector to obtain the sample displacement. However, not many details about the implementation or about the principles of the method were available, except for the theoretical works by Pralle *et al.* (23) and Gittes and Schmidt (22).

During the process, we observed that the curves relating the detector signal $S_x$ and the sample position were suspiciously similar to those relating the force and the position (Fig. 2.1). This brought our attention to the method developed by Smith *et al.*, according to which it was possible to directly measure forces with a setup similar to ours. Although it was generally accepted that the method could not be implemented in single-beam traps, our observations were telling the opposite. Given the potential advantages of this alternative approach, we started working on this.

The crucial point was to determine the amount of light that we could capture with our instrument and whether that was sufficient for the proper operation of the method.

We started by analyzing the amount of back-scattered light for typical samples, finding that this was generally a low fraction of the whole beam (Fig. 2 in the paper). We also checked that the condenser lens used to collect the light fulfilled the Abbe sine condition, necessary to obtain the momentum decomposition of the beam at its back focal plane (Fig. 3 in the paper). In addition, we calibrated the relation between positions in this plane and the transverse components of the momentum, obtaining an absolute map between both. This allowed us to interpret the light patterns at the BFP

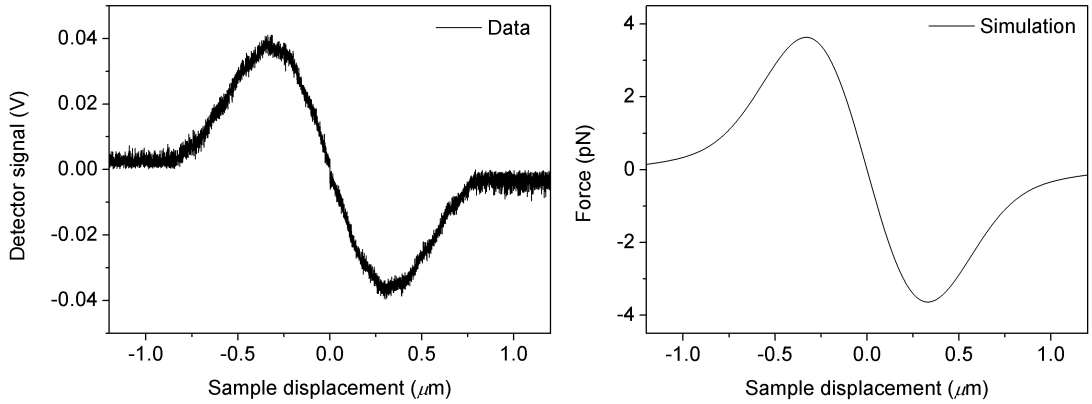


**Figure 2.1:** - Curves of detector signal and force vs. displacement, displaying great similarities.

and determine the amount of forward-scattered light we were collecting (Fig. 5 in the paper).

We found that, for most samples, the captured light corresponded to a large fraction ($> 95\%$) of all the beam, so the implementation of the momentum measurement was feasible.

The verification came with an experiment designed to determine the existence of an absolute relation between detector signal and force. We applied a known hydrodynamic force on trapped microspheres and we compared this value with the detector response for particles with different properties, always obtaining the same relation (Fig. 6 in the paper).

## 2.3 Optimized back-focal-plane interferometry

A. Farré, F. Marsà, and M. Montes-Usategui, *Optimized back-focal-plane interferometry directly measures forces of optically trapped particles*, **Opt. Express** 20, 12270-12291 (2012).

In a second part of this work, we further developed the idea of the connection between this method and back-focal-plane displacement measurements. The setup for measuring forces in the counter-propagating design is essentially equivalent to that of BFPI, so the properties should be shared to some degree. The relation between posi-

tion and momentum measurements was shown by Smith *et al.* for counter-propagating beams and indicated for optical tweezers by Gittes and Schmidt, although only theoretically. Here, we took advantage of our optimized BFPI instrument developed in the previous stage to further explore experimentally this connection for single-beam optical traps.

We found an extended range of force measurements beyond the region where positions are typically measured with BFPI and larger than the harmonic regime of the trap where force is linear with position (Fig. 1 in the paper). This could only be possible because the product $\kappa \cdot \beta$ was constant throughout the curve. On the other hand, we showed that the product was also constant regardless of the physical properties of the sample (Fig. 3 in the paper). We calibrated the trap for beads of different sizes, made of different materials, trapped with different objectives and for a range of laser powers, and found a linear relation between $\kappa$ and $1/\beta$. We explained these connected observations as simple consequences of the same principle: BFPI signals are momentum measurements. We demonstrated that, in fact, the product of the two parameters is constant because it corresponds to the calibration factor that converts detector signals into forces and it only depends on three construction features of the apparatus (Fig. 7 in the paper). Namely, its total focal length, the detector radius and the relation between the detector intensity reading and the laser power at the sample plane.

We have further shown that the results could be extended to more standard systems. Basically, we proved that even when the instrument is not fully optimized to capture all the light carrying information about the momentum change of the beam, it is still possible to find a certain range where an absolute calibration holds (Fig. 8 in the paper). We also discussed that this has strong implications in the use of BFPI and that should be kept in mind when the ultimate goal is the measurement of forces.

## 2.4 Combining holography and high-force measurements

A. Farré, A. van der Horst, G. A. Blab, B. P. B. Downing, and N. R. Forde, *Stretching single DNA molecules to demonstrate high-force capabilities of holographic optical tweezers*, **J. Biophoton.** 3, 224-233 (2010).

In parallel, we worked in the integration of holographic optical traps with quantitative experiments. In a first study, we addressed the question of what were the possibilities of a holographic system for exerting high forces. HOTs have been typically used to manipulate large numbers of particles with weak traps, but their application to measure high forces has been scarce.

In fact, there are different effects that can contribute to make high-force experiments difficult or even impossible. For example, the hologram displayed on the liquid crystal changes in time, because it is constantly updated at video rate and at the addressing frequency of the electronics. The impact on the stability of the phase and the intensity of holographic traps, which can fluctuate in time, has been recently observed (53). We deeply analyzed the effect on position and force measurements in the paper *"Positional stability of holographic optical traps"*.

On the other hand, the hologram changes when the trap is steered so there is not a continuous and smooth transition from one position to another. Thus, we can consider that two traps at two positions are intrinsically different. During this change, there is the so-called "dead time". This is the time lapse between the moment at which the trap at a certain position goes off and that when it turns on again at a different location. The result of this effect on the ability to displace samples has been recently analyzed (59). Eriksson *et al.* applied a constant flow while the trap was steered in the perpendicular direction and studied the motion of the bead between the two positions for different step sizes. They found that the decrease in the laser intensity at the trapping foci during hologram change strongly affected the motion of the particle.

Using DNA as a standard to investigate the response of holographic traps at high forces, we showed that we could exert forces as high as 65 pN within the previously calibrated harmonic region of the trap (Fig. 5 in the paper), and that even forces larger than 100 pN could not pull beads off the trap. This allowed us to confirm that trap fluctuations due either to "dead time" or instabilities did not impair the trapping of micron-sized particles at these high forces.

We observed reproducible ripples of some piconewtons in the DNA force-extension curves at both low and high forces (Fig. 5 in the paper). These oscillations did not show up when we repeated the experiment using a single-beam, non-holographic system. We attributed this artifact in the signal to the use of traps with the same polarization, which could be creating an spatially-extended interference and producing the modulations.

However, we could not confirm this hypothesis and we are still intently studying its origin.

## 2.5 High-frequency stability of holographic optical tweezers

A. Farré, M. Shayegan, C. López-Quesada, G. A. Blab, M. Montes-Usategui, N. R. Forde, and E. Martín-Badosa, *Positional stability of holographic optical traps*, **Opt. Express** 19, 21370-21384 (2011).

The phase and intensity instabilities due to the SLM's refreshing and addressing seemed to have a limited impact on the trapping but their effect could be relevant in position and force measurements.

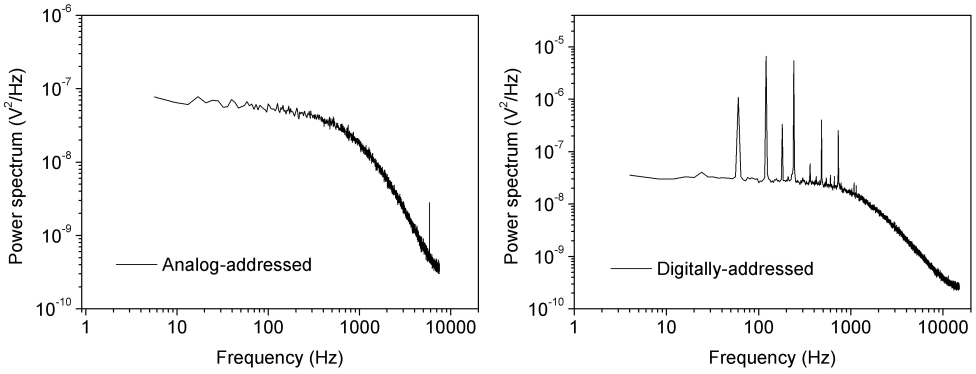


**Figure 2.2:** - Different stabilities for analog- and digitally-addressed SLMs observed in the power spectra of trapped particles.

When we were calibrating holographic traps, we observed that peaks showed up in the power spectra depending on whether the SLM was on or off. By then, we were collaborating with the laboratory of Nancy Forde in Canada and, comparing the power spectra, we realized that the SLMs from the two groups seemed to behave with remarkable differences regarding stability (Fig. 2.2).

We studied this feature and found that the origin was the different electronic technology of the SLMs backplanes. First, we investigated the characteristics of the two electronics and their effect on the phase modulation. Digital modulators are advantageous because of their lower cost, as they are manufactured using mass market tech-

nologies. However, we discovered that they suffer from a stronger phase fluctuation than analog-addressed SLMs because of the binary nature of the electronic signals sent to the liquid crystal (LC). The electronics can only provide two voltages so any intermediate state is achieved by pulse width modulation. With this technique, the LC molecules can be oriented at any angle between the minimum and the maximum, but at the expense of a larger fluctuation.

Then, at a second level of analysis, we directly measured the phase stability of a beam reflected onto the modulator for different gray levels displayed on the LC (Fig. 2 in the paper). The phase showed oscillations that corresponded to the addressing frequency for both modulators, that is, at the rate at which the electronic signal is sent to the modulator. Nevertheless, we found a clear difference between the two addressing technologies. The digitally-addressed SLM (HEO 1080P Holoeye) exhibited oscillations several orders of magnitude larger than the analog-addressed SLM (X10468-03 Hamamatsu).

Finally, we studied the effect of these fluctuations in the position stability of the traps. For this, we analyzed using high-speed video microscopy the power spectrum of trapped particles (Fig. 4 in the paper). The spectra showed peaks at the addressing frequencies. From their amplitude we determined the oscillation of the trap at the sample plane. We found that, despite the larger fluctuations, the stability of the traps generated with a digitally-addressed modulator were small, only a few nanometers (Table 1 in the paper). On the other hand, the stability of the analog-addressed SLM was excellent ($< 1nm$), comparable to non-holographic traps.

Our result in HOTs show that this kind of optical traps, despite widespread expectations to the contrary because of limitations of current SLMs, fare well when applied to single-molecule experiments.

Together with our method for measuring force based on momentum conservation, we hope to advance the study of mechanochemical processes at the molecular scale inside living samples.

# Chapter 3

# Contributions

## 3.1 Papers

- C. López-Quesada, M. D. Ludevid, M. Joseph, A. Farré, A. S. Fontaine, J. Selva, G. Egea, E. Martín-Badosa, and M. Montes-Usategui, *Artificially-induced organelles as optimized handles for optical trapping experiments inside living cells*, **J. Biophoton.** (in preparation).

- F. Marsà*, A. Farré*, E. Martín-Badosa, and M. Montes-Usategui, *Highly-stable holographic dumbbell combined with back-focal-plane displacement detection*, **Opt. Express** (in preparation).

- A. Farré, F. Marsà, and M. Montes-Usategui, *Optimized back-focal-plane interferometry directly measures forces of optically trapped particles*, **Opt. Express** 20, 12270-12291 (2012).

- A. Farré, M. Shayegan, C. López-Quesada, G. A. Blab, M. Montes-Usategui, N. R. Forde, and E. Martín-Badosa, *Positional stability of holographic optical traps*, **Opt. Express** 19, 21370-21384 (2011).

- I. Verdeny, A. Farré, J. Mas, C. López-Quesada, E. Martín-Badosa*, and M. Montes-Usategui*, *Optical trapping: a review of essential concepts*, **Opt. Pur. Apl.** 44, 527-551 (2011).

- J. Mas, A. Farré, J. Cuadros, I. Juvells, and A. Carnicer, *Understanding optical trapping phenomena: a simulation for undergraduates*, **IEEE Trans. Educ.** 54,

133-140 (2011).

- A. Farré, C. López-Quesada, J. Andilla, E. Martín-Badosa, and M. Montes-Usategui, *Holographic optical manipulation of motor-driven membranous structures in living NG-108 cells*, **Opt. Eng.** 49, 085801(2010).

- A. Farré and M. Montes-Usategui, *A force detection technique for single-beam optical traps based on direct measurement of light momentum changes*, **Opt. Express** 18, 11955-11968 (2010).

- A. Farré, A. van der Horst, G. A. Blab, B. P. B. Downing, and N. R. Forde, *Stretching single DNA molecules to demonstrate high-force capabilities of holographic optical tweezers*, **J. Biophoton.** 3, 224-233 (2010).

## 3.2 Patents

- E. Martín-Badosa, M. Montes-Usategui, A. Farré, and J. Mas, *Method for manipulating microscopic samples and measuring forces acting thereon*, Patent (application ES 201130783) (2011).

- M. Montes-Usategui and A. Farré, *Method and apparatus for measuring optical forces acting on a particle*, Patent (application ES200901259) (2009).

## 3.3 Other publications

- I. Verdeny, A-S. Fontaine, A. Farré, M. Montes-Usategui, and E. Martín-Badosa, *Heating effects on NG108 cells induced by laser trapping*, **Proc. SPIE** 8097, 809724 (2011).

- J. Mas, A. Farré, C. López-Quesada, E. Martín-Badosa, and M. Montes-Usategui, *Measuring stall forces in vivo with optical tweezers through light momentum changes*, **Proc. SPIE** 8097, 809726 (2011).

- C. López-Quesada, M. Joseph, J. Selva, A. Farré, G. Egea, M. D. Ludevid, E. Martín-Badosa, and M. Montes-Usategui, *High-speed tracking of intracellular structures: understanding the transport mechanisms in living plant cells*, **Proc. SPIE** 8097, 80970 (2011).

- A. Farré, E. Martín-Badosa, and M. Montes-Usategui, *Back-focal-plane interferometry: position or force detection?*, **Proc. SPIE** 8097, 809705 (2011).

## 3.4 Conferences

- I. Verdeny, A-S. Fontaine, A. Farré, M. Montes-Usategui, and E. Martín-Badosa
  "Heating effects on NG108 cells induced by laser trapping"
  Optical Trapping and Optical Micromanipulation VIII
  San Diego (United States), August 2011

- C. López-Quesada, M. Joseph, J. Selva, A. Farré, G. Egea, M. D. Ludevid, E. Martín-Badosa, and M. Montes-Usategui
  "High speed tracking of intracellular structures: understanding the transport mechanisms in living plant cells"
  Optical Trapping and Optical Micromanipulation VIII
  San Diego (United States), August 2011

- J. Mas, A. Farré, C. López-Quesada, E. Martín-Badosa, and M. Montes-Usategui
  "Measuring stall forces in vivo with optical tweezers through light momentum changes"
  Optical Trapping and Optical Micromanipulation VIII
  San Diego (United States), August 2011

- A. Farré, E. Martín-Badosa, and M. Montes-Usategui
  "Back-focal-plane interferometry: position or force detection?"
  Optical Trapping and Optical Micromanipulation VIII
  San Diego (United States), August 2011

- I. Verdeny, A.-S. Fontaine, A. Farré, M. Montes-Usategui, and E. Martín-Badosa
  "Study of thermodamage to Neuroblastoma NG108 cells due to manipulation with optical tweezers"
  EOS Annual Meeting
  Paris (France), October 2010

- A. Farré, A. van der Horst, G. A. Blab, M. Shayegan, B. P. B. Downing, and N. R. Forde

"Stretching single DNA molecules to demonstrate high-force capabilities of holographic optical tweezers"
Optical Trapping and Optical Micromanipulation VII
San Diego (United States), August 2010

- A. Farré and M. Montes-Usategui
"Force detection method for single-beam-gradient traps based on the measurement of light momentum change"
ESF Research Conference on Trends in Optical Micromanipulation II
Obergurgl (Austria), April 2010

- Arnau Farré, Josep Mas, and Mario Montes-Usategui
"A force detection technique for molecular experiments in living cells using gradient optical traps"
Optical Tweezers in Life Sciences
Berlin (Germany), October 2009

- Arnau Farré, Josep Mas, and Mario Montes-Usategui
"Método de medida de fuerzas en el interior de células vivas con pinzas ópticas de gradiente"
IX Reunión Nacional de Óptica
Ourense (Spain), September 2009

- Josep Mas, Carol López-Quesada, Arnau Farré, Estela Martín-Badosa, and Mario Montes-Usategui
"Sistema de pinzas ópticas combinado con microscopía de fluorescencia para la realización de experimentos de biofísica celular."
IX Reunión Nacional de Óptica
Ourense (Spain), September 2009

- Arnau Farré, Josep Mas, and Mario Montes-Usategui
"A force detection technique for molecular experiments in living cells using gradient optical traps"
11th Annual Metting of the Northwest Section of APS
Vancouver (Canada), May 2009

- Arnau Farré, Carol López-Quesada, Josep Mas, Jordi Andilla, Estela Martín-Badosa, and Mario Montes-Usategui
  "Holographic optical manipulation of motor-driven subcellular structures"
  OSA Topical Meetings. Optical Trapping Applications (OTA).
  Vancouver (Canada), April 2009

- Arnau Farré, Carol López-Quesada, Jordi Andilla, Estela Martín-Badosa, and Mario Montes-Usategui
  "Exploring the vesicle trafficking mechanisms in living cells using optical tweezers"
  XXIV Trobades Científiques de la Mediterrània. La física a les ciències de la vida.
  Menorca (Spain), October 2008

- Arnau Farré, Jordi Andilla, Encarnación Pleguezuelos, Mario Montes-Usategui, Estela Martín-Badosa, Artur Carnicer, Ignasi Juvells, and Santiago Vallmitjana
  "Construcción de un sistema de pinzas ópticas holográficas y calibración de fuerzas"
  XXII Trobades Científiques de la Mediterrània. Nanociència i Nanotecnologia.
  Menorca (Spain), October 2006

# Chapter 4

# Conclusions

The conclusions of this thesis follow:

1. We trapped and manipulated freely-diffusing structures within living NG108 cells. We used the flexibility of our holographic tweezers to further stop motor-protein driven structures moving rapidly within the cytoplasm. Forces generated by molecular motors were estimated using the escape force method.

2. We analyzed the requirements to obtain correct measurements of the light momentum. We first studied the image formation through the lens used to capture the light and developed a method to determine whether it fulfilled the Abbe sine condition, necessary to obtain the momentum structure of the beam at its back focal plane. We calibrated this plane by converting positions into transverse components of the momentum and, using the light patterns here, we determined that the fraction of scattered light collected by the detection instrument was close to 100% for most samples.

3. Following the previous work, we designed (with a ray optics simulation) and built a force sensor apparatus compatible with optical tweezers.

4. We determined the calibration constant of this instrument for different experimental conditions and found that it did not vary. In connection with this, we also proved that forces could be measured beyond the harmonic approximation of the trap.

5. Our setup was essentially an optimized BFPI system, so, in a second step, we used it to explore the connection between position and momentum measurements. We showed that the product of the stiffness, $\kappa$, and the inverse of the position sensitivity, $1/\beta$, was constant and equal to the calibration factor that converted detector signals into momentum measurements. We evaluated the extent to which the absolute force calibration could be recognized in practice in the measurements with a conventional BFPI instrument, and found that the momentum could be determined even when the system was not fully optimized.

6. We studied the variability of force calibration with several parameters: the trapping depth, the position of the condenser lens, the position of the relay lens used to image the BFP onto the detector, and the type of photodetector.

7. We obtained double-stranded DNA by digestion of plasmid pPIA2-6 and labelled it with biotin and digoxigenin groups. We coated microspheres with streptavidin and anti-digoxigenin and prepared them within solutions with oxygen scavengers (PCA/PCD). We built a fluid chamber for single-molecule experiments.

8. We studied the high-force capabilities of optical traps generated with SLMs and found that it was possible to measure the characteristic transition of double-stranded DNA at 65 pN and even reach forces larger than 100 pN. We thus showed that trapping was not compromised at high forces despite the instabilities of the SLM due to refresh, "dead time" and addressing.

9. We further verified that these effects had also an insignificant influence on the stability of traps. We made this analysis with two modulators with different electronics: a digitally-addressed one (HEO 1080P Holoeye) and an analog-addressed (X10468-03 Hamamatsu). We measured the oscillation of the beam phases after being reflected off the SLMs and observed modulations at the corresponding addressing frequencies. For the digital modulator, fluctuations were several orders of magnitude larger and also showed up at overtones of the fundamental frequency. The origin was the pulse width modulation used in this case to adapt the binary nature of the electronic signal sent to the liquid crystal to the continuous variation of the phase required to correctly modulate the laser. We further showed the effect of these oscillations on the traps and found that the stability of the

digitally-addressed SLM could be reduced down to 2 nm, and that this stability was better than 1 nm for the analog-addressed SLM, comparable to regular non-holographic systems.

In summary, we have shown capabilities of holographic optical trapping that were previously undemonstrated (high force and positional stability), which indicate a promising potential for this technology in single-molecule research and other precision applications.

On a parallel track, we have adapted force measurements based on the method of Smith *et al.* of momentum conservation to single-beam traps and therefore made it compatible with HOTs as well. We hope to use the combined power of these methods in applications involving living cellular samples in the near future.

# Chapter 5

# Papers

# Holographic optical manipulation of motor-driven membranous structures in living NG-108 cells

Arnau Farré, Carol López-Quesada, Jordi Andilla, Estela Martín-Badosa, and Mario Montes-Usategui

Optical Engineering
Vol. 49, 085801 (2010)

Optical Engineering 49(8), 085801 (August 2010)

# Holographic optical manipulation of motor-driven membranous structures in living NG-108 cells

**Arnau Farré**
**Carol López-Quesada**
**Jordi Andilla,** MEMBER SPIE*
**Estela Martín-Badosa**
**Mario Montes-Usategui**
Universitat de Barcelona
Departament de Física Aplicada i Òptica
Optical Trapping Lab—Grup de Biofotònica
Martí i Franquès, 1
Barcelona 08028, Spain
E-mail: arnau.farre@ub.edu

**Abstract.** Optical tweezer experiments have partially unveiled the mechanical properties of processive motor proteins while driving polystyrene or silica microbeads *in vitro*. However, the set of forces underlying the more complex transport mechanisms in living samples remains poorly understood. Several studies have shown that optical tweezers are capable of trapping vesicles and organelles in the cytoplasm of living cells, which can be used as handles to mechanically interact with engaged (active) motors, or other components regulating transport. This may ultimately enable the exploration of the mechanics of this trafficking mechanism *in vivo*. These cell manipulation experiments have been carried out using different strategies to achieve dynamic beam steering capable of trapping these subcellular structures. We report here the first trapping and manipulation, to our knowledge, of such small motor-propelled cargos in living cells using holographic technology.  [DOI: 10.1117/1.3475950]

Subject terms: optical tweezers; real-time holography; vesicle transport.

Paper 100194R received Mar. 11, 2010; revised manuscript received Jun. 9, 2010; accepted for publication Jun. 19, 2010; published online Aug. 13, 2010.

## 1 Introduction

Optical tweezers are currently used in a range of different molecular biology experiments.[1] A highly focused infrared laser beam enables the manipulation of biological samples and the measurement of the forces involved in many relevant molecular processes.[2] Results of primary importance have been obtained with this biophotonic tool, such as information regarding the elastic properties of DNA molecules,[3] precise values of the basic mechanical properties of the RNA polymerase,[4] or a detailed picture of the mechanism by which bacteriophage $\phi 29$ infects bacteria.[5] Its noninvasive behavior renders this technique highly suitable for *in-vivo* experiments within living cells. One of the areas in which notable progress has been made is intracellular transport.

Both anterograde and retrograde intracellular transports mediate many important cellular processes in living neurons and other motile cells, such as the NG-108 cells that we used in this study. The disruption of these mechanisms may eventually compromise the cell's main functions, and may lead to the appearance of neurodegenerative diseases.[6] Specifically, transport disorders associated with the overexpression of the microtubule-associated protein (MAP) tau, which inhibits the engagement of plus-end-directed motor proteins, appear to play an important role in Alzheimer's disease.[7] Vesicle trafficking disruptions may also be involved in Huntington's chorea and amyotrophic lateral sclerosis.[6]

The cytoskeleton is the cellular component governing vesicle trafficking in eukaryotic cells. Different enzymatic motor proteins drive cargos along the crowded branched networks of cytoskeletal filaments by means of the chemical energy obtained from the hydrolysis of ATP molecules. Working in coordination with other accessory proteins, they constitute an extremely complex mechanism by which the cellular components are packaged in small vesicles and transported between inner and peripheral regions.

The mechanical and chemical processes underlying this mechanism have been extensively studied *in vitro*. Optical tweezer experiments, in particular, have provided many important results related to the fundamental molecular processes involved in transport. The force exerted by the polymerization of the cytoskeletal filaments, as well as their stiffness,[8,9] or the mechanochemical processes that give motor proteins the ability to sequentially bind and detach from the filaments,[10,11] are just a few examples.

Despite their success, these experiments generally provide a simplified picture of vesicle trafficking. They focus mainly on the properties of processive motors, thus avoiding the complex mechanical interplay arising between the cargo and cytoskeletal and accessory proteins. However, these secondary actors also promote cargo transport in living cells and may play a fundamental role in the regulation of the mechanism *in vivo*. Specifically, mechanical effects derived from the presence of recruiting proteins that increase the number of motors moving the cargo, or the tug-of-war between actin- and microtubule-based motors, are known to modify fast axonal transport.[12] It has been suggested that these additional processes, which partially govern intracellular trafficking, could be responsible for the regulation of the entire mechanism.

*Currently at Imagine Optic, Orsay, France

Unfortunately, although optical tweezers constitute a powerful technique for studying these molecular processes, they still exhibit some limitations when working within living cells. A robust calibration method to measure forces in an optically nonhomogeneous medium, such as the cytoplasm of the cell,[13] is not currently available. In the past decade, a few isolated studies have reported several ways to obtain quantitative data within living samples.[14,15] However, these remain unsuitable, either because it is difficult to combine them with advanced microscopy techniques (e.g., phase contrast microscopy, fluorescence, etc.) for observing the cells, or they lack accuracy.

Despite the paucity of optical tweezer results *in vivo* due to experimental difficulties, increasing interest is being shown in the use of such quantitative techniques to unveil the underlying processes in vesicle trafficking. Recently, several optical trapping experiments have demonstrated the manipulation of lipid granules in living cells, and have made a significant contribution to *in-vivo* calibration methods.[16–18] Together with earlier results,[19] these studies have provided important information about trapping free-floating vesicles. Nevertheless, the results refer only to freely diffusing vesicles, so the conditions necessary for mechanical interaction with motor-driven membranous structures remain unclear. Although this is known to be feasible,[14,20] few details have been given, and there is almost no information available about similar results.

The trapping of rapid motor-driven vesicles and organelles requires, in principle, the use of a fast beam-steering system. To date, several alternatives have been extensively used for different purposes.[21] Among these, dynamic holographic tweezers have proved to be a powerful tool for creating, moving, and removing the trap quickly,[22–24] and have shown, in many applications, a particular ability to generate structured traps and complex light patterns for a wide range of manipulation experiments.[25] These capabilities might improve optical tweezer performance in the trapping of small structures in living cells, and might also favor the design of more sophisticated experiments.[26]

However, caution must be displayed when introducing holography into the setup, since the already difficult task of trapping within cells[19] can be further complicated by the use of a temporally and spatially modulated beam: the time-dependent orientation of the molecules in a spatial light modulator (SLM), related to changes in the applied voltage due to both refreshing and addressing of the apparatus, leads to temporal and spatial instabilities of the beam shape.[27] Therefore, the possibility of holding these small biological particles, with sizes in the range of hundreds of nanometers, against the forces applied by different proteins in the cell, should be addressed.

Here, we show the use of such holographic technology in an interactive dynamic tweezers system to trap motor-driven organelles and vesicles in living NG-108 cells.

## 2 Experimental Setup and Methods

The optical setup used in the experiments is shown in Figs. 1 and 2. An $Nd:YVO_4$ infrared laser (1064 nm) was located on an auxiliary shelf below the optical table to avoid noise from its cooling fans. The beam was brought to the desired traveling height by means of a periscope system (P). A half-wave plate (HWP) provided correct incident beam poarization on the SLM (Hamamatsu X10468-03), which generated steerable holographic traps. Two sets of telescopes (lenses L1 and L2, and L3 and L4) allowed us to adjust beam width to the size of the SLM display and to fill the entrance pupil of the objective in which we generated the modulator image.[23] We employed the objective lens (Nikon Plan Fluor 100× 1.3 NA, oil-immersion, phase contrast) of the microscope (Nikon, Eclipse TE-2000E) to focus the laser beam tightly on the sample while simultaneously observing the cells with a charge-coupled device (CCD) camera (QImaging (Surrey, British Columbia) QICAM). A dichroic mirror inserted in-between, in front of the objective lens, redirected the beam so that the same path could be used for both the laser and illumination light coming from the condenser. The light passed through the mirror and reached the CCD camera at the bottom of the microscope. Finally, the objective focused the laser on a tiny spot at the specimen plane to generate the optical trap. By means of a user-friendly software package, we were able to dynamically create, move, and remove traps to perform the experiments as required.[24] A fast algorithm, based on random mask encoding of Fourier components,[22] was used to compute the holograms that were displayed on the SLM, and allowed us to steer the beam at frequencies of 9 to 10 Hz.

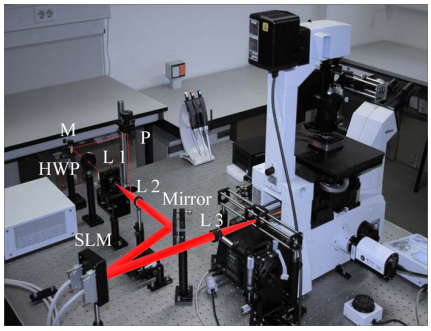


**Fig. 1** General view of the optical setup used in the experiments. (P: periscope, M: mirror, HWP: half-wave plate, L1-L4: lenses, SLM: spatial light modulator.)

Estimation of the size of trapped subcellular structures was desirable for our experiments, since this is an important characteristic of vesicles, which are larger or smaller

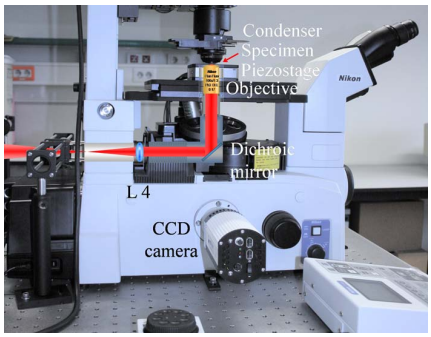


**Fig. 2** Detailed laser pathway inside the microscope.

depending on their function and content. We determined the relation between the dimension of the sample and the corresponding pixel count from the magnification (100×), and the size of the pixels (4.65 $\mu$m) of the CCD camera used to observe the sample. The apparent size of trapped particles was then computed by applying the scale factor m=4.65/100=0.0465 $\mu$m/pix. This result was confirmed by measuring the diameter of polystyrene microspheres of known size.

The differentiated type of neuroblastoma×glioma hybrid cell line (NG-108) used in our experiments has been widely employed for the study of neural function, since it presents easily visible vesicular trafficking under conventional phase contrast microscopy.

NG-108 cells (provided by Ehrlicher at the University of Leipzig) were grown in a culture medium containing 90% Dulbecco's Modified Eagle's Medium (DMEM), supplemented by 10% fetal calf serum, 1% 100 U/ml penicilling/streptomycin, and 1% 1-M HEPES, yielding 10-mM concentration. The cultures were maintained at 37 °C in a humidified atmosphere containing 95% air and 5% $CO_2$. The medium was replaced every 2 days.

For optical manipulation, cells were plated onto a laminin-coated chamber (40 $\mu$g/ml, L2020 Sigma Aldrich, Saint Louis, Missouri) to stimulate neurite outgrowth, cell differentiation, and to promote cell attachment. Optimal cell density was attained by transferring 1500 cells per chamber.

## 3 Results and Discussion

Vesicle trafficking is a set of coordinated molecular processes that ultimately leads to the transport of vesicles and organelles along the cytoskeletal filaments of the cell. Their rapid movement, up to 1 to 2 $\mu$m/s, and the unpredictable trajectories that they take within the cytoplasm [Fig. 3], make the trapping of these cargos especially difficult.

Motor proteins kinesin-1, cytoplasmic dynein, and myosin-V, often called porters, are primarily responsible for this transport. Although these motors exhibit a high processivity, they do not remain bound to the filaments for long periods of time, usually less than 1 s. A more reliable trafficking mechanism is achieved when several motors act on the same cargo simultaneously, which is a common strategy in cells. This enhances the robustness of the process, but also makes it more complex.

Transport is generally composed of consecutive displacements, between which the cargo is released to the cytosol. Depending on the number of motors propelling the vesicle, the mean distance of these displacements varies drastically, from 1 to 15 $\mu$m. The cross-links between the cargo and the filamentous proteins usually range from 1 to 5.[14] However, not only the number, but also the type of motors modifies the transport. When a structure is driven by different kinds of proteins, these compete with each other, pulling in different directions. Thus, a certain tug-of-war may emerge between them, which can result in a sharp change in the direction of movement.

Unfortunately, alterations in transport features make the trapping of these driven vesicles more difficult, as they take place very rapidly. The rate of recruitment and release of motor proteins at the surface of driven-membranous structures varies constantly. It is a highly dynamic process in which the type and amount of active motors on vesicles and organelles changes rapidly.

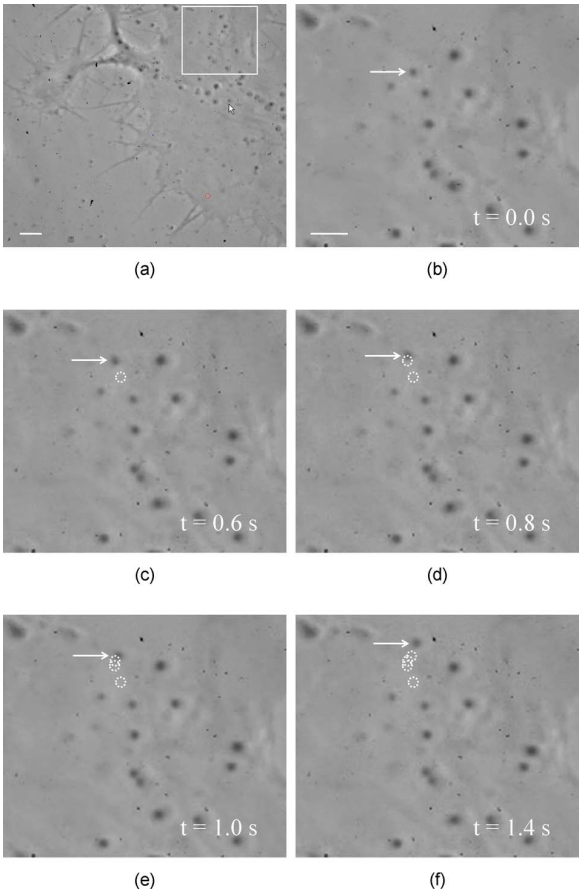


**Fig. 3** Video showing the irregular movement of a fast-driven ~400-nm vesicle within an NG-108 cell is shown in a sequence of phase contrast images. (a) General view. The following frames show a zoom into the highlighted area. Scale bar is 5 $\mu$m. (b) through (f) A horizontal arrow shows a membranous structure that is moving very rapidly, ~1.7 $\mu$m/s, for some 2.3 $\mu$m. The dotted circles indicate the position of the vesicle in the previous images. Scale bar is 2 $\mu$m (QuickTime, 6.7 MB).
[URL: http://dx.doi.org/10.1117/1.3475950.1].

Consequently, the use of dynamic tweezers capable of being moved quickly, together with an interactive user interface, may present an effective solution to the problem of trapping particles while they are moving. Under certain circumstances, one could block vesicle traffic with a standard, manually steered, optical tweezers setup. Nevertheless, experiments where it is necessary to repeat the trapping process systematically would greatly benefit from such an interactive system.

During the experiments, we discovered that it was generally easier to capture vesicles just after they had stopped moving, even though this required moving the trap quickly over a long distance, and to trap the vesicles before motor proteins resumed transportation, rather than trying to stop those passing by. In some cases, the vesicle did not continue with its path after being released, so this required

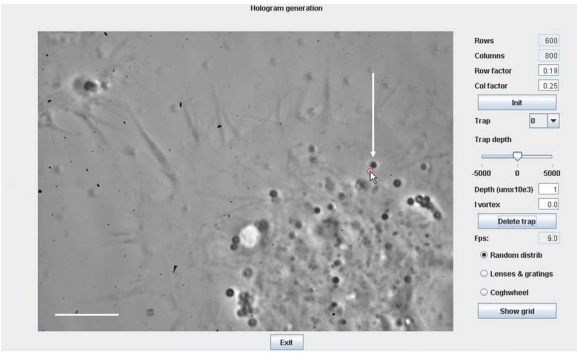


(a)

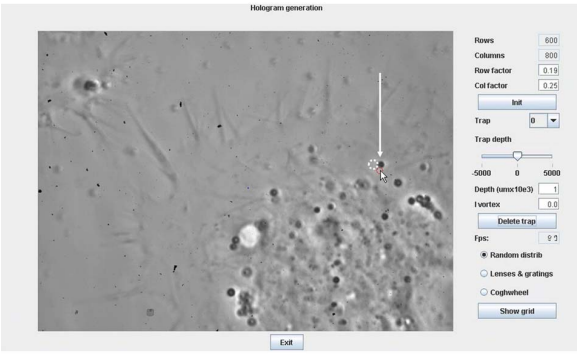


(b)

**Fig. 4** Video showing the interactive manipulation of a ~900-nm subcellular structure (endosome, lysosome, etc.) near the nucleus of an NG-108 cell. The arrow indicates the position of the vesicle that is being moved by means of the holographic trap, while the dotted circle shows the original location of the cargo. Scale bar is 10 $\mu$m (QuickTime, 15 MB).
[URL: http://dx.doi.org/10.1117/1.3475950.2].

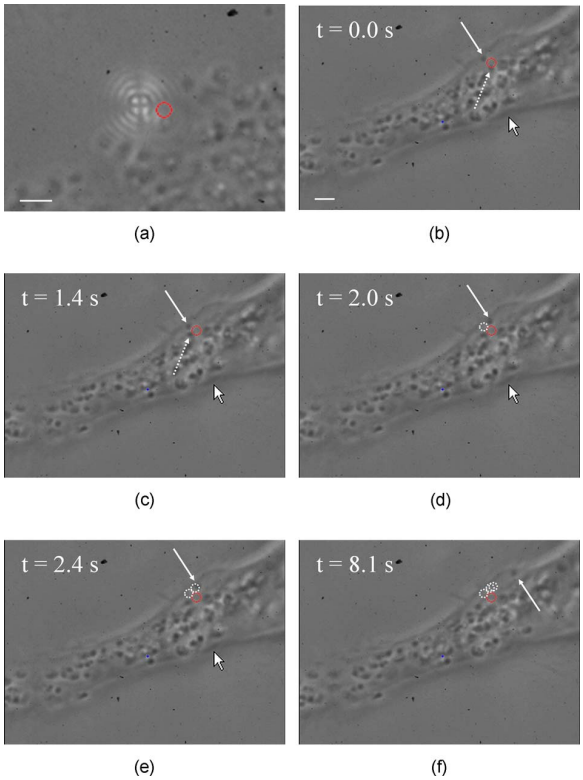


(a) (b) (c) (d) (e) (f)

**Fig. 5** Video showing experiment in which a ~400-nm vesicle was immobilized. (a) Although hidden in the following frames, the position of the holographic trap lies close to the solid circle throughout all the experiments. Scale bar is 2 $\mu$m. (b) A solid arrow shows an ~400-nm stalled vesicle, while a second freely moving cargo is indicated with a dotted arrow. (c) After 1.4 s, this latter vesicle is transported ~0.65 $\mu$m away from its initial position, whereas the trapped vesicle remains at the same point. (d) Over these seconds, the power of the laser beam is reduced until the motor is able to overcome the force from the trap. (e) Just one second later, the vesicle is moved 0.8 $\mu$m. (f) Finally, the cargo, apparently unaffected by the laser, continues to be transported and continues on its path several microns away. Considering that the growth cone is on the left side of the image, the motor driving the cargo is presumably a cytoplasmic dynein, since neurites are microtubule-rich areas. Scale bar is 2 $\mu$m (QuickTime, 7 MB). [URL: http://dx.doi.org/10.1117/1.3475950.3].

changing to another driven vesicle (which at times could be located some microns away) and trapping it rapidly before movement was resumed. This procedure was repeated until one of these trapped particles was apparently once again pulled by a motor after stopping.

To ensure that we could interact effectively with the vesicles, we first checked whether we were able to manipulate free-floating particles moving at low speeds generated by thermal agitation alone. Figure 4 shows a ~900-nm membranous structure near the cell nucleus that was trapped and interactively moved using our software. These free vesicles often seemed to be surrounded by stiff filamentous networks that confined their movement to small regions. We could move these easily within the limits of these inner compartments.

Although more difficult, manipulation of long-directed-driven cargos was also possible. By using the laser, we were able to block single-vesicle transport along neurites. Specifically, with our holographic system, we performed experiments similar to those carried out independently by Ashkin et al.[14] and Welte et al.,[20] in which they measured the stall forces of motor proteins in living giant amoeba *Reticulomyxa* and in *Drosophila* cells. They used the trapped cargo as a sensing probe to obtain quantitative data about the operation of motor proteins *in vivo*; grabbing organelles and holding them against the pulling forces allowed them to interact with the engaged motors. However, we were not interested at this stage in determining the stall forces precisely. We estimated the applied forces with the sole purpose of obtaining evidence that we were effectively interacting with enzymatic motors.

It is worth pointing out that the trapping of driven vesicles is further complicated by their small size (a few hundred nanometers). A well-corrected optical system was necessary for interacting with such tiny particles. Figure 5 shows an example of one of these experiments in which a ~400-nm vesicle was immobilized using 80 mW at the sample plane. The vesicle, which had been transported some microns through the neurite, was trapped just after stopping. Some seconds later, we observed that the vesicle was being pulled once again by a motor protein. At this point, laser power was gradually reduced until the force generated by the motor was greater than that exerted by the

light. Then, the vesicle escaped from the trap and continued on its path. The motor propelling the cargo was presumably a cytoplasmic dynein, since the movement was directed toward the microtubule minus-end.[28] Throughout the experiments, transport always seemed to resume normally, thus motors seemed to remain unaltered by the laser. Furthermore, the beam did not appear to cause any damage to the living cells after a few hours of performing experiments.

To ensure that the load was effectively applied on motor proteins, we estimated the forces involved in vesicle movement. Following Ashkin et al., the applied force in the example given in the previous paragraph was a few picoNewtons, which is compatible with the chemical forces exerted by motor proteins *in vitro*. After escaping, the fast-directed motion of the cargo took place along several microns (3.5 $\mu$m), and its velocity (0.8 $\mu$m/s) was similar to that exhibited by these molecules *in vivo*. Considered together, this suggests that the ballistic movement of the cargo was due to the action of one, or several, molecular motors.

In all of these experiments, our holographic system was able to systematically and reliably trap the small particles despite the temporal and spatial variations of the modulated traps reported in other systems.[27] Apparently, the ability to trap subcellular structures in our cells was not altered by the effects of our SLM. If necessary, the use of higher laser power[19] would have enabled us to reach even greater force values, and thus enhance the manipulation of such particles.

The results shown here could also have been obtained using a different system capable of rapidly generating traps at any point of the sample plane. There are several experimental techniques that fit this description. AODs are probably the most common devices for this purpose. Nonetheless, it was the advantages offered by holographic tweezers that led us to choose this solution.[24] The powerful features exhibited by this technology have prompted the increasing development of important optical applications.[25] Specifically, such features could enable the vesicle or organelle to be moved not just on the sample plane, as happens with AODs, but also in the axial direction. Also, non-Gaussian beams might be generated, such as size-selective traps,[29] which could be useful in certain cases to avoid trapping other undesired vesicles. Finally, holography could be used to compensate for the aberrations of the laser beam due to cell shape irregularities, to the varying cytosol index of refraction, or to the optical setup itself. This is particularly relevant here, because the maximum force applied *in vivo* is almost halved with respect to *in-vitro* experiments, since the vesicle refractive index ($n \sim 1.52$) is close to that of the surrounding medium ($n_m \sim 1.39$).[19] Aberrations, which reduce the elastic constant of the trap, could be corrected to generate greater forces.

## 4 Conclusion

We describe the holographic trapping of small structures within living cells. This is a powerful technology that may provide some advantages with respect to other beam-steering techniques in such experiments. Vesicles lying free in the cytosol of NG-108 cells are moved to ensure that we are able to interact with these small particles, and afterward, motor-driven cargos moving along neurite microtubule bundles are blocked. Throughout the entire set of experiments, the point-and-click capabilities of our system proved advantageous for dealing with these fast moving particles.

### Acknowledgments

We would like to thank M. S. Roth for her help with the experimental setup, A. Ehrlicher for providing the cell line used in the experiments, and G. Egea for fruitful discussions about the biological content. This work has been funded by the Spanish Ministry of Education and Science under grant FIS2007-65880. A. Farré and C. López-Quesada are sponsored by PhD grants FI from the Generalitat de Catalunya (Spain) and APIF from the University of Barcelona (Spain), respectively.

### References

1. M. J. Lang and S. M. Block, "Resource letter: Lbot-1: laser-based optical tweezers," *Am. J. Phys.* **71**, 201–215 (2003).
2. A. Ashkin, J. M. Dziedzic, J. E. Bjorkholm, and S. Chu, "Observation of a single-beam gradient force optical trap for dielectric particles," *Opt. Lett.* **11**, 288–290 (1986).
3. S. B. Smith, Y. Cui, and C. Bustamante, "Overstretching B-dna: the elastic response of individual double-stranded and single-stranded dna molecules," *Science* **271**, 795–799 (1996).
4. J. Shaevitz, E. Abbondanzieri, R. Landick, and S. M. Block, "Backtracking by single rna polymerase molecules observed at near-base-pair resolution," *Nature* **426**, 684–687 (2003).
5. D. E. Smith, S. J. Tans, S. B. Smith, S. Grimes, D. L. Anderson, and C. Bustamante, "The bacteriophage $\phi 29$ portal motor can package DNA against a large internal force," *Nature* **413**, 748–752 (2001).
6. J. E. Duncan and L. S. B. Goldstein, "The genetic of axonal transport and axonal transport disorders," *PLOS Gen.* **2**, 1275–1284 (2006).
7. A. Ebneth, R. Godemann, K. Stamer, S. Illenberger, B. Trinczek, E. M. Mandelkow, and E. Mandelkow, "Overexpresion of tau protein inhibits kinesin-dependent tracking of vesicles mitochondria, and endoplasmic reticulum: implications for alzheimer's disease," *J. Cell Biol.* **143**, 777–794 (1998).
8. M. Dogterom and B. Yurke, "Measurement of the force-velocity relation for growing microtubules," *Science* **278**, 856–860 (1997).
9. M. J. Footer, J. W. J. Kerssemakers, J. A. Theriot, and M. Dogterom, "Direct measurement of force generation by actin filament polymerization using an optical trap," *Proc. Natl. Acad. Sci. U.S.A.* **104**, 2181–2186 (2007).
10. R. Mallik, B. C. Carter, S. A. Lex, S. J. King, and S. P. Gross, "Cytoplasmic dynein functions as a gear in response to load," *Nature* **427**, 649–652 (2004).
11. K. Svoboda, C. F. Schmidt, B. J. Schnapp, and S. M. Block, "Direct observation of kinsein stepping by optical trap interferometry," *Nature* **365**, 721–727 (1993).
12. S. P. Gross, M. Vershinin, and G. T. Shubeita, "Cargo transport: two motors are sometimes better than one," *Curr. Biol.* **17**, 478–486 (2007).
13. B. Rappaz, F. Charrire, C. Depeursinge, P. J. Magistretti, and P. Marquet, "Simultaneous cell morphometry and refractive index measurement with dual-wavelength digital holographic microscopy and dye-enhanced dispersion of perfusion medium," *Opt. Lett.* **33**, 744–746 (2008).
14. A. Ashkin, K. Schutze, J. M. Dziedzic, U. Euteneuer, and M. Schliwa, "Force generation of organelle transport measured in vivo by an infrared laser trap," *Nature* **348**, 346–348 (1990).
15. S. B. Smith, Y. Cui, and C. Bustamante, "Optical-trap force transducer that operates by direct measurement of light momentum," *Methods Enzymol.* **361**, 134–162 (2003).
16. M. Fischer and K. Berg-Sørensen, "Calibration of trapping force and response function of optical tweezers in viscoelastic media," *J. Opt. A, Pure Appl. Opt.* **9**, S239–S250 (2007).
17. L. Sacconi, I. M. Tolic-Nørrelykke, C. Stringari, R. Antolini, and F. S. Pavone, "Optical micromanipulation inside yeast cells," *Appl. Opt.* **44**, 2001–2007 (2005).
18. I. M. Tolic-Nørrelykke, E. L. Munteanu, G. Thon, L. Oddershede, and K. Berg-Sørensen, "Anomalous diffusion in living yeast cells," *Phys. Rev. Lett.* **93**, 078102 (2004).
19. S. P. Gross, "Application of optical trap in vivo," *Methods Enzymol.* **361**, 162–174 (2003).
20. M. A. Welte, S. P. Gross, M. Postner, S. M. Block, and E. F. Wie-

schaus, "Developmental regulation of vesicle transport in drosophila embryos: forces and kinetics," *Cell* **92**, 547–557 (1998).
21. K. Visscher, S. P. Gross, and S. M. Block, "Construction of multiple-beam optical trap with nanometer-resolution position sensing," *IEEE J. Sel. Top. Quantum Electron.* **2**, 1066–1076 (1996).
22. M. Montes-Usategui, E. Pleguezuelos, J. Andilla, and E. Martín-Badosa, "Fast generation of holographic optical tweezers by random mask encoding of fourier components," *Opt. Express* **14**, 2101–2107 (2006).
23. E. Martín-Badosa, M. Montes-Usategui, A. Carnicer, J. Andilla, E. Pleguezuelos, and I. Juvells, "Design strategies for optimizing holographic optical tweezers set-ups," *J. Opt. A, Pure Appl. Opt.* **9**, 267–277 (2007).
24. E. Pleguezuelos, A. Carnicer, J. Andilla, E. Martín-Badosa, and M. Montes-Usategui, "Holotrap: interactive hologram design for multiple dynamic optical trapping," *Comput. Phys. Commun.* **176**, 701–709 (2007).
25. D. G. Grier, "A revolution in optical manipulation," *Nature* **424**, 21–27 (2003).
26. J. R. Moffitt, Y. R. Chemla, S. B. Smith, and C. Bustamante, "Recent advances in optical tweezers," *Annu. Rev. Biochem.* **77**, 205–228 (2008).
27. A. van der Horst and N. R. Forde, "Calibration of dynamic holographic optical tweezers for force measurements on biomaterials," *Opt. Express* **16**, 20987–21003 (2008).
28. N. Hirokawa, "Kinesin and dynein superfamily proteins and the mechanism of organelle transport," *Science* **279**, 519–526 (1998).
29. A. Jesacher, S. Furhapter, S. Bernet, and M. Ritsch-Marte, "Size-selective trap with optical 'cogwheel' tweezers," *Opt. Express* **12**, 4129–4135 (2004).

**Arnau Farré** obtained his BSc in physics from the Universitat de Barcelona (Spain) in 2007, and his MSc in biophysics from the same university in 2008. He is currently a PhD student in the field of optical tweezers and biological applications in the Optical Trapping Lab—Grup de Biofotònica at the Universitat de Barcelona (UB).

**Carol López-Quesada** received her BSc in physics from the Universitat de Barcelona (Spain) in 2004, and her MSc in engineering physics in 2006 at the same university. She is currently a PhD student in the Optical Trapping Laboratory—Group de Biofotònica at the Universitat de Barcelona. Her research focuses on biological applications of optical tweezers.

**Jordi Andilla** obtained his BSc in physics from the Universitat de Barcelona (Spain) in 2002, and his PhD degree in the same university in 2008. He has currently a postdoc position as a research and development engineer in the field of adaptive optics for microscopy applications at Imagine Optic (France).

**Estela Martín-Badosa** received her BSc and PhD degrees in physics from the University of Barcelona, in 1992 and 1998, respectively, and her BSEE in 2003. Since 2006, she has been an associate professor in the Department of Applied Physics and Optics at the University of Barcelona. Her research interests include optical tweezers, spatial light modulators, digital holography, and applications of optical manipulation in biological problems.

**Mario Montes-Usategui** obtained his PhD in physics at the University of Barcelona (Spain) in 1995, where he has been an associate professor in the Department of Applied Physics and Optics since 1997. His research interests are centered on the development of optical trapping technologies to tackle problems at the interface between physics and biology.

# A force detection technique for single-beam optical traps based on direct measurement of light momentum changes

Arnau Farré and Mario Montes-Usategui

Optics Express
Vol. 18, 11955-11968 (2010)

# A force detection technique for single-beam optical traps based on direct measurement of light momentum changes

**Arnau Farré* and Mario Montes-Usategui**

*Optical Trapping Lab – Grup de Biofotònica, Departament de Física Aplicada i Òptica, Universitat de Barcelona, Martí i Franquès, 1 08028, Barcelona, Spain*

**arnau.farre@ub.edu*

*www.ub.edu/biopt*

**Abstract:** Despite the tremendous success of force-measuring optical traps in recent years, the calibration methods most commonly used in the field have been plagued with difficulties and limitations. Force sensing based on direct measurement of light momentum changes stands out among these as an exception. Especially significant is this method's potential for working within living cells, with non-spherical particles or with non-Gaussian beams. However, so far, the technique has only been implemented in counter-propagating dual-beam traps, which are difficult to align and integrate with other microscopy techniques. Here, we show the feasibility of a single-beam gradient-trap system working with a force detection technique based on this same principle.



**OCIS codes:** (350.4855) Optical tweezers; (120.4640) Optical instruments; (120.1880) Detection; (180.0180) Microscopy; (170.1420) Biology.

## References and links

1. A. Ashkin, "Acceleration and trapping of particles by radiation pressure," Phys. Rev. Lett. **24**(4), 156–159 (1970), http://prola.aps.org/abstract/PRL/v24/i4/p156_1.
2. M. J. Lang, and S. M. Block, "Resource Letter: LBOT-1: Laser-based optical tweezers," Am. J. Phys. **71**(3), 201–215 (2003), http://scitation.aip.org/getabs/servlet/GetabsServlet?prog=normal&id=AJPIAS000071000003000201000001&idtype=cvips&gifs=yes.
3. A. Ashkin, *Optical Trapping and Manipulation of Neutral Particles Using Lasers*, (World Scientific, 2006).
4. A. Ashkin, J. M. Dziedzic, J. E. Bjorkholm, and S. Chu, "Observation of a single-beam gradient force optical trap for dielectric particles," Opt. Lett. **11**(5), 288–290 (1986), http://ol.osa.org/abstract.cfm?uri=ol-11-5-288.
5. A. Jesacher, S. Fürhapter, S. Bernet, and M. Ritsch-Marte, "Size selective trapping with optical "cogwheel" tweezers," Opt. Express **12**(17), 4129–4135 (2004), http://www.opticsinfobase.org/abstract.cfm?URI=oe-12-17-4129.
6. D. G. Grier, "A revolution in optical manipulation," Nature **424**(6950), 810–816 (2003), http://www.nature.com/nphoton/journal/vsample/nsample/full/nature01935.html.
7. K. Visscher, S. P. Gross, and S. M. Block, "Construction of multiple-beam optical traps with nanometer-resolution position sensing," IEEE J. Sel. Top. Quantum Electron. **2**(4), 1066–1076 (1996), http://ieeexplore.ieee.org/xpls/abs_all.jsp?arnumber=577338&tag=1.
8. K. Svoboda, C. F. Schmidt, B. J. Schnapp, and S. M. Block, "Direct observation of kinesin stepping by optical trapping interferometry," Nature **365**(6448), 721–727 (1993), http://www.nature.com/nature/journal/v365/n6448/abs/365721a0.html.
9. S. B. Smith, Y. Cui, and C. Bustamante, "Overstretching B-DNA: the elastic response of individual double-stranded and single-stranded DNA molecules," Science **271**(5250), 795–799 (1996), http://www.sciencemag.org/cgi/content/abstract/271/5250/795.
10. D. E. Smith, S. J. Tans, S. B. Smith, S. Grimes, D. L. Anderson, and C. Bustamante, "The bacteriophage straight ϕ29 portal motor can package DNA against a large internal force," Nature **413**(6857), 748–752 (2001), http://www.nature.com/nature/journal/v413/n6857/abs/413748a0.html.
11. L. P. Ghislain, and W. W. Webb, "Scanning-force microscope based on an optical trap," Opt. Lett. **18**(19), 1678–1680 (1993), http://www.opticsinfobase.org/DirectPDFAccess/74525E7B-BDB9-137E-C5E24E3A219D736D_11961.pdf?da=1&id=11961&seq=0.
12. W. Denk, and W. W. Webb, "Optical measurement of picometer displacements of transparent microscopic objects," Appl. Opt. **29**(16), 2382–2391 (1990), http://www.opticsinfobase.org/DirectPDFAccess/7459B57C-BDB9-137E-CF84DFA116D13FB7_38312.pdf?da=1&id=38312&seq=0.

#124686 - $15.00 USD Received 25 Feb 2010; revised 30 Apr 2010; accepted 30 Apr 2010; published 21 May 2010

13. A. Ashkin, “Forces of a single-beam gradient laser trap on a dielectric sphere in the ray optics regime,” Biophys. J. **61**(2), 569–582 (1992), http://www.cell.com/biophysj/retrieve/pii/S000634959281860X.
14. Y. Harada, and T. Asakura, “Radiation forces on a dielectric sphere in the Rayleigh scattering regime,” Opt. Commun. **124**(5-6), 529–541 (1996).
15. M. Capitanio, D. Maggi, F. Vanzi, and F. S. Pavone, “FIONA in the trap: the advantages of combining optical tweezers and fluorescence,” J. Opt. A, Pure Appl. Opt. **9**(8), S157–S163 (2007), http://iopscience.iop.org/1464-4258/9/8/S07/?ejredirect=.iopscience.
16. F. Gittes, and C. F. Schmidt, “Interference model for back-focal-plane displacement detection in optical tweezers,” Opt. Lett. **23**(1), 7–9 (1998), http://www.opticsinfobase.org/DirectPDFAccess/7463924C-BDB9-137E-CFB95A10D3C1858A_36510.pdf?da=1&id=36510&seq=0.
17. A. Rohrbach, and E. H. K. Stelzer, “Three-dimensional position detection of optically trapped dielectric particles,” J. Appl. Phys. **91**(8), 5474–5488 (2002), http://scitation.aip.org/getabs/servlet/GetabsServlet?prog=normal&id=JAPIAU000091000008005474000001&idtype=cvips&gifs=yes.
18. K. C. Neuman, and S. M. Block, “Optical trapping,” Rev. Sci. Instrum. **75**(9), 2787–2809 (2004), http://scitation.aip.org/getabs/servlet/GetabsServlet?prog=normal&id=RSINAK000075000009002787000001&idtype=cvips&gifs=yes.
19. J. P. Rickgauer, D. N. Fuller, and D. E. Smith, “DNA as a metrology standard for length and force measurements with optical tweezers,” Biophys. J. **91**(11), 4253–4257 (2006), http://www.cell.com/biophysj/retrieve/pii/S0006349506721397.
20. M. Capitanio, G. Romano, R. Ballerini, M. Giuntini, F. S. Pavone, D. Dunlap, and L. Finzi, “Calibration of optical tweezers with differential interference contrast signals,” Rev. Sci. Instrum. **73**(4), 1687–1696 (2002), http://scitation.aip.org/getabs/servlet/GetabsServlet?prog=normal&id=RSINAK000073000004001687000001&idtype=cvips&gifs=yes.
21. D. C. Appleyard, K. Y. Vandermeulen, H. Lee, and M. J. Lang, “Optical trapping for undergraduates,” Am. J. Phys. **75**(1), 5–14 (2007), http://scitation.aip.org/getabs/servlet/GetabsServlet?prog=normal&id=AJPIAS000075000001000005000001&idtype=cvips&gifs=yes.
22. L. P. Ghislain, N. A. Switz, and W. W. Webb, “Measurement of small forces using an optical trap,” Rev. Sci. Instrum. **65**(9), 2762–2768 (1994), http://scitation.aip.org/getabs/servlet/GetabsServlet?prog=normal&id=RSINAK000065000009002762000001&idtype=cvips&gifs=yes.
23. K. Berg-Sørensen, and H. Flyvbjerg, “Power spectrum analysis for optical tweezers,” Rev. Sci. Instrum. **75**(3), 594–612 (2004), http://scitation.aip.org/getabs/servlet/GetabsServlet?prog=normal&id=RSINAK000075000003000594000001&idtype=cvips&gifs=yes.
24. A. Rohrbach, “Switching and measuring a force of 25 femtoNewtons with an optical trap,” Opt. Express **13**(24), 9695–9701 (2005), http://www.opticsinfobase.org/oe/abstract.cfm?id=86259.
25. E.-L. Florin, A. Pralle, E. H. K. Stelzer, and J. K. H. Hörber, “Photonic force microscope calibration by thermal noise analysis,” Appl. Phys., A Mater. Sci. Process. **66**(7), S75–S78 (1998), http://www.springerlink.com/content/6x7wx7l2fqrfrhn5.
26. S. F. Tolić-No□rrelykke, E. Schäffer, J. Howard, F. S. Pavone, F. Jülicher, and H. Flyvbjerg, “Calibration of optical tweezers with positional detection in the back focal plane,” Rev. Sci. Instrum. **77**(10), 103101 (2006), http://scitation.aip.org/getabs/servlet/GetabsServlet?prog=normal&id=RSINAK000077000010103101000001&idtype=cvips&gifs=yes.
27. S. C. Kuo, and J. L. McGrath, “Steps and fluctuations of Listeria monocytogenes during actin-based motility,” Nature **407**(6807), 1026–1029 (2000), http://www.nature.com/nature/journal/v407/n6807/abs/4071026a0.html.
28. P. C. Seitz, E. H. K. Stelzer, and A. Rohrbach, “Interferometric tracking of optically trapped probes behind structured surfaces: A phase correction method,” Appl. Opt. **45**(28), 7309–7315 (2006), http://www.opticsinfobase.org/ao/abstract.cfm?uri=ao-45-28-7309.
29. A. Ashkin, K. Schütze, J. M. Dziedzic, U. Euteneuer, and M. Schliwa, “Force generation of organelle transport measured in vivo by an infrared laser trap,” Nature **348**(6299), 346–348 (1990), http://www.nature.com/nature/journal/v348/n6299/abs/348346a0.html.
30. P. A. Sims, and X. S. Xie, “Probing dynein and kinesin stepping with mechanical manipulation in a living cell,” ChemPhysChem **10**(9-10), 1511–1516 (2009), http://www3.interscience.wiley.com/journal/122440825/abstract.
31. M. Fischer, and K. Berg-Sorensen, “Calibration of trapping force and response function of optical tweezers in viscoelastic media,” J. Opt. A, Pure Appl. Opt. **9**(8), S239–S250 (2007), http://iopscience.iop.org/1464-4258/9/8/S18/pdf?ejredirect=.iopscience.
32. M. Fischer, A. C. Richardson, S. N. S. Reihani, L. B. Oddershede, and K. Berg-So□rensen, “Active-passive calibration of optical tweezers in viscoelastic media,” Rev. Sci. Instrum. **81**(1), 015103 (2010), http://rsi.aip.org/rsinak/v81/i1/p015103_s1.
33. M. Yanai, J. P. Butler, T. Suzuki, H. Sasaki, and H. Higuchi, “Regional rheological differences in locomoting neutrophils,” Am. J. Physiol. Cell Physiol. **287**(3), C603–C611 (2004), http://ajpcell.physiology.org/cgi/content/abstract/287/3/C603.
34. S. B. Smith, Y. Cui, and C. Bustamante, “Optical-trap force transducer that operates by direct measurement of light momentum,” Methods Enzymol. **361**, 134–162 (2003).
35. W. Grange, S. Husale, H.-J. Güntherodt, and M. Hegner, “Optical tweezers system measuring the change in light momentum flux,” Rev. Sci. Instrum. **73**(6), 2308–2316 (2002),

#124686 - $15.00 USD Received 25 Feb 2010; revised 30 Apr 2010; accepted 30 Apr 2010; published 21 May 2010

http://scitation.aip.org/getabs/servlet/GetabsServlet?prog=normal&id=RSINAK000073000006002308000001&idtype=cvips&gifs=yes.
36. M. Montes-Usategui and A. Farré, "Method and apparatus for measuring optical forces acting on a particle," Patent (application ES200901259).
37. P. Bartlett, and S. Henderson, "Three-dimensional force calibration of a single-beam optical gradient trap," J. Phys. Condens. Matter **14**(33), 7757–7768 (2002), http://iopscience.iop.org/0953-8984/14/33/314/?ejredirect=.iopscience.
38. W. M. Lee, P. J. Reece, R. F. Marchington, N. K. Metzger, and K. Dholakia, "Construction and calibration of an optical trap on a fluorescence optical microscope," Nat. Protocols **2**, 3226–3238 (2007), *http://www.nature.com/nprot/journal/v2/n12/abs/nprot.2007.446.html*.
39. K. Berg-Sørensen, L. Oddershede, E.-L. Florin, and H. Flyvbjerg, "Unintended filtering in a typical photodiode detection system for optical tweezers," J. Appl. Phys. **93**(6), 3167–3176 (2003), http://jap.aip.org/japiau/v93/i6/p3167_s1.
40. F. Czerwinski, A. C. Richardson, and L. B. Oddershede, "Quantifying noise in optical tweezers by allan variance," Opt. Express **17**(15), 13255–13269 (2009), http://www.opticsinfobase.org/VJBO/abstract.cfm?URI=oe-17-15-13255.
41. J. W. Goodman, *Introduction to Fourier optics*, 2nd ed., (McGraw-Hill, San Francisco, 1996).
42. K. von Bieren, "Lens design for optical fourier transform systems," Appl. Opt. **10**(12), 2739–2742 (1971), http://www.opticsinfobase.org/abstract.cfm?URI=ao-10-12-2739.
43. C. J. R. Sheppard, and M. Gu, "Imaging by a high aperture optical system," J. Mod. Opt. **40**(8), 1631–1651 (1993), http://www.informaworld.com/smpp/content~db=all~content=a713823939.
44. C. J. Bustamante, and S. B. Smith, "Light-force sensor and method for measuring axial optical-trap forces from changes in light momentum along an optic axis," US Patent #7133132 (2006).
45. F. Merenda, G. Boer, J. Rohner, G. Delacrétaz, and R.-P. Salathé, "Escape trajectories of single-beam optically trapped micro-particles in a transverse fluid flow," Opt. Express **14**(4), 1685–1699 (2006), http://www.opticsinfobase.org/oe/abstract.cfm?uri=oe-14-4-1685.

## 1. Introduction

Since its discovery in the early 1970s [1], the trapping of micron-sized particles by radiation pressure has attracted the interest of a growing number of research laboratories, especially those involved in molecular and cellular biology. The use of the technique has now become routine [2].

As first noticed by Ashkin [3], the existence of momentum transfer between photons and material particles provides light beams with the ability to exert contactless forces in the piconewton scale under certain conditions. Using this principle, optical traps operate by means of a tightly focused laser beam, which is capable of stably trapping microscopic structures near its focal region due to the balance of forces in the trap [4]. Furthermore, modern photonics technology enables dynamic and precise 3D positioning of the trapped particle, as well as remarkable flexibility in generating structured traps [5] or complex light patterns [6,7], for a wide variety of manipulation experiments.

The technique finds its main application, however, in the measurement of the piconewton forces that dominate many processes at the microscopic scale: that is, as a quantitative tool. The confirmation of kinesin stepping [8], analysis of dsDNA elasticity [9], or the study of the DNA packaging in bacteriophage $\phi$29 [10] are some dramatic examples where the optical tweezers' capability of measuring forces was of primary importance.

However, the way these forces are usually detected has not changed considerably since the method was proposed independently by Svoboda et al. [8] and Ghislain et al. [11] in 1993. The technique, initially motivated by the high spatial and temporal resolution achieved by laser differential interferometry [12], uses the position of the sample in the trap, x, to indirectly measure the optical force, F. When the trapped particle remains in the vicinity of the equilibrium position, the restoring force that maintains the object in a stable location exhibits a linear response to displacements in x, so that F can be readily obtained from an optical equivalent to Hooke's law: $F = -kx$. The performance of the system is reflected in the trap stiffness k, by means of a complex dependence on several experimental parameters, such as particle size, the objective numerical aperture, or the laser power [13,14].

Throughout the 1990s and in to the 21st century, improvement of the technique has focused on looking for alternatives means of accurate position detection, since this lies at the heart of precise force measurements. Differential interference contrast [8,12], CCD imaging [15] and back-focal-plane (BFP) interferometry [7,16,17] are some of the methods that have

#124686 - $15.00 USD Received 25 Feb 2010; revised 30 Apr 2010; accepted 30 Apr 2010; published 21 May 2010

been satisfactorily used thus far. In particular, the last of these has achieved wide acceptance due to its simple implementation, and both its large temporal bandwidth (kHz) and high spatial resolution (< 1 nm). Similarly, a precise determination of stiffness, k, has played a central role in the development of the technique. Different external forces, especially those of thermal or hydrodynamic origin, have been used to calibrate optical traps [18,19]. As an appreciable discrepancy between different methods has been repeatedly reported [20,21], the power spectrum analysis of the Brownian motion of a trapped bead has often been considered the reference calibration procedure [22,23].

Making use of the harmonic approximation, high-precision force measurements have been routinely carried out. Despite its simplicity, this technique provides a powerful method of obtaining accurate information, since the instrument is fine-tuned for a certain experiment, through the specific calibration of both the trap stiffness and the position sensor sensitivity. In this manner, the measurement of minute forces in the femtonewton range has been reported [24].

Ironically, this is, in turn, one of the major drawbacks of the system; the value of k is only valid for a given configuration and it demands recalibration when any of the parameters changes. This makes the detection of forces impossible when properties such as the temperature or the medium viscosity fluctuate in time and/or space. The limitation arises because the harmonic approximation does not provide a direct measurement of the force. Instead it is estimated according to a delicate relation with position, which is extremely sensitive to changes in the conditions.

Furthermore, the mere existence of a stiffness constant which characterizes the trap is intimately tied to meeting some pre-requisites. In particular, it requires the use of non-aberrated Gaussian beams, spherical particles, and optically- and mechanically-homogeneous viscous media. Thus, use of a stiffness constant is inevitably restricted to certain rules, and, hence, to certain experimental conditions. In parallel, a similar situation exists for position detection through BFP interferometry, where a meaningful conversion between the electric signal, S, from the detector and the displacement of the sample, x, exhibits identical restrictions.

Experiments are designed, when possible, so that these requirements are met. In general, polystyrene or silica microbeads are used as ‘handles’ to study the force or the response generated by the sample in a controlled buffer. Nonetheless, a broad spectrum of experiments, ranging from the manipulation of irregular samples to the intracellular trapping of vesicles or organelles, does not meet such requirements. In these cases, more complicated or even unpredictable time-dependent relations between F and x, and between S and x, can appear.

Some calibration methods have addressed these questions and enabled the use of non-harmonic potentials [25] and buffers with arbitrary viscosities [26]. Similarly, some progress has been made to allow BFP interferometry to work with non-spherical particles or in the presence of additional structures that interfere with the beam [27,28]. However, the problem has not been completely solved and optical tweezers still encounter many difficulties when working under certain conditions. Particularly critical are cellular experiments, which have mainly been restricted to *in vitro* conditions, or to prior calibration in a viscous buffer followed by a later correction of k during the experiment [29,30], which might introduce a large error. Recent work has shed light into this problem by enabling the calibration of traps in viscoelastic media [31,32], although the model must still be proved accurate inside cells [33].

The main problem with solutions that try to circumvent the drawbacks of the harmonic approximation is that, as a rule, they are clever but limited modifications of existing calibration methods, which largely rely on the same or similar assumptions. Consequently, they are doomed, to a greater or lesser extent, to suffer the same deficiencies.

In response to this situation, Smith et al. [34] developed a new technique following a completely different approach. The method was based on the detection of the momentum change in the trapping beam, which is directly related to the optical force created by the trap. This is a powerful way of obtaining force information, since it is based on first principles (Newton’s second and third laws) and thus the measurement is not dependent on any

#124686 - $15.00 USD Received 25 Feb 2010; revised 30 Apr 2010; accepted 30 Apr 2010; published 21 May 2010

experimental condition. It may allow the use of both non-spherical particles and trapping beams with arbitrary intensity profiles, the measurement of forces in homogeneous buffers with unknown viscosity and/or refractive index, and it does not require continued recalibration [34]. Experiments in living cells may also benefit from the features of this technique since no *in situ* calibration is needed. However, the accuracy of the force detection will still be subject to the non-homogeneities of the surrounding medium since these might change the angular distribution or intensity of the scattered light, and therefore the momentum of the beam. This is something that will need to be addressed in the future if the method is to be used in such more complex environments.

Unfortunately, this promising alternative has not yet been used with single-beam optical traps since the technique is sensitive to losses of light in the detection process. All the light scattered at the sample must be collected in order to derive the value of the force, which, as has been pointed out in several occasions [18,34,35], is very difficult or impossible with this configuration. This led to the design of an experimental setup where two counter-propagating laser beams were used to trap the sample by the effect of the scattering force. The system cannot be easily implemented in a microscope, as it requires duplicated optical trains, so both the optical alignment and the use of more advanced imaging techniques, such as fluorescence or TIRF, can be considerably cumbersome. As a result, it has not been as widely accepted as other methods.

Here, we show the conditions necessary for using such a force detection technique based on the measurement of the light momentum change in a single-beam configuration, bringing together the advantages of the two techniques [36].

## 2. Experimental setup

We use a modified inverted microscope as the basis for our setup. The detailed layout is depicted in Fig. 1. The force sensor apparatus required herein is akin to that used in BFP interferometry [7], albeit not identical because of some specific features of our method. Despite the apparent theoretical differences between the two approaches, this shared setup suggests an intimate connection between them, which we discuss below.

In BFP interferometry, the calibration of the system provides, when possible, a conversion of the diode electric signal into sample displacements. The relation between the magnitudes then enables the determination of the position of particles with high accuracy. However, the detection process is more closely related to the measurement of forces than to that of positions. Indeed, the momentum structure of the trapping beam and hence the light momentum change responsible for the optical force in the trap becomes visible at the BFP of the condenser. Thus, under the right conditions the position sensing detector (PSD) signal gives a reading of the applied force.

This same idea was used by Smith et al. [34] to measure forces through the beam momentum change in their counter-propagating dual-beam apparatus. Unfortunately, the constraints on the collection of light reported by those authors and others, prevented the development of the single-beam version of this versatile force detection method, leaving the setup used in BFP interferometry to the detection of sample displacements, x. Some years later, Gittes et al. [16] provided the first-order interference theory for the pattern formation at the BFP of the condenser for position detection. They pointed out that their model for small particles was also able to describe the lateral trapping force in this regime. In a similar vein, based on experimental data, Barlett et al. [37] suggested that BFP interferometry may be better understood as a force-sensing rather than as a position–sensing technique.

#124686 - $15.00 USD Received 25 Feb 2010; revised 30 Apr 2010; accepted 30 Apr 2010; published 21 May 2010

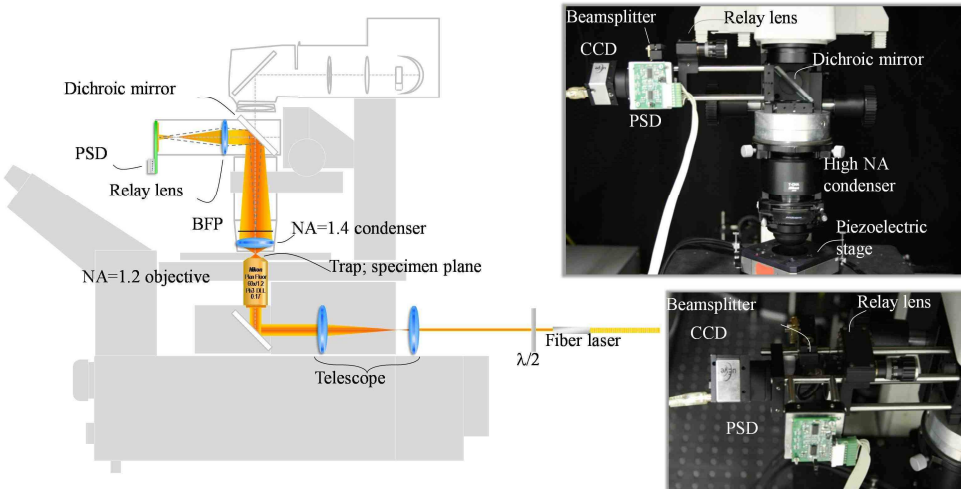


Fig. 1. Layout of the system: optical design. The optical train of an inverted microscope (Nikon, Eclipse TE-2000E) was used to both observe the samples and generate the optical traps. The force detection apparatus consists of a condenser lens, which collects the light from the trap, and a relay lens that simultaneously projects the light pattern at the back focal plane (BFP) of the condenser onto a position sensing detector (PSD) and a CCD camera. The latter was used to observe the structure and properties of the patterns projected onto the PSD.

We will show that only some additional requirements in the setup are necessary to allow direct measurement of forces with the instrument used ordinarily. The determination of position, which is actually feasible because the information at the BFP provides a measurement of the force, which in turn is linear with x, is less strict because the linear conversion from volts to nanometers is still valid despite the loss of light. In this case, the conditions of the setup are strongly relaxed, and it can easily be implemented with low-NA lenses [38]. By contrast, the apparatus that we show here necessarily includes a high-NA condenser lens (Nikon, oil immersion, NA = 1.4). In particular, the numerical aperture must be chosen higher than the refractive index of the medium used to suspend the particle, $n_m <$ NA, and the microchamber containing the sample should not be thick, ~100 µm in our case. Also, a PSD (Pacific Silicon Sensor, DL100-7PCBA3), instead of a quadrant photodiode, is necessary for correctly reading the force, while the relay lens that projects the light pattern from the BFP of the condenser onto that sensor, needs to be carefully selected to avoid vignetting the beam. The use of a PSD provides, on the other hand, the advantage of little parasitic filtering [18,39], which might be useful when a high temporal bandwidth is required. The experimental value for the rolloff frequency that has been previously reported for our PSD [18] is similar to the nominal value provided by the manufacturer ($f_{3dB}$ = 257 kHz), and larger than the typical frequency limit used in the calibration through analysis of the power spectrum of the Brownian motion of a trapped bead. In addition, PSDs seem also slightly less noisy than QPDs as recently pointed out in [40].

With these constraints, the detector can provide a signal proportional to the force exerted on the sample, and the constant relating the two becomes independent of the experimental conditions.

## 3. Theory

The force in an optical trap arises from a rather complex interaction between the laser beam and the sample. Diffraction, internal reflections, scattering and absorption are some of the optical phenomena taking place in this process. As an example, movie 1 shows an FDTD simulation of a 1.3-NA Gaussian beam interacting with a 1-µm polystyrene microsphere. A frame of this movie together with the numerical results of the light intensity scattered by the bead in the same conditions appear in Fig. 2.

#124686 - $15.00 USD Received 25 Feb 2010; revised 30 Apr 2010; accepted 30 Apr 2010; published 21 May 2010

The detection of this force relies on analysis of the changes in the angular distribution of the light. Any net variation in the propagation direction of the photons in the beam gives rise to a force, F, on the particle. Thus, correct measurement of F demands, in principle, the capture of all light interacting with the sample, in order to collect all the information about the changes in angular distribution.

However, detecting the light over the whole solid angle generally proves to be unfeasible. Fortunately, as can be observed in the example, the light travelling in the backward direction usually corresponds to a small fraction of all the emitted light. As a result, the information about the momentum change is mainly concentrated on the forward-scattered light, and, therefore, only one detection lens is needed to collect the light and retrieve the force with reasonable accuracy.

The forward-scattered electric field, **u**, at the sample plane can be decomposed into a set of plane waves weighted with the corresponding 2D-Fourier transform of **u** [17]:

$$\mathbf{u}(x_0, y_0, z) = \iint \mathbf{U}(k_x, k_y) e^{i\mathbf{k}\cdot\mathbf{r}} \mathrm{d}k_x \mathrm{d}k_y \,. \tag{1}$$

This is relevant because the photons in a plane wave all have the same elementary momentum, $\mathbf{p} = \hbar\mathbf{k}$, so Eq. (1) can also be regarded as the momentum spectrum of the field **u**. That is, weights $\mathbf{U}(k_x, k_y)$ are related to the number of photons in **u** having transverse momentum components $(\hbar k_x, \hbar k_y)$.

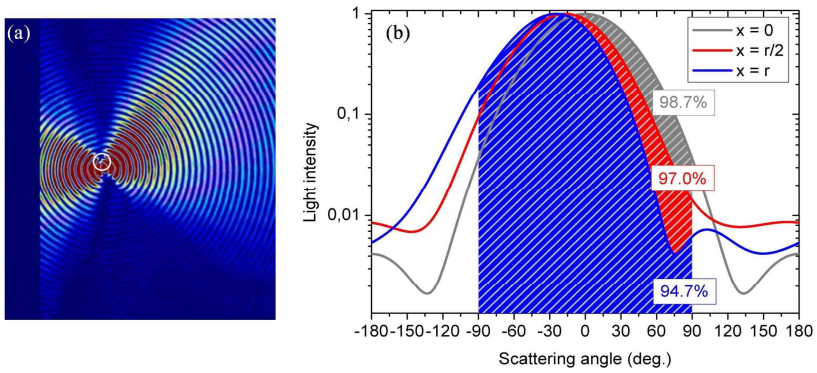


Fig. 2. (a) Image of the x-component of the electric field when a 1064-nm laser beam is focused by a 1.3-NA lens and is scattered by a 1-μm polystyrene sphere suspended in water. Light travels from left to right (Media 1). (b) Intensity distribution of light scattered by the bead. The results for three different positions of the trap are presented: centered with the bead, at half of the radius and at the edge of the bead. The forward-scattered light is contained in the region between –90° and 90°, as indicated on the plot by the shaded area. The amount of light in this region was computed for each curve.

After being collected by the condenser lens, the electric field at the BFP is projected onto the PSD by means of a relay lens (Fig. 1). In the paraxial approximation, disregarding some unimportant phase terms, this light corresponds to the Fourier transform of the field at the sample. That is, to factors, **U**, of the plane wave decomposition [41], so that at the PSD the momentum structure of the beam becomes visible, as mentioned. Any force exerted will cause a change in this structure that may thus be easily detected.

Some care must be taken if, by contrast, a high-NA lens is used to collect the light. The same result can be extended to large angles only if the lens fulfills the Abbe sine condition [42], otherwise, the pattern at the BFP will be warped, more difficult to interpret as a momentum decomposition of the beam, and will cause the PSD to give a wrong result.

If the optical system is also well corrected [42], according to the sine condition the plane wave with momentum $p_r = p_0 n \sin\theta$ before the lens focuses at a position:

$$r = f' n \sin\theta = \frac{f'}{p_0} p_r = \frac{f'}{k_0} k_r \tag{2}$$

#124686 - $15.00 USD Received 25 Feb 2010; revised 30 Apr 2010; accepted 30 Apr 2010; published 21 May 2010

in the BFP. Here f' and n are the focal length and the refractive index of the immersion medium (oil for our condenser) of the capturing lens, and $p_0$ and $k_0$ are the light momentum and the wave vector in vacuum. Therefore, coordinates here represent the transverse components of light momenta in a proper scale.

The intensity pattern I(x,y), given by **U**, is then projected onto the PSD which, according to [34], produces an electric signal given by:

$$S_x = \psi \iint \tfrac{x}{R_D} I(x,y)\mathrm{d}x\mathrm{d}y \qquad (3)$$

where $R_D$ and ψ are the size and the efficiency of the detector, respectively.

Since I(x,y)dxdy is the radiant power at point (x,y) and thus proportional to the number of photons per unit time having transverse momentum ($p_x$, $p_y$), the integral in Eq. (3) represents the orderly addition of the x-component of all the momenta (similarly for y). Change in signals $S_x$ and $S_y$ before and after the light passes through the sample are thus proportional to the light force. Signals without a trapped sample, $S_x^{\text{empty}}$, are usually zero since the trapping laser profile is often center-symmetric, which further simplifies the measurement.

Furthermore, the conversion factor, α, between V and pN does not depend on the experimental parameters:

$$F_x = \iint p_x(x,y)\tfrac{I(x,y)}{E}\mathrm{d}x\mathrm{d}y = \frac{1}{f'c}\iint xI(x,y)\mathrm{d}x\mathrm{d}y = \frac{R_D}{\psi f'c}S_x \equiv \alpha S_x . \qquad (4)$$

In this equation, E and $p_x$ are the energy and the x-component of the momentum per photon, and c is the speed of light in vacuum.

## 4. Experiments

Although the theory is straightforward, the experimental implementation is difficult, since many problems may arise with the collection of the light. We believe that a previous quantitative analysis of the light patterns formed at the BFP of the condenser is enlightening and provides insights into the main issues concerning light capture and utilization. The reason for this is that they provide an explicit and intuitive picture of the interaction between the trap and sample. All the information about the light momentum change is comprehended in a single clear image, where it is possible to visualize the formation of the measurement. In particular, the loss of light can be readily observed and quantified.

Our first step is to calibrate the BFP, that is, to measure the relation between positions on that plane and the momentum of the photons at the sample. This is important to better understand the light patterns but also to check the correct operation of the technique: a linear map between positions and momenta establishes a globally valid p-coordinate system on the BFP. This is necessary if the momentum structure, that is, the Fourier transform, of the beam must appear here undistorted. Otherwise, the PSD will not provide a correct measurement of the force, according to Eq. (4). This is equivalent to showing that the lens fulfills the Abbe sine condition [Eq. (2)].

#124686 - $15.00 USD Received 25 Feb 2010; revised 30 Apr 2010; accepted 30 Apr 2010; published 21 May 2010

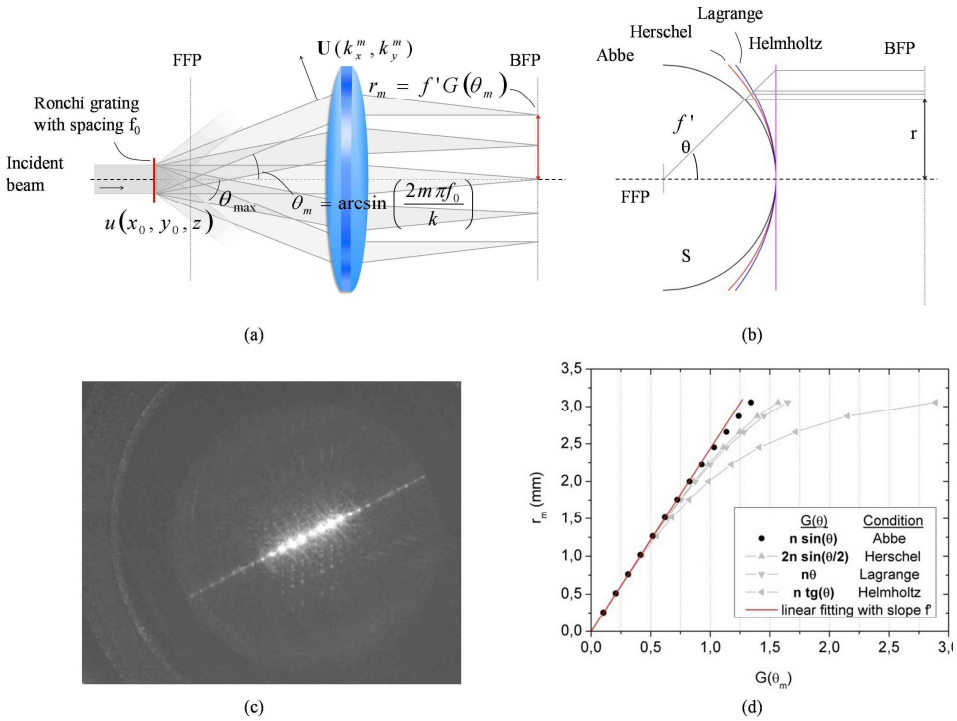


Fig. 3. (a) The field after the diffraction grating is composed of a discrete set of plane waves with amplitude (**U**)($k_x$,$k_y$) and with the angle given by Eq. (5). Each of the waves is focused on a different position at the BFP of the condenser. (b) The focusing positions, r, depend strongly on the condition that the lens follows, that is, on the shape of the principal surface S. Adapted from Sheppard et al. [43]. (c) CCD image of the light pattern at the BFP of the condenser. The bright disk surrounding the spots corresponds to the light scattered within the grating substrate, which generates a disk at the BFP with an associated numerical aperture of 1.4. (d) Plotting of the positions of the spots in the plane as a function of G(θ), according to different conditions. The linear fitting at low angles provides the calibration of the plane.

The placement of a Ronchi ruling at the sample plane provides a particularly simple and intuitive way to determine this relation. In this experiment, the objective is removed, so the source of light interacting with the grating is a collimated beam [Fig. 3(a)]. After diffraction by the ruling, the electric field, **u**, given by Eq. (1) turns into a discrete sum of plane waves (the Fraunhofer diffraction orders). In particular, only those waves fulfilling the relation:

$$\sin\theta_m = \frac{k_r^m}{k} = \frac{2m\pi f_0}{k} \tag{5}$$

propagate, that is, only those having equally spaced transverse momentum components $\hbar k_r^m = 2\hbar m\pi f_0$. In the equation, $k = 2\pi n/\lambda_0$ ($\lambda_0$ = 1064 nm) is the magnitude of the wave vector (the wavenumber) in the immersion oil, m is the diffraction order, and $f_0$ is the spatial frequency of the grating (97 lines/mm in our case).

Once collected by the lens, the waves are focused at different locations on the BFP. In general, these positions, $r_m$, will be related to the angle of propagation before the condenser, $\theta_m$, according to a certain expression r = f'G(θ), where f' is the focal length. Different shapes of the condenser principal surface, S, lead to different expressions and hence, to different focusing positions [43] [Fig. 3(b)]. Specifically, when the lens fulfills the Abbe sine condition, its principal surface is spherical, and every point on the plane is assigned to a single transverse component of the momentum through a linear relation. In this case, the light pattern provided by the diffraction grating would correspond to an array of equi-distributed spots at positions:

#124686 - $15.00 USD Received 25 Feb 2010; revised 30 Apr 2010; accepted 30 Apr 2010; published 21 May 2010

$$r_m = f'G(\theta_m) = f'n\sin\theta_m = \frac{f'}{k_0}k_r^m = m\lambda\varphi f'. \quad (6)$$

The analysis of the CCD images showed that a similar distribution of light is obtained with our setup [Fig. 3(c)]. The positions of the peaks were measured and plotted against G(θ), where the expressions for the conditions were extracted from [43], and the angles were computed according to Eq. (5). In this plot, the real G(θ) that best fits the condenser behavior should appear as a straight line with slope f'. The data obtained with the Abbe sine condition provided the best results, whereas other options, such as Herschel or Lagrange, clearly deviated from linear behavior at large angles [Fig. 3(d)]. The fitting was performed at low values of θ, where all G(θ) collapse to the Lagrange condition, and the free parameter (the focal length f' of the system formed by the condenser plus the relay lens) gave us the calibration of the plane. We can also check that the maximum angle accepted by the lens did indeed correspond to the NA of the condenser, 1.4, so that there is no vignetting elsewhere in the system.

From the results, we can safely assume that the condenser provides the Fourier transform of the field over its whole BFP and, in doing so, discloses the beam momenta.

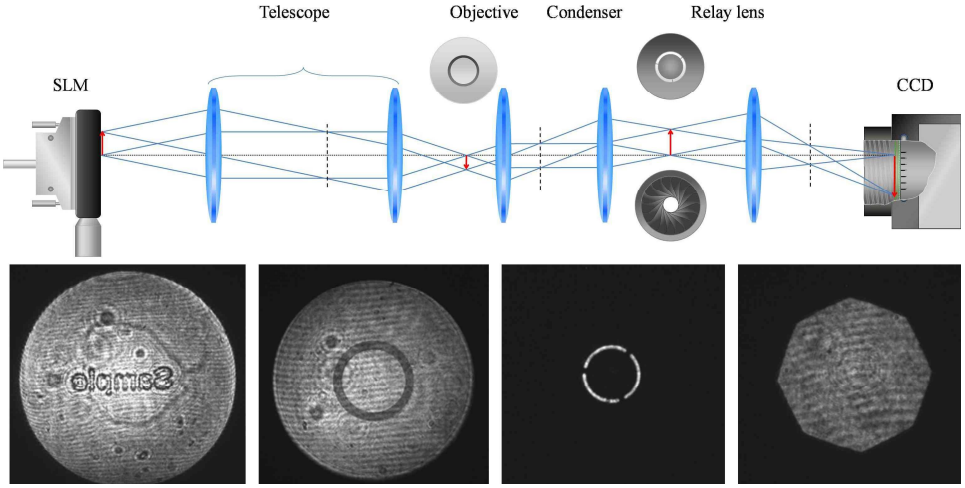


Fig. 4. Layout of the optical system between the spatial light modulator and the PSD (or CCD). The different elements at the conjugated planes of the PSD are indicated with solid arrows, and are visible with the CCD when the trapping laser passes through them. The correction hologram of the SLM, the phase plate of the objective, the annulus of the condenser and the aperture diaphragm of the microscope are shown.

Also, the known relation between the transverse components of the momentum (and thus angles of propagation prior to focusing) and the positions in the plane allows us to easily estimate the amount of light that the condenser lens is collecting, which is the most critical part of the technique.

If no beads are trapped and the NA of the objective is smaller than that of the condenser the light cone coming out from the former is completely captured by the latter and, therefore, all the light from the trap reaches the detector. A circular pattern appears with a diameter determined by the angle of propagation of its marginal ray, as shown in Figs. 4 and 5(a).

Also, in a different interpretation, that circle corresponds to the image of the entrance pupil of the objective. In general, when the system is well adjusted throughout its whole length, a set of planes is conjugate to that of the PSD (or the CCD), as illustrated in Fig. 4. The image shows the simultaneous conjugation of the spatial light modulator (our system is holographic), the circular entrance pupil of the microscope objective, its phase plate (it is a phase contrast lens), the annulus of the (phase-contrast) condenser, and, finally, the condenser aperture stop. This property is useful for setting and tuning the relay lens.

#124686 - $15.00 USD Received 25 Feb 2010; revised 30 Apr 2010; accepted 30 Apr 2010; published 21 May 2010

We studied the set of patterns created with different numerical aperture objectives, focusing the trap inside a sample chamber filled with water buffer. Using the calibration of the plane, the effective NA associated with the radius of these circular patterns was computed, and it matched the nominal values given by the manufacturer in all cases. Figure 5(a) shows the example of a 1.2 water immersion objective.

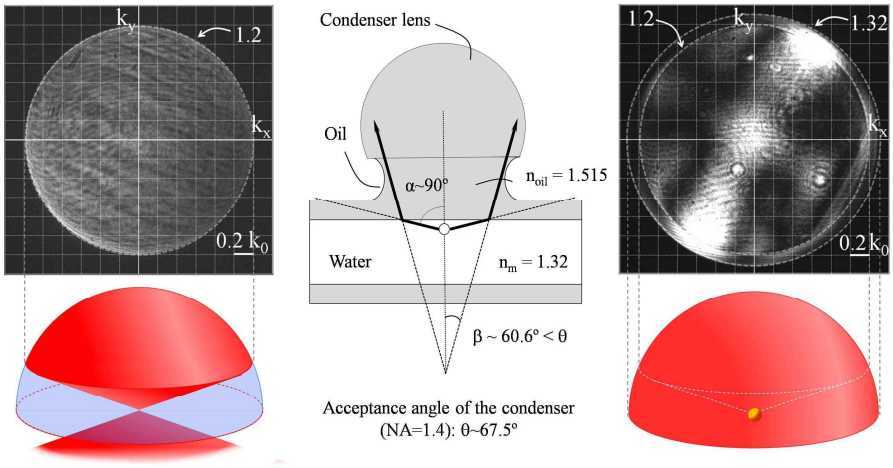


Fig. 5. (a) CCD image of the light pattern at the BFP of the condenser when a 1.2-NA objective focuses in a sample chamber filled with water. (b) If a particle interacts with the beam, the light changes its propagation direction. When this particle remains close to the microscope slide, the light within a cone of semi-angle α, very close to 90°, refracts within the capture angle of a high numerical aperture condenser (see text), which then collects all the forward-scattered light, since the acceptance angle, θ, of the lens is larger than the angle, β, of the refracted beam. (c) A 3-μm bead close to the upper surface of the chamber is trapped with the same objective.

The main difficulty regarding the collection of light arises when the trap is drawn near to a sample, because the particle deflects the beam. In principle, the scattered photons are distributed over a 4π surface, and they may not all enter the condenser. However, the lens is capable of collecting nearly all the forward-scattered light when certain precautions are taken. Specifically, the sample must be close to the upper cover-slip (exit surface) of the suspension chamber, for the light to quickly reach the buffer-glass interface, and the buffer must have a refractive index lower than the numerical aperture of the condenser. Under these constraints, shortly after being scattered by the sample, the beam refracts at the interface between the sample medium and the coverslip, so the rays propagating almost parallel to this surface (α~90°) are collected by the condenser [Fig. 5(b)] . Mathematically, the following condition must be met:

$$\theta \geq \beta \Rightarrow n_{oil} \sin\theta \geq n_{oil} \sin\beta = n_m \sin\alpha \;\sim\; n_m \Rightarrow NA_{condenser} \geq n_m \qquad (7)$$

where $n_m$ and $n_{oil}$ are the refractive indexes of the medium and the immersion oil, respectively, θ is the acceptance angle of the condenser, α is the angle of incidence on the suspension medium-glass interface (ideally 90°) and β the corresponding refraction angle (ideally the critical angle). This way, all the light coming from the sample with relevant information (again, back-scattered light is disregarded as unimportant) reaches the PSD and, therefore, the apparatus provides the force despite the presence of scattering structures.

It is worth pointing out that the change of propagation direction at the interface does not affect the lateral momentum of the beam, since the transverse components of the wave vector are preserved by Snell's law ($k_r' = k_r$). So the detector still provides a correct measurement.

The images of the light patterns confirm that we are capturing all the light when the trapped particle is in contact with the interface [Fig. 5(c)]. The calibration of the plane gave us

#124686 - $15.00 USD Received 25 Feb 2010; revised 30 Apr 2010; accepted 30 Apr 2010; published 21 May 2010

an effective numerical aperture of 1.32 for the light scattered at largest angles, which is equal to the refractive index of water in the infrared. This fulfills Eq. (7) for our condenser of NA = 1.4, and proves that the light was travelling at right angles to the surface normal inside the chamber.

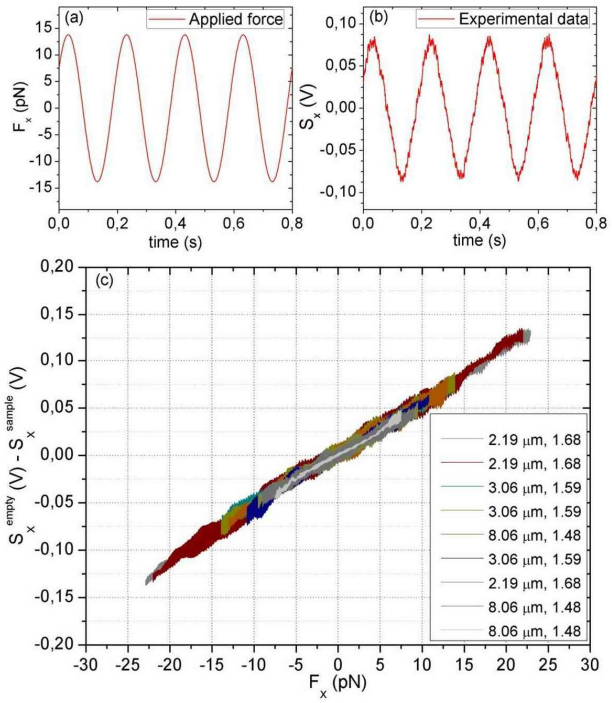


Fig. 6. (a) Temporal modulation of the hydrodynamic force applied to the trapped microspheres. (b) PSD signal obtained when dragging the bead with the fluid. (c) Comparison of the previous variables for different experimental conditions.

The amount of light collected depended weakly on the size and optical properties of the sample but it always remained a high percentage: between 95% and 99%. On the contrary, this result relied heavily upon the axial positions of both the sample in the flow chamber and the condenser. We needed to finely adjust these two distances in order to recover all the light. However, this was facilitated by the calibration of the BFP.

Experiments were performed in a range of 10-30 µm from the upper surface of the microchamber. The results indicate that the method provides a robust measurement of the force when the sample is maintained in a region of some tens of micrometers below the slide, even if the axial position is not kept constant. This small separation of the trap from the coverglass is required to collect a large percentage of the light scattered by the sample, as discussed above, and, to a lesser degree, to avoid the effects of the aberrations of the condenser lens. In particular, spherical aberrations induce a distortion of the light pattern at the BFP of the condenser when the sample is moved down into the chamber, with detrimental effects on the measurement of the force.

As a result of these restrictions in the particle axial position, it becomes necessary the use of aberration-free objectives with long working distances (water-immersion typically providing better performance than oil-immersion lenses). Alternatively, if the thickness of the construction is not a concern, one can directly build a thin flow chamber (~50 µm) so any accessible location in the sample fulfills the requirement.

Finally, we calibrated the sensor, that is, we determined the constant, α, which relates the PSD signal in V and the applied force in pN. To this effect, we used the hydrodynamic forces

#124686 - $15.00 USD Received 25 Feb 2010; revised 30 Apr 2010; accepted 30 Apr 2010; published 21 May 2010

created by the surrounding fluid on a trapped bead. A piezoelectric stage (Piezosystem Jena, TRITOR 102 SG) was moved sinusoidally and the PSD response was plotted against the force applied to the sample. We repeated the experiment with different values of the laser power, the refractive index and the radius of the particle (Fig. 6 shows a typical run). All the data fitted a single straight line with slope 5.18 mV/pN almost perfectly. The value of the calibration factor was then $\alpha_x = (0.193 \pm 0.007)$ pN/mV (two different constants along the perpendicular axes, x and y, of the detector were found), where the error is the standard deviation of α. Importantly, the method does not measure the force in the axial direction, but it may be modified to do so by incorporating a second detector, following [44].

The important result of this experiment is that α can then be used regardless of the experimental conditions, since the detection of the force does not depend on them: it is an absolute measurement. As we mentioned in the Introduction, this has enormous advantages with respect to other calibration methods for single-beam traps.

## 5. Discussion and conclusions

The results shown here indicate that our method for measuring forces through the beam momentum change in a single-beam trap provides a robust measurement of the force despite the changes in the experimental conditions. The error in the calibration factor α, coming from the standard deviation is around 4%, which, despite limited experimental data, is similar to that reported in the counter-propagating trap configuration and in the conventional calibration techniques. There still exist, however, different questions that will need to be addressed in order to improve the accuracy.

Some preliminary experiments indicate the reliability of the calibration factor, α, under both the loss of light in the measurement process and the effect of the aberrations of the condenser lens. However, a more systematic analysis of these effects would allow us to quantify the actual robustness of the method. In particular, we want to explore the variability of α with the use of different numerical apertures of the condenser and different axial positions of the sample, and evaluate their relation with the accuracy in the measurement of α. Likewise, it is necessary to check the contribution of the backscattered light to the precision of the method, although we envision a small effect due to the low percentage of light reflected back at the sample, as shown in the simulations.

The calibration of the sensor should also be extended to greater forces. The maximum values used in each experiment, so far, do not correspond to the escape force, $F_{max}$, of the trap [45]. They only represent a fraction of it, around 0.6 $F_{max}$. The maximum force of the trap is achieved when moving the bead along a certain curve in the x-z plane. The calibration experiments were performed by moving the sample chamber only in one dimension, so the particle was pulled away from the trap before reaching the maximum force value (escaping in the axial direction). An experiment that compensates for this effect would allow us to explore the linearity of the conversion between V and pN at larger forces.

The study of the system at large forces will also include a deeper analysis of the bending of the calibration curves (Fig. 6). A small curvature effect at the ends of the straight lines has been systematically observed, leading to a non-linear relation between the PSD signal and the force. We believe that the effect is related to the calibration method itself (of hydrodynamic origin, for example) rather than to light loss in the detection step, because the bending in this case is in the opposite direction to the one previously reported [34]. Also, the images of the light pattern at the BFP of the condenser are strong evidence in favor of the collection of most, if not all, forward-scattered light.

Finally, the angle dependency of the Fresnel coefficients at the water-glass interface of the microchamber should also be taken into account when studying the precision of this method. The correction of this effect should be small, but it could be compensated for by adding a filter at the BFP with an appropriate radial transmission profile.

#124686 - $15.00 USD Received 25 Feb 2010; revised 30 Apr 2010; accepted 30 Apr 2010; published 21 May 2010

**Acknowledgements**

We would like to thank J. Mas and A. Carnicer for their help with the programming of the software used to acquire the PSD data. This work has been funded by the Spanish Ministry of Education and Science, under grant FIS2007-65880, as well as by the Agency for Assessing and Marketing Research Results (AVCRI) of the University of Barcelona. A. Farré is sponsored by a doctoral research fellowship from the Generalitat de Catalunya (grant FI).

#124686 - $15.00 USD Received 25 Feb 2010; revised 30 Apr 2010; accepted 30 Apr 2010; published 21 May 2010

# Optimized back-focal-plane interferometry directly measures forces of optically trapped particles

Arnau Farré, Ferran Marsà, and Mario Montes-Usategui

Optics Express
Vol. 20, 12270-12291 (2012)

# Optimized back-focal-plane interferometry directly measures forces of optically trapped particles

**Arnau Farré, Ferran Marsà, and Mario Montes-Usategui***

*Optical Trapping Lab–Grup de Biofotònica, Departament de Física Aplicada i Òptica, Universitat de Barcelona, Martí i Franquès 1, Barcelona 08028, Spain*

*mario_montes@ub.edu

http://biopt.ub.edu

**Abstract:** Back-focal-plane interferometry is used to measure displacements of optically trapped samples with very high spatial and temporal resolution. However, the technique is closely related to a method that measures the rate of change in light momentum. It has long been known that displacements of the interference pattern at the back focal plane may be used to track the optical force directly, provided that a considerable fraction of the light is effectively monitored. Nonetheless, the practical application of this idea has been limited to counter-propagating, low-aperture beams where the accurate momentum measurements are possible. Here, we experimentally show that the connection can be extended to single-beam optical traps. In particular, we show that, in a gradient trap, the calibration product $\kappa \cdot \beta$ (where $\kappa$ is the trap stiffness and $1/\beta$ is the position sensitivity) corresponds to the factor that converts detector signals into momentum changes; this factor is uniquely determined by three construction features of the detection instrument and does not depend, therefore, on the specific conditions of the experiment. Then, we find that force measurements obtained from back-focal-plane displacements are in practice not restricted to a linear relationship with position and hence they can be extended outside that regime. Finally, and more importantly, we show that these properties are still recognizable even when the system is not fully optimized for light collection. These results should enable a more general use of back-focal-plane interferometry whenever the ultimate goal is the measurement of the forces exerted by an optical trap.



**OCIS codes:** (350.4855) Optical tweezers; (140.7010) Laser trapping; (170.4520) Optical confinement and manipulation; (120.4640) Optical instruments; (120.1880) Detection; (170.1420) Biology.

## References and links

1. A. Ashkin, J. M. Dziedzic, J. E. Bjorkholm, and S. Chu, "Observation of a single-beam gradient force optical trap for dielectric particles," Opt. Lett. **11**(5), 288–290 (1986).
2. A. Ashkin, "Forces of a single-beam gradient laser trap on a dielectric sphere in the ray optics regime," Biophys. J. **61**(2), 569–582 (1992).
3. K. Svoboda and S. M. Block, "Biological applications of optical forces," Annu. Rev. Biophys. Biomol. Struct. **23**(1), 247–285 (1994).
4. S. C. Kuo and M. P. Sheetz, "Force of single kinesin molecules measured with optical tweezers," Science **260**(5105), 232–234 (1993).
5. J. T. Finer, R. M. Simmons, and J. A. Spudich, "Single myosin molecule mechanics: piconewton forces and nanometre steps," Nature **368**(6467), 113–119 (1994).
6. K. Svoboda and S. M. Block, "Force and velocity measured for single kinesin molecules," Cell **77**(5), 773–784 (1994).
7. S. Kamimura and R. Kamiya, "High-frequency vibration in flagellar axonemes with amplitudes reflecting the size of tubulin," J. Cell Biol. **116**(6), 1443–1454 (1992).
8. K. Svoboda, C. F. Schmidt, B. J. Schnapp, and S. M. Block, "Direct observation of kinesin stepping by optical trapping interferometry," Nature **365**(6448), 721–727 (1993).

#167413 - $15.00 USD Received 26 Apr 2012; accepted 27 Apr 2012; published 15 May 2012

9. W. Denk and W. W. Webb, "Optical measurement of picometer displacements of transparent microscopic objects," Appl. Opt. **29**(16), 2382–2391 (1990).
10. L. P. Ghislain and W. W. Webb, "Scanning-force microscope based on an optical trap," Opt. Lett. **18**(19), 1678–1680 (1993).
11. L. P. Ghislain, N. A. Switz, and W. W. Webb, "Measurement of small forces using an optical trap," Rev. Sci. Instrum. **65**(9), 2762–2768 (1994).
12. S. B. Smith, Y. Cui, and C. Bustamante, "Overstretching B-DNA: the elastic response of individual double-stranded and single-stranded DNA molecules," Science **271**(5250), 795–799 (1996).
13. S. B. Smith, "Stretch transitions observed in single biopolymer molecules (DNA or protein) using laser tweezers," Doctoral Thesis, University of Twente, The Netherlands (1998).
14. W. Grange, S. Husale, H.-J. Güntherodt, and M. Hegner, "Optical tweezers system measuring the change in light momentum flux," Rev. Sci. Instrum. **73**(6), 2308–2316 (2002).
15. S. B. Smith, Y. Cui, and C. Bustamante, "Optical-trap force transducer that operates by direct measurement of light momentum," Methods Enzymol. **361**, 134–162 (2003).
16. K. Visscher, S. P. Gross, and S. M. Block, "Construction of multiple-beam optical traps with nanometer-resolution position sensing," IEEE J. Sel. Top. Quantum Electron. **2**(4), 1066–1076 (1996).
17. F. Gittes and C. F. Schmidt, "Interference model for back-focal-plane displacement detection in optical tweezers," Opt. Lett. **23**(1), 7–9 (1998).
18. P. Bartlett and S. Henderson, "Three-dimensional force calibration of a single-beam optical gradient trap," J. Phys. Condens. Matter **14**(33), 7757–7768 (2002).
19. M. Jahnel, M. Behrndt, A. Jannasch, E. Schäffer, and S. W. Grill, "Measuring the complete force field of an optical trap," Opt. Lett. **36**(7), 1260–1262 (2011).
20. A. Farré and M. Montes-Usategui, "A force detection technique for single-beam optical traps based on direct measurement of light momentum changes," Opt. Express **18**(11), 11955–11968 (2010).
21. M. J. Lang, C. L. Asbury, J. W. Shaevitz, and S. M. Block, "An automated two-dimensional optical force clamp for single molecule studies," Biophys. J. **83**(1), 491–501 (2002).
22. K. C. Neuman and S. M. Block, "Optical trapping," Rev. Sci. Instrum. **75**(9), 2787–2809 (2004).
23. A. Rohrbach, H. Kress, and E. H. K. Stelzer, "Three-dimensional tracking of small spheres in focused laser beams: influence of the detection angular aperture," Opt. Lett. **28**(6), 411–413 (2003).
24. S. Perrone, G. Volpe, and D. Petrov, "10-fold detection range increase in quadrant-photodiode position sensing for photonic force microscope," Rev. Sci. Instrum. **79**(10), 106101 (2008).
25. T. A. Nieminen, V. L. Y. Loke, A. B. Stilgoe, G. Knöner, A. M. Brańczyk, N. R. Heckenberg, and H. Rubinsztein-Dunlop, "Optical tweezers computational toolbox," J. Opt. A, Pure Appl. Opt. **9**(8), S196–S203 (2007).
26. J. R. Moffitt, Y. R. Chemla, D. Izhaky, and C. Bustamante, "Differential detection of dual traps improves the spatial resolution of optical tweezers," Proc. Natl. Acad. Sci. U.S.A. **103**(24), 9006–9011 (2006).
27. T. Godazgar, R. Shokri, and S. N. S. Reihani, "Potential mapping of optical tweezers," Opt. Lett. **36**(16), 3284–3286 (2011).
28. K. Berg-Sørensen and H. Flyvbjerg, "Power spectrum analysis for optical tweezers," Rev. Sci. Instrum. **75**(3), 594–612 (2004).
29. I.-M. Tolić-Nørrelykke, K. Berg-Sørensen, and H. Flyvbjerg, "MatLab program for precision calibration of optical tweezers," Comput. Phys. Commun. **159**(3), 225–240 (2004).
30. See Table 1 in: A. Wozniak, "Characterizing quantitative measurements of force and displacement with optical tweezers on the Nanotracker™," JPK Instruments Technical Report, *http://www.jpk.com/optical-tweezers.233.en.html*; the product of stiffness and parameter $\beta$ changes by a factor of more than two, for polystyrene beads between 100 nm and 4260 nm (similarly for silica beads, Table 2). Also, in Table 1 and Fig. 5 in: A. Buosciolo, G. Pesce, and A. Sasso, "New calibration method for position detector for simultaneous measurements of force constants and local viscosity in optical tweezers," Opt. Commun. 230, 375–368 (2004), a factor of two or more is observed between the values of $\kappa \cdot \beta$ obtained for different positions of the trap. Finally, Fig. 9 in: M. Capitanio, G. Romano, R. Ballerini, M. Giuntini, F. S. Pavone, D. Dunlap, and L. Finzi, "Calibration of optical tweezers with differential interference contrast signals," Rev. Sci. Instrum. **73**, 1687–1696 (2002), shows a product factor $\kappa \cdot \beta$ that apparently changes more than sevenfold for beads between 500 and 5000 nm in size (position detection is through DIC interferometry).
31. E. Wolf, "Electromagnetic diffraction in optical systems. I. An integral representation of the image field," Proc. R. Soc. Lond. A Math. Phys. Sci. **253**(1274), 349–357 (1959).
32. B. Richards and E. Wolf, "Electromagnetic diffraction in optical systems. II. Structure of the image field in an aplanatic system," Proc. R. Soc. Lond. A Math. Phys. Sci. **253**(1274), 358–379 (1959).
33. S. Hell, G. Reiner, C. Cremer, and E. H. K. Stelzer, "Aberrations in confocal fluorescence microscopy induced by mismatches in refractive index," J. Microsc. **169**(3), 391–405 (1993).
34. A. Rohrbach and E. H. K. Stelzer, "Optical trapping of dielectric particles in arbitrary fields," J. Opt. Soc. Am. A **18**(4), 839–853 (2001).
35. K. von Bieren, "Lens design for optical Fourier transform systems," Appl. Opt. **10**(12), 2739–2742 (1971).
36. C. J. R. Sheppard and M. Gu, "Imaging by a high aperture optical system," J. Mod. Opt. **40**(8), 1631–1651 (1993).
37. A. Rohrbach and E. H. K. Stelzer, "Three-dimensional position detection of optically trapped dielectric particles," J. Appl. Phys. **91**(8), 5474–5488 (2002).
38. K. C. Neuman, E. H. Chadd, G. F. Liou, K. Bergman, and S. M. Block, "Characterization of photodamage to *Escherichia coli* in optical traps," Biophys. J. **77**(5), 2856–2863 (1999).
39. N. B. Viana, M. S. Rocha, O. N. Mesquita, A. Mazolli, and P. A. Maia Neto, "Characterization of objective transmittance for optical tweezers," Appl. Opt. **45**(18), 4263–4269 (2006).

#167413 - $15.00 USD Received 26 Apr 2012; accepted 27 Apr 2012; published 15 May 2012

40. J. Mas, A. Farré, C. López-Quesada, X. Fernández, E. Martín-Badosa, and M. Montes-Usategui, "Measuring stall forces *in vivo* with optical tweezers through light momentum changes," Proc. SPIE **8097**, 809726, 809726-10 (2011).
41. I. Verdeny, A.-S. Fontaine, A. Farré, M. Montes-Usategui, and E. Martín-Badosa, "Heating effects on NG108 cells induced by laser trapping," Proc. SPIE **8097**, 809724, 809724-12 (2011).
42. S. P. Gross, "Application of optical traps in vivo," Methods Enzymol. **361**, 162–174 (2003).
43. M. P. Landry, P. M. McCall, Z. Qi, and Y. R. Chemla, "Characterization of photoactivated singlet oxygen damage in single-molecule optical trap experiments," Biophys. J. **97**(8), 2128–2136 (2009).
44. J. Dong, C. E. Castro, M. C. Boyce, M. J. Lang, and S. Lindquist, "Optical trapping with high forces reveals unexpected behaviors of prion fibrils," Nat. Struct. Mol. Biol. **17**(12), 1422–1430 (2010).
45. E. Schäffer, S. F. Nørrelykke, and J. Howard, "Surface forces and drag coefficients of microspheres near a plane surface measured with optical tweezers," Langmuir **23**(7), 3654–3665 (2007).
46. A. H. Firester, M. E. Heller, and P. Sheng, "Knife-edge scanning measurements of subwavelength focused light beams," Appl. Opt. **16**(7), 1971–1974 (1977).
47. W. H. Wright, G. J. Sonek, and M. W. Berns, "Radiation trapping forces on microspheres with optical tweezers," Appl. Phys. Lett. **63**(6), 715–717 (1993).
48. M. Mahamdeh, C. P. Campos, and E. Schäffer, "Under-filling trapping objectives optimizes the use of the available laser power in optical tweezers," Opt. Express **19**(12), 11759–11768 (2011).
49. A. Pralle, M. Prummer, E.-L. Florin, E. H. K. Stelzer, and J. K. H. Hörber, "Three-dimensional high-resolution particle tracking for optical tweezers by forward scattered light," Microsc. Res. Tech. **44**(5), 378–386 (1999).
50. K. Berg-Sørensen, L. Oddershede, E.-L. Florin, and H. Flyvbjerg, "Unintended filtering in a typical photodiode detection system for optical tweezers," J. Appl. Phys. **93**(6), 3167–3176 (2003).
51. T. Otaki, "Condenser lens system for use in a microscope," US Patent no. 5657166 (1997).
52. T. Čižmár, M. Mazilu, and K. Dholakia, "*In situ* wavefront correction and its application to micromanipulation," Nat. Photonics **4**(6), 388–394 (2010).
53. W. M. Lee, P. J. Reece, R. F. Marchington, N. K. Metzger, and K. Dholakia, "Construction and calibration of an optical trap on a fluorescence optical microscope," Nat. Protoc. **2**(12), 3226–3238 (2007).

## 1. Introduction

Detailed knowledge of the force exerted by a single-beam optical trap on a microsphere [1] and its variation with position [2] provide the theoretical basis for the utilization of optical tweezers as "picotensiometers" [3]. The optical trap acts as an elastic spring, since the force is proportional to the displacement of the sample from its equilibrium position (within a small range; only some 100-200 nm in many practical cases [4–6]). Measuring the position of the sample can thus eventually be used to calculate the force; to be useful, however, it is necessary for this to be carried out with nanometer and millisecond accuracy as well as being integrated into an experimental device that minimizes the different sources of instability (laser, microscope, etc.) [4].

Almost simultaneously, three procedures compatible with these requirements were devised in the early 1990s. Finer *et al.* [5], relying on previous work by Kamimura and Kamiya [7], utilized a method consisting of imaging the sample on a quadrant photodetector (QPD), which replaced the video camera, and using the trapping laser for illumination. Although the instrumental error was notably reduced (from ~10 nm [4] to ~1 nm [7]) and the acquisition rate increased to 4 kHz [5], the method requires repeated and delicate alignment.

This problem does not occur in non-imaging methods. Svoboda *et al.* [8] advanced by adapting the uniaxial differential laser microinterferometer devised by Denk and Webb [9] to be used simultaneously as an optical trap. Their approach was based on the determination of the polarization changes of two overlapping light beams when intercepted by the trapped microsphere. This method, together with the reduction in Brownian noise caused by laser trapping, enabled, for example, the measurement of the processive motion of kinesin at the molecular scale (8 nm) [8] and later of other mechanical properties (maximum force, force–velocity curve, etc.) [6].

Nonetheless, it was the procedure devised by Ghislain and Webb that was to have the greatest impact on the subsequent evolution of the measurement methods. Possibly inspired by the operation of scanning probe microscopes [10], this method measured the deflection of the trapping beam when it traversed the sample [11]. An intensity detector in a non-imaging plane generated a signal that was a function of the overlap between its active area and the deflected light cone, thus enabling precise three-dimensional tracking of the sample without requiring the polarizing optics of the Svoboda *et al.* approach.

#167413 - $15.00 USD Received 26 Apr 2012; accepted 27 Apr 2012; published 15 May 2012

However, using the deflection of the trapping beam to measure the motion of the sample connected the measurements of positions and of momenta. The deflection of the light cone used by Ghislain and Webb naturally contains information on the change in the momentum of the photons, as S. Smith *et al.* [12] noticed shortly thereafter. If this light is captured with a lens that fulfills the Abbe sine condition, the spatial position of the light distribution after the collecting lens is not merely proportional to the displacement of the sample, but it directly and immediately indicates the force exerted by the trap [13–15].

Measuring forces directly by means of the analysis of the angular distribution of scattered light has many advantageous features [15]. Unfortunately, the light that goes through the sample has to be captured in full, at least nominally, which is notoriously difficult with an optical trap based on a large-aperture beam [13–15]. Smith *et al.* solved this problem by using two weakly focused counter-propagating beams, but, because of the simplicity and flexibility of single-beam optical traps compared to this much more complex geometry, this direct force method has not generally been adopted. Instead, the indirect route via the harmonic approximation has been the method of choice; specifically, determining positions through back-focal-plane interferometry (BFPI), a method finally proposed by Visscher *et al.* [16] in 1996 and theoretically explained by Gittes and Schmidt two years later [17]. The result is a setup equivalent to that of Smith *et al*., but for single-beam traps where the light scattered by the sample is only collected in part. In this case, asymmetries in the far-field distribution of the radiated intensity can only be related to the transverse displacements of the sample, and not directly to trapping forces.

Despite the ideas of Ghislain and Webb being a common ingredient in the genesis of the method of Smith *et al.* and BFPI, the degree to which the latter incorporates the clear advantages of the method based upon momentum conservation has not been sufficiently studied. The relationship between the two methods has been theoretically highlighted by Gittes and Schmidt in their first-order interference model [17], and exploited specifically for counter-propagating traps by Smith himself [15]. However, the difficulty in correctly measuring the light momentum with large-aperture beams has impeded similar results for gradient traps. This eventually led the two methods to develop in different directions. To the best of our knowledge, only in two unrelated experiments have particular aspects of BFPI been identified as seeming to imply direct measurements of the force in optical tweezers [18,19]. Bartlett and Henderson [18], studying the functional dependence of the elastic constant on different experimental variables, found a linear relationship between stiffness and detector sensitivity (equivalent to our Eq. (6) and Fig. 3, below). More recently, by means of an experimental setup consisting of two traps of different stiffness simultaneously trapping the same sample, Jahnel *et al.* [19] observed that the range over which their sensor output was proportional to the force is larger than the linear (with position) range of the trap itself.

Following the work of Smith *et al.*, we recently reported the conditions under which the momentum changes of a large-aperture beam can be measured accurately [20], which opens the door to experimentally tackling this question. Here we explore the connection between BFPI and the measurement of the light momentum for single-beam gradient traps. We start by indicating the possibility that there is an extraordinary range of validity for the force measurements and show the existence of a relationship between the calibration constants $\beta$ and $\kappa$. We then proceed to prove that the product of the two factors does not depend on the trapping conditions and, more specifically, that this product corresponds to the calibration factor that converts the detector signals into momentum changes, according to Ref [15]. More importantly, we demonstrate that these observations are not necessarily restricted to fully optimized instruments but are valid more generally, depending only on the proportion of light collected.

We point out that this has clear practical consequences so that the link between BFPI and the method of Smith *et al.* must always be kept in mind when measuring the force that optical tweezers exert on a trapped particle.

#167413 - $15.00 USD Received 26 Apr 2012; accepted 27 Apr 2012; published 15 May 2012

## 2. Setup

The instrument used here has been briefly described in Ref [20]. and is presented in more detail in the Appendix. It has the same structure as a conventional BFPI system [16]. A high-numerical-aperture lens collects the light deflected by the sample and a photodetector placed in a plane conjugate to its back focal plane (BFP) provides a measurement of the optical force in volts. Some specific requirements ensure the proper measurement of the light momentum. In particular, we use a position sensitive detector (PSD), an aplanatic, long-focal-length condenser lens with a numerical aperture (NA) of 1.4 and the sample is kept close (< 30 $\mu$m) to the upper surface of the microchamber. Experiments were first carried out with this optimized setup as the effects we want to show are more clearly displayed under these favorable conditions. Then we discuss more widely valid results obtained under more typical BFPI conditions.

## 3. Results and discussion

In BFPI, sample displacement is measured by means of *in situ* calibration that converts the electric photodetector signal (volts) into a length (micrometers). Figures 1(a) and 1(b) show, respectively, a typical V-to-$\mu$m curve for an 8.06-$\mu$m polymethacrylate microsphere and the intensity at the detector plane (see *Methods*). Beads were left to settle on the coverslip and then the signals were recorded as one of the adhered particles was moved across the laser beam (NA = 1.2) with a piezoelectric stage. Although the particle motion generates a single-valued signal [21], $S_x(x_0)$, even for large displacements (as much as $x_0$ ~4 $\mu$m in this case), only a small range of positions around the trap centre ($x_0$ = 0) is generally used. In that region of the curve, position is proportional to the detector signal ($x_0 = \beta_x \cdot S_x$) so changes in voltage are easily translated into sample displacements once $\beta$ is known.

From the different possibilities [22], we chose power spectrum analysis of the thermal motion of the trapped sample to obtain the constant of proportionality, $\beta$. In this analysis, comparison between one of the free parameters in the theoretical expression and the value of the diffusion constant of the sample, $D = k_B T/\gamma$, gives the value of $\beta$; so position can be calibrated if the medium viscosity, the particle size and the sample temperature are all known. We used the value from the calibration ($\beta_x$ = 39 $\mu$m/V) to convert the detector signal in Fig. 1(a) into displacements in real units ($\mu$m), and thus explore the position detection capabilities of our instrument. We observed that the position was correctly measured only for displacements smaller than 2 $\mu$m (Fig. 1(c)). Beyond that range, changes in the angular distribution of the light scattered by the sample do not correlate linearly with sample positions, so that correct measurements are not possible with this method.

The region in which linearity is valid, although dependent on the physical properties of the object [17] as well as on the NA of the collecting lens [23], is smaller than the harmonic region of the trap (as we discuss below), which in turn typically covers a small range of forces [2]. The range can be increased by normalizing the detector signal, which in addition provides a measurement of $\beta$ that is insensitive to laser power. Further improvements along these lines were proposed by Svoboda and Block [6] and Lang *et al.* [21], who applied a polynomial fit to the curve $S_x(x_0)$, and by Perrone *et al.* [24], who took advantage of the cross-talk between the *x* and the *sum* channel to achieve a ten-fold increase in the working range. However, even when the position is measured in this more general fashion, it still remains very sensitive to the particular experimental conditions.

#167413 - $15.00 USD Received 26 Apr 2012; accepted 27 Apr 2012; published 15 May 2012

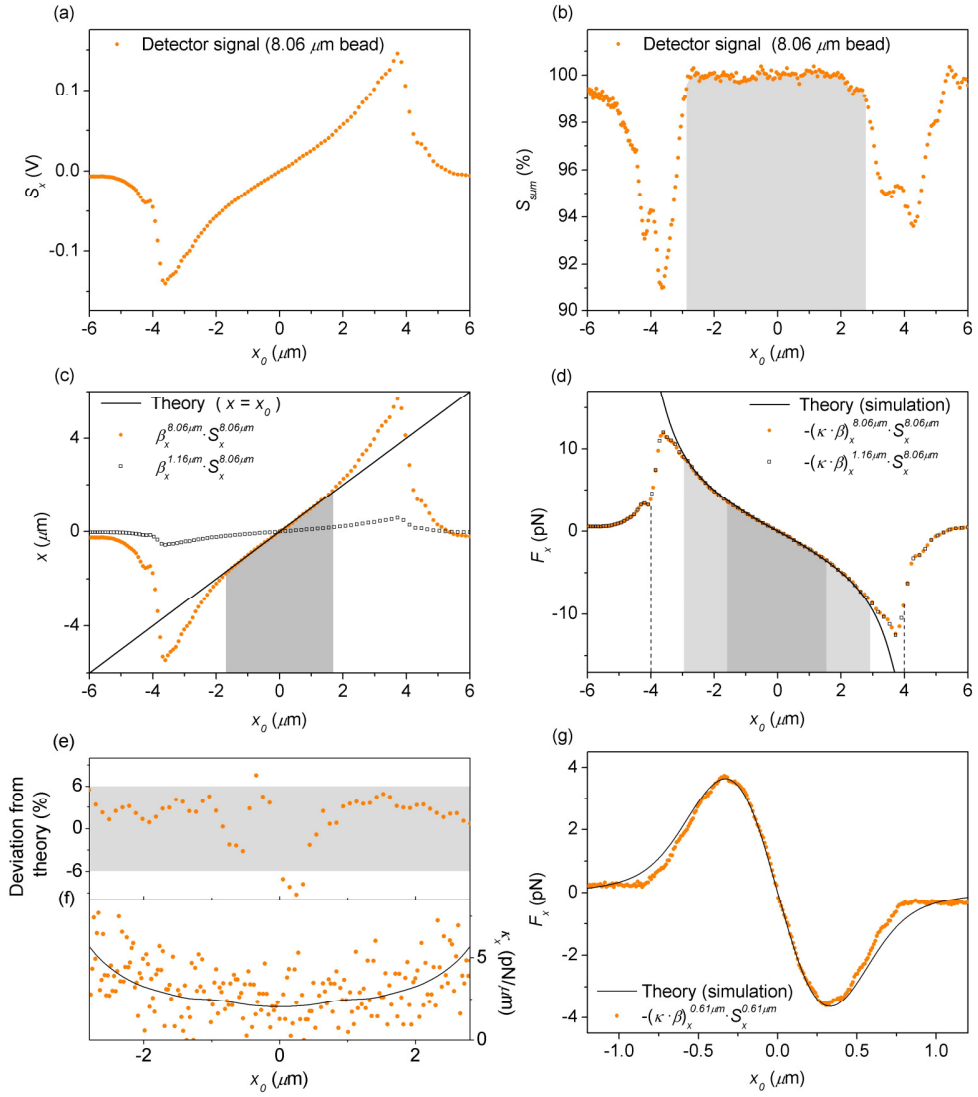


Fig. 1. Position and force detection capabilities of the BFPI instrument. (a) Position signal and (b) fraction of total intensity. (c) Comparison between the position reading from the detector and the actual piezo displacement. Two different V-to-$\mu$m conversions are shown: one obtained with the correct $\beta$ (orange dots) and the other by multiplying by the $\beta$ corresponding to a different bead size, (a 1.16-$\mu$m particle; hollow squares). The dark shaded area indicates the region where positions are correctly measured with the first calibration factor. (d) The orange dots in (c) are multiplied by the trap stiffness to indicate the force. The light shaded area shows the region where this matches the theoretical force–displacement curve. The hollow squares are obtained by multiplying the corresponding curve in (c) (that with a mismatched $\beta$) by the 1.16-$\mu$m-bead stiffness. The product of the two mismatched factors gives a puzzlingly accurate force curve. Finally, the dashed vertical lines indicate the bead limits. (e) Error between theory and experiment in (d). The recorded data match the force curve for values up to 2.8 $\mu$m within a 6% error, comparable to the uncertainty of the absolute calibration of the instrument (Table 1). (f) Variation of trap stiffness as a function of bead position. (g) Theoretical and experimental force curves for a 0.61-$\mu$m bead corresponding to a measured laser power of 17.5 ± 0.9 mW.

Motion of the probe is indirectly determined from changes in the angular distribution of the light scattered by the sample [17], which in turn are due to the difference between the refractive indices of the object and of the surrounding medium, so any variation in either the sample or

#167413 - $15.00 USD Received 26 Apr 2012; accepted 27 Apr 2012; published 15 May 2012

the laser properties may require new calibration. The parameter $\beta$ critically depends on the size of the sample so that, for instance, the value for the 8.06-$\mu$m microsphere in Fig. 1 ($\beta_x$ = 39 $\mu$m/V) is ten times that for a 1.16-$\mu$m microsphere ($\beta_x$ = 4 $\mu$m/V).

It is therefore evident that when we multiply the 8.06-$\mu$m curve in Fig. 1(a) by the calibration factor for the 1.16-$\mu$m particle, the instrument cannot provide an accurate measurement (Fig. 1(c)). Typically the system needs to be recalibrated before every experiment, which is a serious drawback for several potential uses of BFPI.

If we go a step further and calibrate the trap stiffness, $\kappa$, we can use the position measurement to calculate the optical force. In our experiment, the value of $\kappa$ was also determined from a fit of the power spectrum data. The force for the different positions of the sample (Fig. 1(d)) was obtained by multiplying the curve in Fig. 1(c) by the constant $\kappa$. The range over which our data matched the theoretical curve, to within the 6% error associated with the absolute calibration of the instrument (see Table 1), was found to extend to 0.7 times the particle radius (Fig. 1(e)), notably beyond the region where positions are accurately measured in (c), and also further than the linear regime of the trap, where $\kappa$ is defined. The theoretical curve was obtained with a T-matrix simulation [25] using an estimated laser power at the sample plane of 11.4 ± 0.6 mW, which was derived previously from measurements of the transmittance of the objective (see below).

An extended force detection region has similarly been observed by Jahnel *et al.* for a 2.01-$\mu$m bead [19]. Using an experimental design similar to that in Ref [26], they compared the force exerted by a stiff trap calibrated using thermal analysis with the force exerted by a second, less powerful trap on a single trapped microsphere. Although unaware of the reasons, they point out that the force could be measured with this second beam beyond the linear regime. Smith *et al.* [15] found an analogous result with a counter-propagating beam system.

For the force to be measured correctly in the extended region, the stiffening of the trap for large displacements of the sample, also observed in Ref [27], has to be compensated by changes in $\beta$ along the curve in such a way that its product with the trap stiffness remains constant. The derivative of the trace in Fig. 1(d) varies by a factor 3 when the trap is moved from the centre of the bead to the edge (Fig. 1(f)), so the calibration of the detection instrument must change by the same amount. These results indicate that the product $\kappa \cdot \beta$ is more universal than each parameter separately. The two calibration factors, $\kappa$ and $\beta$, are local magnitudes, defined in the vicinity of a certain position (typically the trap centre), but their product can be used at all sample positions. In our case, a single constant value describes almost the entire force curve. As we discuss below, the range over which the detector readings provide an accurate measurement of the force is connected solely to the amount of light collected, so theory and experiment start diverging at large forces because the recorded intensity decreases (due to the larger angles through which light gets deflected), as indicated in Fig. 1(b). This is not observed, by contrast, when we repeat the experiment for a 0.61-$\mu$m bead (Fig. 1(g)). For Rayleigh scatterers, the measuring error (small in our case) is independent of the sample position (see discussion on the fraction of light collected below).

More importantly, when we use the trap stiffness corresponding to the 1.16-$\mu$m particle to obtain the second force curve for the larger bead in Fig. 1(d), the result is essentially correct (solid line vs. hollow squares). That is, although the position calibration parameter, $\beta$, was not interchangeable between the different samples, the calibration of the detector signal into force measurements seems to be independent of the sample properties, i.e. $\kappa_{1\mu m} \cdot \beta_{1\mu m} = \kappa_{8\mu m} \cdot \beta_{8\mu m}$. This therefore suggests that $\beta$ is such that its product with the trap stiffness becomes constant not only along the curve but also regardless of the sample.

In order to show the extent to which the product of the two calibration factors remains fixed, we systematically compared trap stiffness, $\kappa$, and position sensitivity, $1/\beta$, for different samples and trapping conditions. We obtained the values from the power spectra of the Brownian motion of trapped particles (Fig. 2(a), see also *Methods*). The Lorentzian fitting to the experimental data was corrected to include different effects [28]: aliasing, the detector transparency in the infrared and the frequency dependence of the drag coefficient (Figs. 2(b)

#167413 - $15.00 USD Received 26 Apr 2012; accepted 27 Apr 2012; published 15 May 2012

and 2(c)). The fitting software [29] was also modified to include the A/D converter quantization noise and to eliminate high-frequency noise from the laser when necessary (Fig. 2(d)).

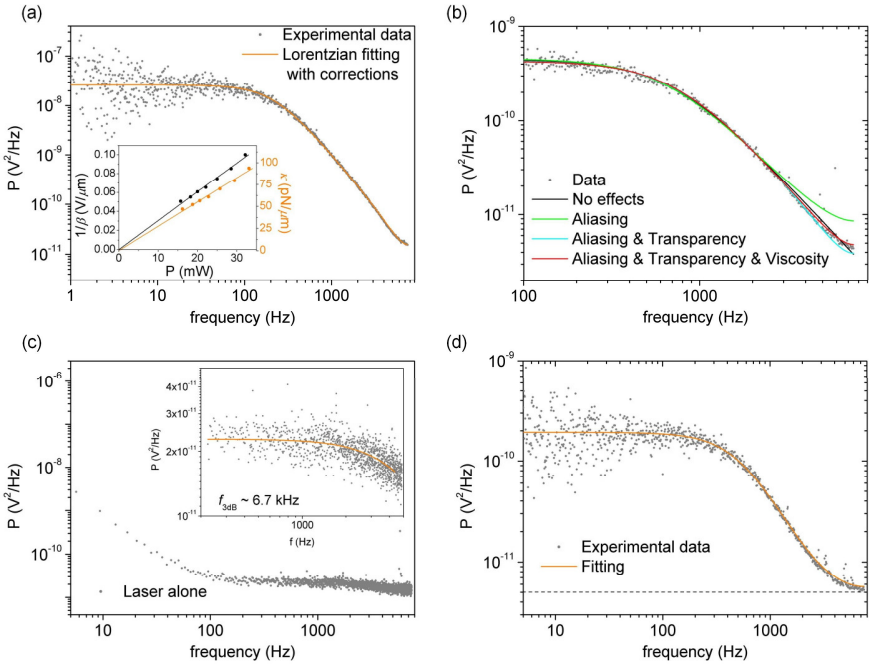


Fig. 2. Power spectrum calibration. (a) Typical two-sided power spectrum of the Brownian motion of a trapped bead (grey dots) and fitting to a corrected Lorentzian curve (orange line). More details about the data recording and analysis are given in the *Methods* section. The linear dependence of both stiffness, $\kappa$, and sensitivity, $1/\beta$, on the laser power (inset) is evidence of correct measurement of the two parameters. (b) Different effects were taken into account to obtain correct measurements of the two constants $\kappa$ and $\beta$. (c) From the fitting of the power spectrum data to a corrected Lorentzian curve, we obtained a mean value for the 3dB-frequency used to characterize the frequency response of the photodetector as a first-order filter, at $\lambda$ = 1064 nm ($f_{3dB}$ = 6830 ± 170 Hz; mean + SD; n = 60). We checked this result by fitting a simple Lorentzian function to the power spectrum of the laser alone, obtaining a value of 6.7 kHz. (d) In some cases, the digitization error from the analogue-to-digital converter of our detection system showed up in the spectra. We took this into account in the fitting. The dashed line indicates the noise level in this experiment.

The experiment shows that the sensitivity, $1/\beta$, is proportional to $\kappa$ regardless of the properties of the sample or the trapping laser (Fig. 3). We trapped beads of five different sizes (0.61 $\mu$m, 1.16 $\mu$m, 2.19 $\mu$m, 3.06 $\mu$m and 8.06 $\mu$m), made of three different materials (n = 1.48, n = 1.57 and n = 1.68), with both water-immersion and oil-immersion objectives (NA = 1.2 and NA = 1.3, respectively) under different laser powers, from 50 mW to 150 mW. The 30 points lie perfectly along a straight line with only 4% dispersion, despite each factor varying by up to 1500%. Clearly, there is a parameter associated with the instrument which is a constant and results from multiplying $\kappa$ and $\beta$.

The existence of such a hidden parameter in single-beam traps has often been overlooked since a constant relationship between $\kappa$ and $\beta$ does not typically appear in BFPI measurements. More often, variation by a factor of two or more can be observed for different experimental conditions [30] (to reproduce our results the conditions explained in the Appendix have to be met). To the best of our knowledge, only Barlett and Henderson [18] have reported an experimental correlation between $\kappa$ and $\beta$ similar to ours. However, their data show a larger dispersion for a smaller range of stiffness (probably because they use a QPD, see the Appendix for a discussion) and were obtained mainly by modifying the refractive index of the sample.

#167413 - $15.00 USD Received 26 Apr 2012; accepted 27 Apr 2012; published 15 May 2012

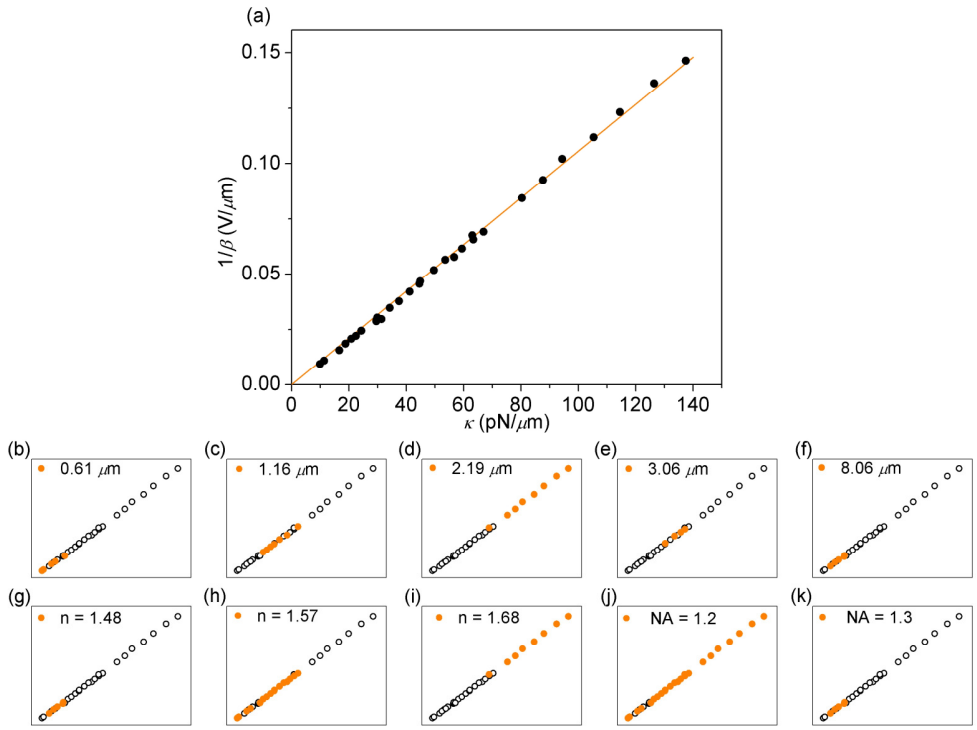


Fig. 3. Relationship between $\kappa$ and $\beta$. (a) Sensitivity is plotted against stiffness for every pair of parameters; the experiment was repeated for 30 different sets of experimental conditions. The linear fit shows the proportionality of the two constants. The variety of experimental conditions is highlighted in (b-k).

This is the first time that this clear-cut, characteristic relationship between the two calibration parameters, regardless of the trapping conditions, and its connection with an extraordinary force-measuring range has been reported. The results suggest that BFPI is better interpreted as a method for measuring forces than for measuring positions. This can be explained on the basis of a relationship between BFPI and the determination of light momentum. The following theoretical development follows a prior exposition in Ref [15].

In the presence of a particle, the beam in an optical trap undergoes a change in its momentum structure (Fig. 4). This is naturally reflected in the angular spectrum of the time-independent part of the field, which is a solution of the Helmholtz equation [31,32]:

$$\begin{aligned}\mathbf{e}^i(\mathbf{r}) &= \frac{-i}{\lambda}\iint_{\sin\theta\le NA_{obj}} \mathbf{A}^i(\theta,\varphi)e^{ik\hat{\mathbf{s}}\cdot\mathbf{r}}\mathrm{d}\Omega \\ &= \frac{-i}{\lambda}\iint_{\sin\theta\le NA_{obj}} f'a(\theta)\cdot A_0^i\left(f'\sin\theta\cos\varphi, f'\sin\theta\sin\varphi\right)\cdot\hat{\mathbf{P}}(\theta,\varphi)e^{ik\hat{\mathbf{s}}\cdot\mathbf{r}}\sin\theta\mathrm{d}\theta\mathrm{d}\varphi,\end{aligned} \tag{1}$$

where: $-i/\lambda$ corresponds to the inclination factor for small obliquities (small focal region) [31,33]; $a(\theta)$ represents the apodization for the objective lens; the unit vector $\hat{\mathbf{P}}$ is the polarization function (see Refs [32,34].); $A_0^i$ is the incident amplitude at the entrance pupil of the lens; $f'$ is the focal length of the objective and $\lambda$ the laser wavelength.

#167413 - $15.00 USD Received 26 Apr 2012; accepted 27 Apr 2012; published 15 May 2012

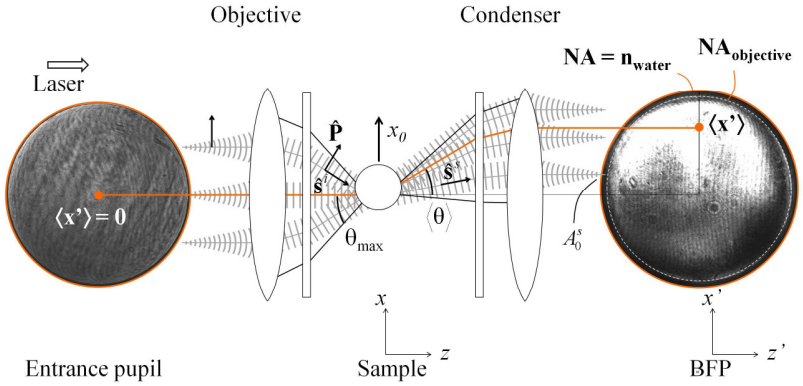


Fig. 4. Schematic representation of the telecentric system used for position detection (not to scale). After interacting with the sample, the focused laser beam is scattered in all directions, but mostly concentrated in the forward direction. When the sample remains at the centre of the trap, the light pattern at the BFP of the condenser lens is symmetric, as it is for the incident beam, and the detector signal is zero. The distribution of light in this plane changes when the position, $x_0$, of the trapped sample relative to the incident beam varies. The refraction of the beam at the water–glass interface at the exit surface of the microchamber allows a large fraction of all the scattered light to be captured (Appendix and Ref [20].). The initial structure of the beam, observed at the front focal plane of the objective, and the changes due to the sample are shown.

Every plane wave that makes up the field at the sample plane, $\boldsymbol{A}^i(\theta, \varphi)e^{iks\cdot r}$, experiences a change in its direction of propagation (Fig. 4). Due to this, the laser transfers part of its momentum to the sample thus producing a net force on it. The modification of the individual momentum of each plane wave, from $\hbar k\hat{\mathbf{s}}^i$ to $\hbar k\hat{\mathbf{s}}^s$ ($\hat{\mathbf{s}}$ being the ray vector with components ($sin\theta\ cos\varphi,\ sin\theta\ sin\varphi,\ cos\theta$), and the superscript $s$ indicating the scattered field), gives rise to an asymmetric distribution of the scattered light. If we picture the beam as a whole, the mean deflection angle of the radiant intensity, $I_\Omega(\theta,\varphi)$, which is related to the square of the Fourier transform of $\mathbf{e}^s(\mathbf{r})$, gives, for small excursions from the centre of the trap, a measurement of the sample displacement, $x_0$:

$$F_x = -\oint p_x(\theta,\varphi)\frac{I_\Omega(\theta,\varphi)}{E}\,d\Omega = -\frac{n}{c}\oint \sin\theta I_\Omega(\theta,\varphi)d\Omega \equiv -\frac{n}{c}P\langle\sin\theta\rangle = -\kappa x_0. \qquad (2)$$

For the sake of simplicity, we restrict the analysis to the $x$-$z$ plane ($\varphi = 0$). In Eq. (2): $E$ is the energy of a photon of wavelength $\lambda$; $n$ corresponds to the refractive index of the suspending medium; $P$ is the laser power at the sample plane; $\kappa$ is the trap stiffness; and $\langle\ \rangle$ indicates the mean value. The negative sign in the expression for $F_x$ shows up because it represents the force that the light exerts on the particle, so it must equal the difference, $\dot{p}_{initial} - \dot{p}_{final}$, where the initial net rate of transfer of momentum is zero due to the radial symmetry of the light distribution.

After the interaction with the object, the beam is collected by a condenser lens. A high-NA system can be used to increase the position sensitivity [23]. Displacements of the sample are easily tracked at the BFP of this collecting lens since, according to Eq. (1), it contains the Fourier transform information (that is, the new amplitudes $A_0^s$) and therefore, the irradiance at this plane, $I(x',y')$, is the projection of the scattered intensity, $I_\Omega(\theta,\varphi)$. The intensity can only be projected without distortion, for the large solid angles used in these experiments, if the lens is aplanatic, that is if plane waves are stigmatically imaged at its BFP according to the Abbe sine condition [35] ($x' = f'nsin\theta$). If that is the case, the position of the light distribution centroid, $\langle x'\rangle$, is proportional to the sample displacement. Using Eq. (2), we obtain:

$$\langle x'\rangle = \frac{f'c\kappa}{P}x_0, \qquad (3)$$

#167413 - $15.00 USD
Received 26 Apr 2012; accepted 27 Apr 2012; published 15 May 2012

where we assumed that the apodization takes the form $cos^{1/2}\theta$ for both the objective and the condenser [36] (see also Appendix), and we used the following identity in Gaussian units:

$$\begin{aligned} f'nP\langle\sin\theta\rangle &= f'n\oint\oint \sin\theta\cdot I_{\Omega}(\theta,\varphi)\,\mathrm{d}\Omega = \oint\oint f'n\sin\theta\cdot\tfrac{nc}{8\pi}\left|f'\sqrt{\cos\theta}A_0^s\hat{\mathbf{P}}\right|^2\mathrm{d}\Omega \\ &= \int_{\Re^2} x'\tfrac{nc}{8\pi}\left|A_0^s(x',y')\right|^2\mathrm{d}x'\mathrm{d}y' = \int_{\Re^2} x'I(x',y')\,\mathrm{d}x'\mathrm{d}y' = \langle x'\rangle P. \end{aligned} \tag{4}$$

So, if the angular distribution is not truncated by the collecting lenses, that is, if neither the laser power, $P$, nor the centroid position, $\langle x'\rangle$, is significantly modified by the pupil of the collection optics, the voltage signal generated by a PSD would measure the sample displacement according to:

$$S_x = \frac{S_{sum}}{R_D}\langle x'\rangle = \frac{\psi f'c\kappa}{R_D}x_0 = \frac{1}{\beta}x_0, \tag{5}$$

where: $R_D$ is the detector size and $\Psi$ is the light efficiency of the instrument in V/W, which relates the laser power at the sample plane to the detector intensity output, $S_{sum}$. Thus, an explicit connection between the trap stiffness and the sensitivity of the instrument shows up:

$$\frac{1}{\beta} = \frac{\psi f'c\kappa}{R_D}. \tag{6}$$

The factor $1/\beta$, although dependent in a complicated fashion on different experimental parameters [17], becomes linear against trap stiffness when a significant fraction of the angular distribution of light reaches the detector. More importantly, the proportionality constant depends only on features of the detection instrument:

$$F_x = -\kappa x_0 = -\kappa\beta S_x = -\frac{R_D}{\psi f'c}S_x \equiv -\alpha S_x. \tag{7}$$

The V-to-pN conversion constant, $\alpha$, in Eq. (7) is identical to the calibration parameter that appears in the measurement of the light momentum [15]. The derivation of this constant was already shown by Smith *et al.* in Ref [15]. Here, in contrast, we stress the connection between BFPI and the measurement of momentum by explicitly dividing the determination of the force into two steps so that we can illustrate the origin of the position sensitivity, $1/\beta$, as a magnitude derived from the trap stiffness. More rigorous and comprehensive descriptions of BFPI can be found, for example, in Ref [37].

The connection between the measurements of positions and momenta can finally be summarized in the following identity:

$$\alpha_{trap} \equiv \kappa_i\cdot\beta_i = \frac{R_D}{\psi f'c} \equiv \alpha_{\mathrm{det}ector}, \tag{8}$$

where the subscript $i$ indicates the two transverse directions $x$ and $y$.

We next supply experimental evidence for the validity of Eq. (8). In a new experiment, we calibrated the instrument using the two different routes: through the product of $\kappa$ and $\beta$, and from separate determinations of $R_D$, $\psi$ and $f'$. We then compared the results. The latter approach required some extra measurements.

The force exerted by the laser, $F_x = -(n/c)\,P\langle sin\theta\rangle$, is described by only its energy rate and the change in the propagation direction; magnitudes which can easily be measured by a position-sensitive photodetector located at the BFP of a lens, where angles are converted into positions. The problem then is reduced to the calibration of the conversion from angles and laser power at the sample plane, to the detector position and intensity readings, respectively. In

#167413 - $15.00 USD Received 26 Apr 2012; accepted 27 Apr 2012; published 15 May 2012

practice, this corresponds to measuring the total focal length of the instrument, $f'$, and the efficiency, $\psi$.

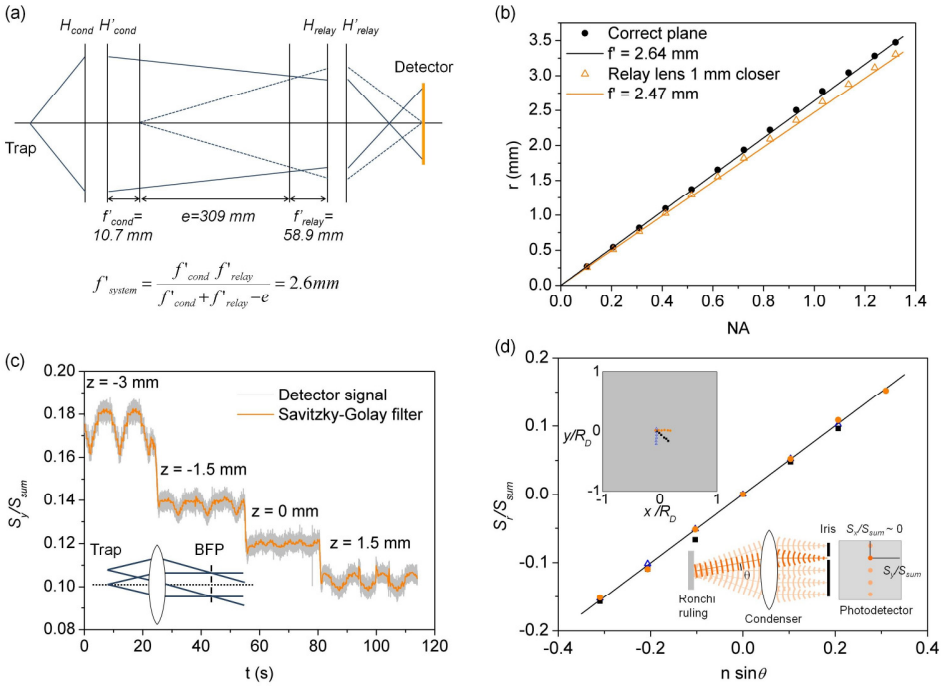


Fig. 5. Determination of $f'$. (a) Layout of our BFPI instrument. $H$ and $H'$ indicate the principal planes of both the condenser and the relay lens. (b) The relay lens (or the PSD) position affects the effective focal length of the system. A change of 1 mm in the relay lens position leads to a variation of 6% in $f'$, which translates into a similar error in $\alpha_{detector}$ ($\delta\alpha_{detector}/\alpha_{detector} = \delta f'/f'$). This was observed in the calibration experiments where we found a change from 100 to 109 pN/V. We also found that a further reduction of the distance between the lens and the detector (~10 mm) eventually led to a 100% difference in $\alpha_{detector}$. In contrast, such changes in the position of the optical elements did not have any impact on the calibration of the instrument efficiency, $\psi$. (c) In order to establish the correct position of the relay lens, the photodetector signal was recorded as an empty trap was holographically moved in steps of 10 $\mu$m across the field of view between two extreme points separated by 100 $\mu$m. Taking advantage of the Fourier transform relation between the sample plane and the BFP of the condenser and its shift property (inset), the proper axial position of the relay lens was identified as the one for which the variation in the voltage was minimum. (d) An alternative Ronchi ruling experiment with the photodetector was used both to measure the focal length of the instrument and to determine the contribution of the asymmetries of the PSD responsivity along its two independent axes. Plane waves with known transverse momentum were generated and sequentially projected onto the PSD; they were selected by means of an iris located at the BFP of the condenser lens. The sequence of points was first along the $x$-axis, then the $y$-axis and at 45° between the two. The normalized signal for each plane wave, $S_r/S_{sum} = r/R_D$, where $r$ is the position of the focused wave on the detector and $R_D$ is the detector radius, was plotted against its transverse momentum, that is, $n{\cdot}sin\theta$. The fitting was used to determine the quotient $f'/R_D$. No significant differences were observed between the results for the three directions (~1%).

A Ronchi ruling experiment, analogous to that described elsewhere [20], gave us a measurement of the total focal length of $f'$ = 2.62 ± 0.08 mm (3% error). A paraxial calculation based on the distance between the condenser and relay lenses and on their focal lengths (Fig. 5(a)), as a first approximation, and a computer simulation with Zemax as an additional verification (Fig. 5(b), black line) provided very similar results ($f'$ = 2.6 mm and $f'$ = 2.64 mm respectively). However, in the experiment, the main source of error was the difference between the axial positions of an auxiliary CCD camera and the PSD. The latter was positioned as shown in Fig. 5(c). We determined, both through experiment and simulation, that a 1-mm error

#167413 - $15.00 USD Received 26 Apr 2012; accepted 27 Apr 2012; published 15 May 2012

translated into ~6% uncertainty in the effective value of $f$' (Fig. 5(b), orange line). To minimize this, an alternative method that involved obtaining the focal length from the photodetector itself was devised (Fig. 5(d)). The same Ronchi ruling that was used earlier was again employed to generate discrete plane waves with known angles of propagation. An iris was placed at the BFP of the condenser lens to select a single diffraction order and the voltage from the detector was recorded as the iris was slid across the plane. This method allowed us, furthermore, to establish that no significant discrepancies in detector size, $R_D$, existed in the $x$ and $y$ directions. According to the manufacturer, its half-size was $R_D$ = 4.5 mm, the value we utilized in our calculations.

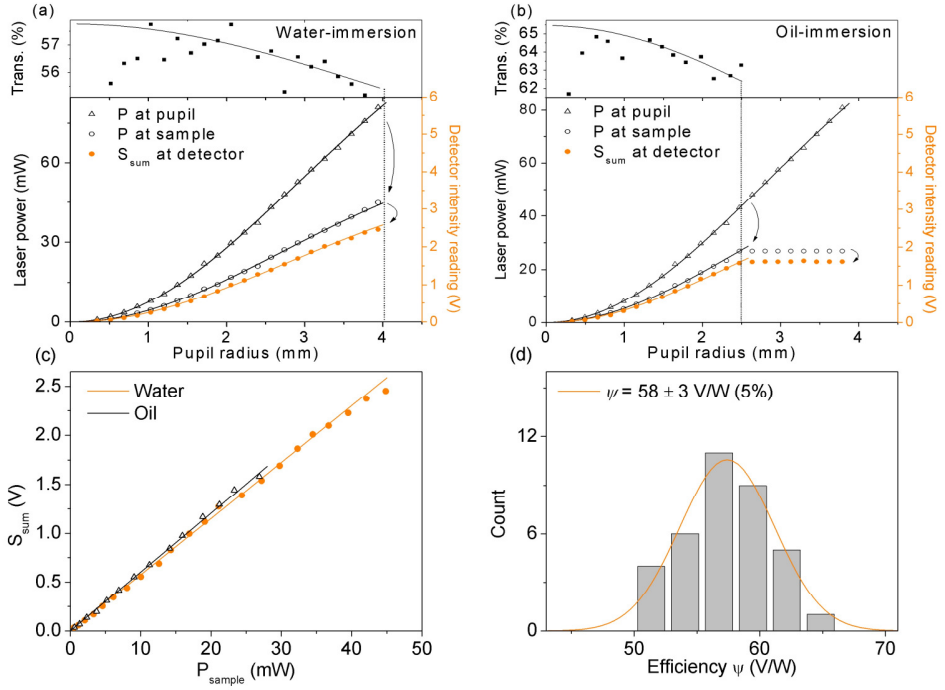


Fig. 6. Determination of the efficiency, $\psi$, of the detection instrument. The infrared laser ($\lambda$ = 1064 nm), with circular polarization, was focused by the objective lenses: (a) Nikon CFI Plan Apo VC 60xA WI and (b) Nikon CFI Plan Fluor 100xH. The former is an NA = 1.2 water-immersion lens with an entrance pupil diameter $r_{pupil}$ = 4 mm ( = $f$'$NA$, $f$' = 3.33 mm); the latter is an NA = 1.3 oil-immersion objective with $r_{pupil}$ = 2.6 mm ($f$' = 2 mm). The laser power at the back aperture of the objective (triangles) was measured as the diameter of an iris, $r$, located in a conjugate plane before the telescope was changed. The beam waist, $w$ = 5.6 ± 0.2 mm, was calculated by fitting the data to $P(r) = P_0(1 - exp(-2r^2/w^2))$, where $P_0$ is the incident laser power, and it was found to be coincident, to within the error, with the product $m \cdot r_{beam}$, where $m$ = 2.22 is the magnification between the laser fiber diameter and the back aperture of the objective in our setup, and $r_{beam}$ = 2.55 mm is the output laser radius. The power in the sample plane (circles) was then modulated by the transmittance function of the objective (top plots), which was measured using the dual objective method [38]. As pointed out in Ref [39], we found a non-homogeneous radial transmission. The profile, obtained for each value of the pupil radius as the ratio $(P_{out}(r)/P_{in}(r))^{1/2}$, fitted a function $T_{offset} + T_0 exp(-r^2/2\,\sigma^2)$ with $T_{offset}$ = 52.6 and $\sigma$ = 3.6 mm for the water-immersion lens, and $T_{offset}$ = 52.9 and $\sigma$ = 3.3 mm for the oil-immersion objective. The measured transmissions were 55% and 62%, respectively, in good agreement with Ref [38]. The error between these values, corresponding to $\langle T^2 \rangle^{1/2}$, and the actual transmissions $\langle T \rangle$ [39] were 5% and 1.5%. Finally, the detector intensity reading (orange dots) was measured and was used (c) to determine the efficiency, $\psi$, for both objectives as the ratio $S_{sum}(r)/P_{sample}(r)$, with values of 56 V/W and 59 V/W, respectively. We found that these values were independent of the laser power (as expected) but they showed a certain (small) dependence on radial distance. (d) The mean value of the efficiency was obtained from the distribution of $\psi$ for all the data analyzed, 58 ± 3 V/W, where the standard deviation represents a 5% error. The value depends on the filters in front of the PSD, but it can be corrected by their attenuation without a recalibration.

#167413 - $15.00 USD Received 26 Apr 2012; accepted 27 Apr 2012; published 15 May 2012

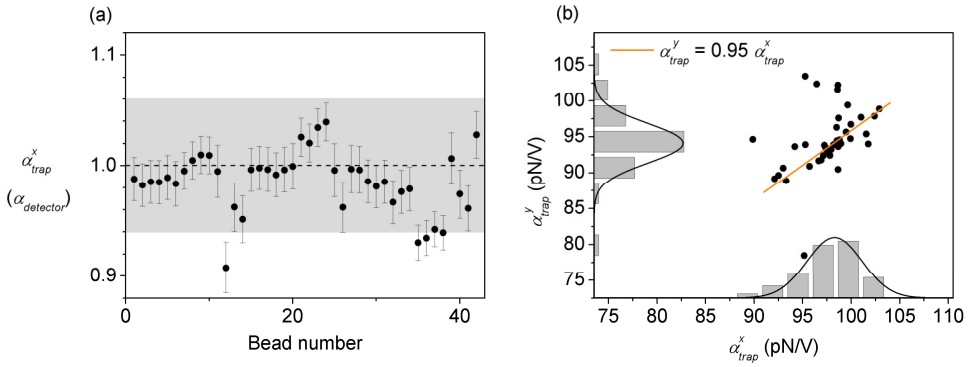


Fig. 7. Comparison between $\alpha_{trap}$ and $\alpha_{detector}$. (a) Values of $\alpha_{trap}$ in units of $\alpha_{detector}$ obtained from the power spectra for different experimental conditions. The bead size (1.16 $\mu$m, 3.06 $\mu$m and 8.06 $\mu$m) its refractive index (1.48 and 1.57) and the laser power were varied. The shaded area indicates the 6% error in $\alpha_{detector}$, which was determined from the propagation of errors in $f'$ (3%) and $\Psi$ (5%). The error bars were also obtained from the propagation of errors. (b) The separate distributions for $x$ and $y$ show that the two components follow Gaussian functions and are centered at different values: 98 ± 3 pN/V (mean ± SD; 3% error) and 94 ± 4 pN/V (mean ± SD; 4% error), respectively. The result for the $y$-component is 5% smaller than that for the $x$-component.

The other parameter required to determine $\alpha_{detector}$ is the efficiency, $\psi$ (Fig. 6). This relates laser power at the sample plane with the PSD detector intensity output in volts, so it is a measurement of the optical transmittance of the detection apparatus as well as of the responsivity of the PSD. We employed the dual-objective method [38,39] to calibrate the amount of light transmitted by our trapping lens (Nikon, NA = 1.2, water-immersion) and therefore that reaching the sample. An iris was placed in a plane conjugate to the entrance pupil of the objective and a second identical objective was aligned with the optical axis of the first making their focal planes coincident. Then, as the iris diameter was increased, the light transmitted through the system was measured with a power meter, and the transmission was calculated as $T = (P_{out}/P_{in})^{1/2}$. The same experiment was repeated for a different objective (Nikon, NA = 1.3, oil-immersion). The results were 55% and 62%, respectively; the latter in agreement with Ref [38].

**Table 1. Values of α.**

| | $\alpha_{detector}$ | $\alpha_{trap}{}^x$ | $\alpha_{trap}{}^y$ |
|---|---|---|---|
| α[a] | 99 ± 6 | 98 ± 3 | 94 ± 4 |

[a]All measurements are in pN/V.

We followed the same procedure to find the value of $\psi$. In this case, we changed the second objective for the force measuring apparatus, using the position sensitive detector to record the intensity in volts. The laser power at the sample was deduced from the laser power reading at the entrance pupil of the objective multiplied by the transmission, $T$, that we just obtained. The ratio between the two measurements gave an efficiency of $\psi$ = 58 ± 3 V/W (5% error).

Finally, we computed the factor $\alpha_{detector}$ and found that, as expected from Eq. (8), it matched the mean value of $\alpha_{trap}$ in both $x$ and $y$ directions to within the estimated error (Fig. 7 and Table 1). The constants $\alpha_{trap}{}^x$ and $\alpha_{trap}{}^y$ followed distributions with a standard deviation of 3-4% in both cases (Fig. 7(b)).

The independence of the product $\kappa \cdot \beta$ from experimental conditions such as particle size or refractive index is demonstrated in Fig. 3. However, from the theoretical discussion culminating in Eq. (8) and the results of the last experiment summarized in Table 1, we can state a more general conclusion: the calibration only depends on three properties of the sensor apparatus (its focal length, the detector size and the efficiency), and is hence totally independent of the trapping phenomenon. We find it illustrative in this regard that the 14%

#167413 - $15.00 USD Received 26 Apr 2012; accepted 27 Apr 2012; published 15 May 2012

difference in $\kappa_x$ and $\kappa_y$ observed in some experiments does not automatically translate into an equivalent discrepancy between $\alpha_{trap}^{x}$ and $\alpha_{trap}^{y}$. However, although very similar, the results for the two components exhibited a small difference (Fig. 7(b)). We found that $\alpha_{trap}^{y} = 0.95\ \alpha_{trap}^{x}$. The origin of this discrepancy lies in radial asymmetries of the light patterns projected onto the photodetector. Small losses of light during the measurements translated into slightly different calibration along the two axes.

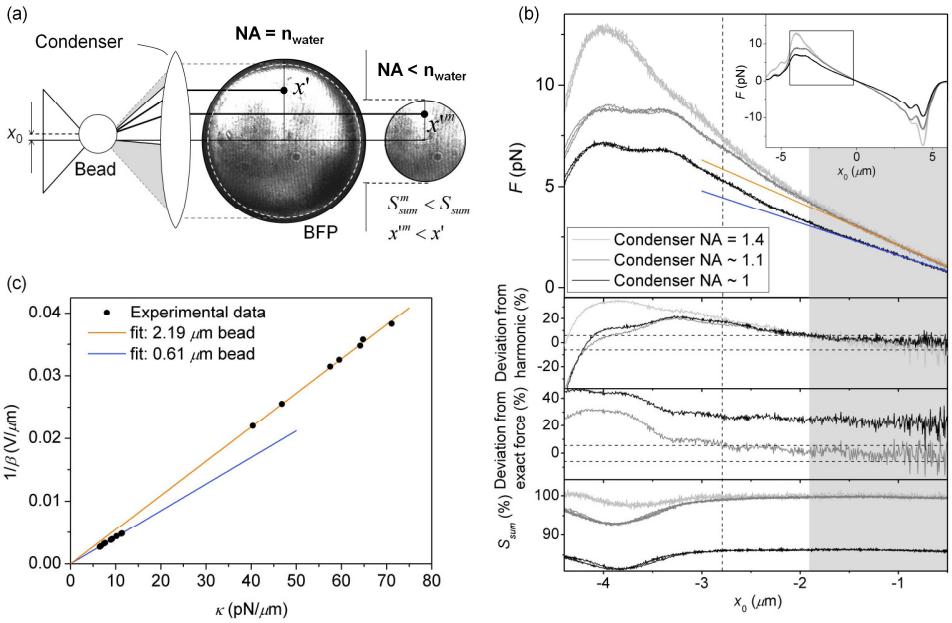


Fig. 8. Effect of light losses on force measurements. (a) Sketch of the measurement process for a collecting lens with a small NA. (b) As for the results in Fig. 1, we show experimental curves of force for an 8.1-$\mu$m bead for different NAs of the condenser lens. The vertical dashed line indicates the limit where the results with NA~1.1 overlap with the correct force curve to within a 6% error. The shaded area corresponds to the harmonic region of the trap, where the force can be described by the orange (and blue) line ($-\kappa x_0$) to within a 6% error. The deviation from the linear approximation starts at 1.8 $\mu$m for NA = 1.1, although exact force measurements can be obtained at up to 2.8 $\mu$m. The horizontal dashed lines indicate again a 6% error. The range where measurements are correct for the reduced NA correlates with the amount of light collected. (c) An excessive reduction in the amount of light captured can make the system lose the robustness in the force calibration even for small displacements of the sample, as shown in (b) for NA~1. This may eventually restrict the use of the instrument to position detection only. This plot shows the relationship between stiffness and detector sensitivity for two different bead sizes and several laser powers for small NA values of the condenser (we chose 0.65 for this example, since it is a typical value [53]). The data obtained at different laser powers are still correlated, but show two different slopes for the two beads. There is no single calibration constant, $\alpha_{trap}$, that characterizes the instrument, so recalibration for different experimental conditions would be necessary in this case.

The experimental proof of the connection between the method of Smith *et al.* and BFPI for single-beam traps has important consequences for the latter. First, it means that we can achieve a robust and permanent calibration of the apparatus. The value of $\alpha_{trap}$ obtained inside a homogeneous buffer or for a regular sample should still be valid, for instance, in a more complex environment such as the cytoplasm of a cell (preliminary results in Ref [40].), or for an arbitrarily shaped object. Second, the calibration is not restricted to the harmonic approximation of the trap; the measurement of the force is valid across a larger range, minimizing the power used for a given trapping force, which is of interest for different biological applications [41–44]. We thus close the loop by giving a unified explanation of the apparently unconnected results in Figs. 1 and 3. Now, the two properties follow as simple

#167413 - $15.00 USD Received 26 Apr 2012; accepted 27 Apr 2012; published 15 May 2012

corollaries from the interpretation of BFPI measurements as changes in light momentum, and therefore, as direct force determinations.

These results were clearly observed with our instrument since it was intentionally built to fulfill specific conditions, which are typically not met in other setups. The distinctive element, provided that a PSD is used (instead of a QPD, see Appendix), is the high-NA condenser that captures and analyzes most of the scattered light. Deviation from the optimal configuration hides, to a varying degree, the properties that we have discussed. That may explain why our observations have few precedents; however, the preceding results should still be generally recognizable since the method is intrinsically the same.

In practice, the effect of a loss of information regarding momentum translates simply into a larger dispersion of the product $\kappa.\beta$ and a reduction of the range within which absolute calibration of the instrument is maintained. In a typical BFPI system, the calibration factor may diverge from $\alpha_{detector}$, as the measured intensity, $S_{sum}^{m}$, and the measured position of the centroid of the captured light distribution, $x'^{m}$, differ from their original values, $S_{sum}$ and $x'$, (Fig. 8(a)):

$$\alpha_{trap} = \alpha_{\det ector} \frac{S_{sum} x'}{S_{sum}^{m} x'^{m}}. \tag{9}$$

This happens, for example, with sample displacements that cause large beam deflections or it may be observed even at the equilibrium position when the NA of the collecting lens is small. Figure 8(b) shows curves for an 8.1-$\mu$m sphere where the force is calculated as the product of the detector signal and factor $\alpha_{detector}$ (as opposed to $\alpha_{trap}$). As the NA is decreased from NA = 1.4 to NA~1.1, the measured quantity exhibits a larger divergence from the correct curve but at forces which are still outside the harmonic regime of the trap, which indicates that there is still an absolute calibration. When the collection angle is further reduced to NA~1, the loss of light modifies the force calibration even at $x_0$ = 0, making correct measurement of momenta unfeasible. At no sample position can the force be measured through the calibration factor $\alpha_{detector}$. In this case, only calibration of $\kappa$ and $\beta$ restores the measurements, although at the

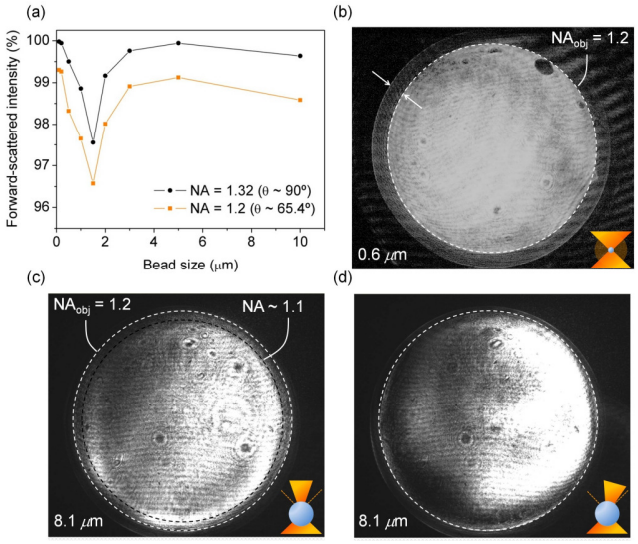


Fig. 9. Fraction of light collected. (a) The value of the force at which the experimental data deviates from the exact force curve in Fig. 8(b) for the low-NA condenser, depends on the sample, and more particularly, on its size. This is observed in a Mie scattering simulation of the fraction of forward-scattered light for different sizes of a polystyrene bead. The beam waist was 0.4 $\mu$m. (b) A faint scattering disk is the only evidence of the presence of a trapped sample for Rayleigh scatterers (arrows). (c, d) For large microspheres, the deflected beam (NA~1.1) remains inside a cone of NA = 1.2 (dashed circle) for a large range of displacements.

#167413 - $15.00 USD Received 26 Apr 2012; accepted 27 Apr 2012; published 15 May 2012

expense of a loss in calibration robustness. New samples, then, will require new calibration (Fig. 8(c)).

The size of the sample is important in this regard. The angular distribution of scattered light is different for different sizes of trapped particle, so the loss of momentum information varies between samples (Fig. 9(a)). For example, for dipoles (particles of only a few hundred nanometers) or large particles (several microns) the most relevant information is concentrated within a reduced-angle cone [15]. So, for both large and small particles, the effect of reducing the NA of the capturing lens is less significant. With small beads, the beam is scattered in the form of a spherical wave that carries zero net transverse momentum (Fig. 9(b)). In addition, all the momentum change arises due to interference with the unscattered light, so the information remains limited to the cone defined by the NA of the trapping objective, $NA_{obj}$, regardless of the sample position. In this case, the decrease of the condenser NA is only noticeable for values smaller than $NA_{obj}$. In contrast, large samples behave roughly as converging lenses; the incident beam is focused, thus reducing its NA (Figs. 9(c) and 9(d)). The force calibration may still be valid for wide displacements of the sample, even if the NA of the collecting system is further reduced.

Equation (9) and Figs. 8 and 9 clearly indicate that force measurements bypass the Hookean approximation of the trap and are ultimately conditioned solely by the capacity to collect a significant fraction of the light, which can be achieved with relative ease. In the range where this fraction is close to 100% (where $\alpha_{trap} = \alpha_{detector}$) the measurement displays the properties that we have discussed here.

## 4. Methods

*Analysis of position and force measurement capabilities*

For the analysis of the position and force detection capabilities of our BFPI instrument, we recorded the detector signal as an 8.06-$\mu$m polymethacrylate microsphere attached to a coverslip was moved across the beam, in a direction perpendicular to the trap axis (Fig. 1). The sample was moved with a piezoelectric stage (Piezosystem Jena, TRITOR 102 SG) in steps of 8.4 nm.

It should be noted that this procedure entails some difficulties and is often ruled out as a method to determine the voltage-to-position calibration factor of the instrument. For example, the scattered field can be affected by the presence of the glass surface [45], which can interfere with the position signal. However, we did not find differences between the results obtained with beads stuck to coverslips and those with particles embedded in an agarose gel for any of the sizes used in the experiments.

A second typical problem is the imprecise three-dimensional positioning of the particle relative to the trap. We addressed this issue by using the light pattern from a trapped particle at the BFP of the condenser as a visual reference. Since such patterns provide a very sensitive measurement of the location of the sample, the adhered bead could be positioned precisely, both transversally and axially.

In the comparison of the experimental results with the T-matrix simulations, we used the beam waist at the focus, $\omega_0$, as an adjustable parameter. This is, in general, a magnitude that is difficult to measure. The knife-edge scanning method [46], for example, can introduce errors as large as 13% (50 nm) [47] or more [46]. Other approaches, such as the analysis of the image of the focused laser spot reflected from a coverslip can reach a 20% error [48]. In several papers, the value has been estimated [17] or simulated [34]. Given the uncertainties, we used $\omega_0$ as a free parameter to match the theoretical curves to the experimental data in a similar way to [49]. The results for the 8-$\mu$m and the 0.6-$\mu$m beads, 340 nm and 410 nm, respectively, are in agreement with values that we obtained from images of the focused beam spots and similar to those reported by others. The difference between the two values may arise from changes in the correction collar of the water-immersion objective, whose position was not fixed.

#167413 - $15.00 USD Received 26 Apr 2012; accepted 27 Apr 2012; published 15 May 2012

*Calibration through spectral analysis of the Brownian motion of the sample*

We calculated the trap stiffness, $\kappa$, and the sensitivity, $1/\beta$, from the power spectra of the thermal motion of trapped beads (Fig. 2). All the experiments were carried out with the microspheres (Spherotech and Sigma-Aldrich) suspended in deionized water inside a flow chamber (model RC-30WA, Warner Instruments). Five different sizes (0.61 ± 0.01 $\mu$m, 1.16 ± 0.04 $\mu$m, 2.19 ± 0.05 $\mu$m, 3.06 ± 0.08 $\mu$m and 8.06 ± 0.10 $\mu$m; mean ± SD) and three materials (polymethacrylate, n = 1.48, polystyrene, n = 1.57, and melamine resin, n = 1.68) were selected. The laser power at the sample plane was determined from the transmission factor of the objective, which was previously measured following the dual-objective method [38,39] (Figs. 6(a) and 6(b)). We used two different objective lenses for trapping: water-immersion and oil-immersion (Nikon CFI, PlanApo VC 60xA NA = 1.2 and PlanFluor 100xH NA = 1.3, respectively).

The two calibration constants displayed linear relationships with laser power (Fig. 2(a), inset). Spectra were obtained from 40-s series of 15000 points at $f_{sample}$ = 15 kHz after blocking (blocks of 350 points). Following the results from [28,29], aliasing, the photodetector transparency at 1064 nm ($f_{3dB}$ ~6.8 ± 0.2 kHz for our photodetector, similar to previous results [50]; mean ± SD; n = 60; see also Fig. 2(c)), the frequency dependence of the drag coefficient, $\gamma$, and the analogue-to-digital converter noise were taken into account for fitting the experimental data to a Lorentzian curve (Figs. 2(b)-2(d)). To determine the two constants $\kappa$ and $\beta$ from the fitted parameters, the bead size calibrated by the manufacturer, Faxén's correction of $\gamma$ [3], and the nominal value of water viscosity at the operating temperature were considered. Measurements were performed at stable room temperature ( ± 2 K), which was monitored with an electronic thermometer.

Errors in $\kappa$, $\beta$, and $\kappa \cdot \beta$ were determined through the propagation of errors. When, in addition, the final value was obtained as a mean of $n$ different measurements (Table 1), the total error was computed as the standard deviation, SD.

## Appendix

In this appendix we give further details of the particular working conditions under which the results in Figs. 1, 3 and 7 were obtained. They are set to ensure the correct measurement of light momentum changes of an optical trap based on a high-NA beam.

Figure 10 shows a ZEMAX simulation of our optimized BFPI optical system, which primarily consists of a high-NA lens (an oil-immersion DIC condenser, Nikon T-CHA, NA=1.4) and an auxiliary lens (a Thorlabs doublet AC254-100-C and an additional singlet LA1986-C). The light scattered by the sample, represented by a set of plane waves propagating within a solid angle of ~2π, is collected by the condenser lens and the relay lens projects the light pattern at the BFP of the condenser onto a photodetector with 1/4 magnification. The NA of the condenser lens, $NA_{condenser}$, has to be larger than the refractive index of the suspension medium, $n_{medium}$, in order to collect the light propagating almost parallel to the upper surface of the microchamber [20] (inset). In this case: $n_{medium} \sim n_{medium}\ sin\theta = n_{glass}\ sin\theta' < NA_{condenser}$, where $\theta$ and $\theta'$ are the convergence angle of the beam before and after refraction at the water–glass interface, respectively. In our case this condition is fulfilled as $NA_{condenser}$ = 1.4 and $n_{medium}$ ~ 1.33.

The second major requirement of our setup is the use of an aplanatic optical system, that is, the system must fulfill the Abbe sine condition. This ensures the proper decomposition of the beam into the transverse momentum ($p_r/p_0 = n \cdot sin\theta$, where $p_0 = h/\lambda$) in the detector plane (that is, ensures that the spatial coordinates at the PSD plane are proportional to momentum). Although this is a typical correction in microscopy optics, we checked our system for compliance with this requirement, as illustrated in Fig. 11. Figure 11(a) plots the results of a ray tracing simulation of the condenser (Nikon T-CHA, oil-immersion, NA=1.4), based on the specifications found in US patent no. 5657166 [51]. Rays travelling at different angles, $\theta$, hit the BFP of the condenser at positions $r = f' \cdot n \cdot sin\theta$ ($f'$ = 10.66 mm) with high fidelity. We observed that, even for far off-axis rays, the geometric image was smaller than the Airy disk (140 $\mu$m), thus being, in addition, diffraction limited.

#167413 - $15.00 USD Received 26 Apr 2012; accepted 27 Apr 2012; published 15 May 2012

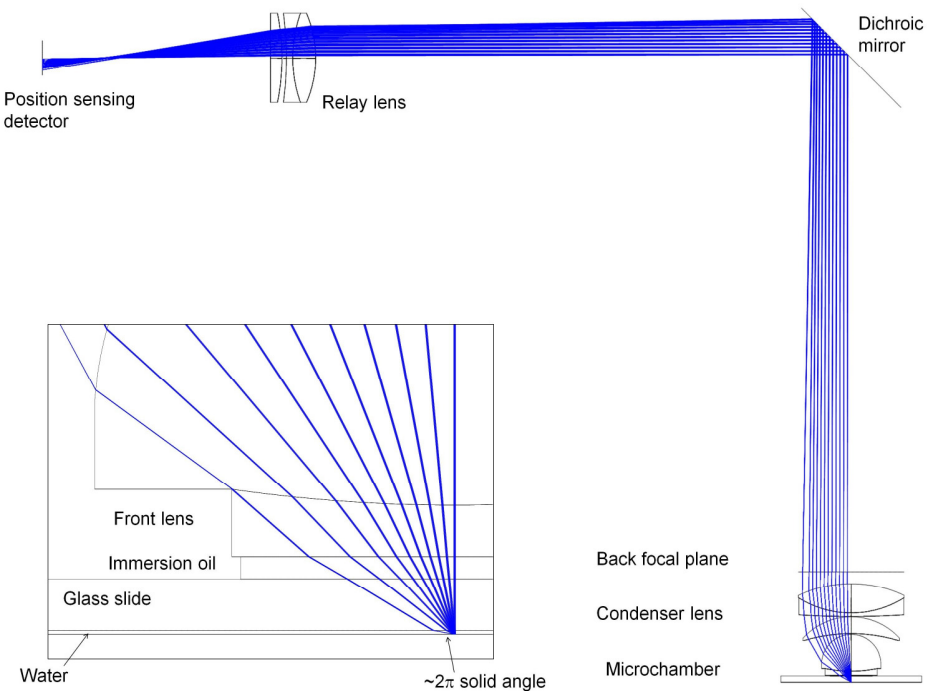


Fig. 10. Computer simulation of the setup using ZEMAX. The inset is a magnified view of the sample region showing how the front lens captures plane waves scattered at high angles.

Figure 11(b) plots the small deviations found with respect to the Abbe condition for large angles. The difference between the position $r$ and the expected value, $r_0 = f' \cdot n \cdot \sin\theta$, is a power (b = 4.77 ~ 5) of the transverse component of the momentum, and is always smaller than 5%. The spherical aberration, $\phi = (S_1/8)r'^4$ (where $0<r'<1$ and $S_1$ is the Seidel coefficient), which is the main optical aberration of an aplanatic oil-immersion condenser, lies at the heart of this small discrepancy, as shown in Fig. 11(c). In an aberration-free lens, the light propagating in direction $\theta$ exits the optical system at position $r_0$. However, due to the spherical aberration, the actual position in our system is $r_0 - \phi \sin\theta$. This gives rise to the polynomial dependency with sinθ (of order 5) observed in (b). The effect on the detector reading is nevertheless small. A Matlab simulation confirmed that the effect of the spherical aberration depends on the scattered pattern and on the deflection of the beam, but it is typically below 2%. This contrasts with the reported poorer performance of the condenser when used as a trapping lens [52]. Finally, Fig. 11(d) shows simulated and experimental data of the fulfillment of the Abbe sine condition by the total optical system (including the auxiliary lens). We chose a combination of elements for the relay lens, so the momentum structure of the beam was not degraded when projected onto the position sensitive detector. A diffraction grating made holographically in-house with an Agfa holotest plate, type 8E75HD (substrate with n~1.53 at 1064 nm), was used to generate plane waves of known transverse momentum. The position of the diffracted orders in the PSD plane was determined from a CCD image (on the right of Fig. 11(d)). This experiment also allowed us to determine the focal length of the total system ($f'$ = 2.62 ± 0.08 mm).

#167413 - $15.00 USD Received 26 Apr 2012; accepted 27 Apr 2012; published 15 May 2012

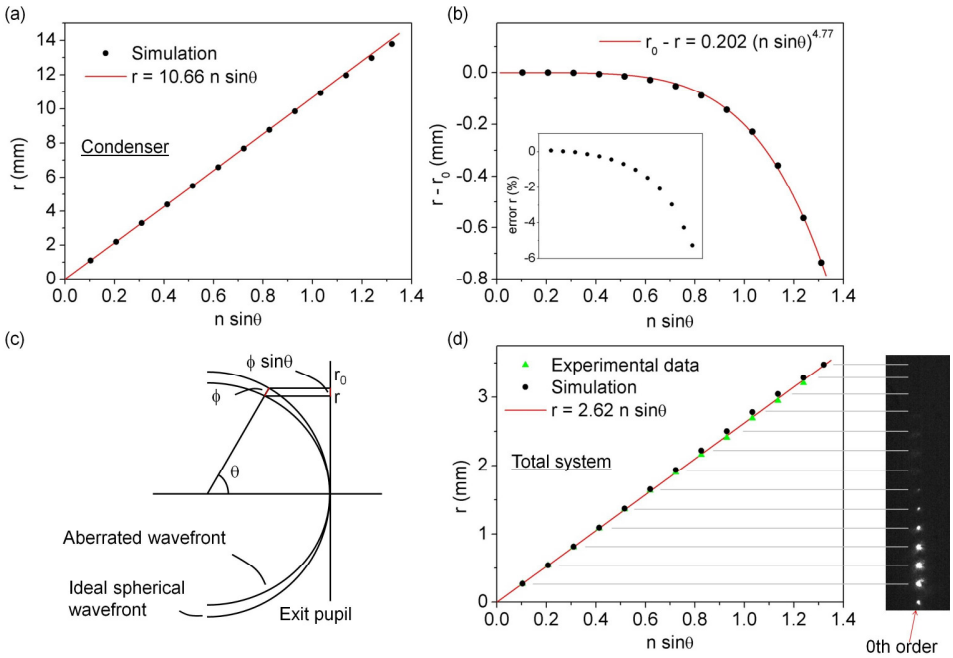


Fig. 11. Analysis of the aplanatic lens requirement. (a) ZEMAX Simulation of the condenser lens alone. Light rays travelling at angles specified by their numerical aperture at the *x*-axis hit the BFP at positions given by coordinate *r* in the *y*-axis. (b) The residues are small and can be fitted to a power law. (c) Spherical aberrations are probably behind the observed discrepancies as they would shift rays following a five-order power law, close to that found in (b). (d) Experimental results for the compound system (condenser + relay) and simulation.

In practice, to capture highly skewed light rays, it is also necessary to work as close to the upper coverslip as possible. Failing to work close to the exit surface reduces the performance of the system in two ways: when the axial distance, *z*, between the trap and the glass increases, 1) the amount of captured light decreases and 2) the degree of agreement with the Abbe sine condition worsens. These effects can be partly reduced through the use of a long-focal-length collecting lens, as shown in Fig. 12. In our case, $f' = 10.66$ mm. Figure 12(a) shows light patterns at the BFP of the condenser lens (inset), which provide direct information about the solid angle captured (the amount of light collected). We observed, both with a simulation and experimentally, that the effective NA changes as the trap is moved in the axial direction. For our system, the effective NA is 1.3 when the trap is kept within a range of 50 $\mu$m from the glass and 1.29 if the distance is greater than this but less than 100 $\mu$m. These values correspond to a large fraction of all the scattered light for most samples (Fig. 9). The fit in Fig. 12(a) corresponds to the curve (derived using geometrical optics) $z\ tg\theta_{max} + (wd - z)\ tg\theta'_{max} = r_{pupil}$, where $\theta_{max}$ is the acceptance angle of the condenser for the cone of light in the sample, $\theta'_{max}$ is the refracted angle at the water–glass interface, $wd$ is the working distance ($wd = 1.72$ mm) and $r_{pupil}$ is the pupil radius, which was used as a free parameter, with a final value of 3 mm. Similarly, the condenser still fulfills the Abbe sine condition when the trap is moved deep into the microchamber (Fig. 12(b)), beyond the plane for which the spherical aberration is corrected (i.e. the working distance). The displacement of the laser introduces a certain error but the deviation from the optimal condition is <5%. In contrast, the use of a short-focal-length lens, such as an oil-immersion objective, does not provide the same performance (Figs. 12(c) and 12(d)). A computer simulation of our objective lens (with a much shorter focal length than the condenser, $f' = 2$ mm) using ZEMAX (data taken from US patent no. 5805346) shows how the pattern at its back aperture is completely modified when the trap position changes as little as from 3 to 20 $\mu$m (Fig. 12(c)). The effective focal length varies by 6%, the linearity for large

#167413 - $15.00 USD Received 26 Apr 2012; accepted 27 Apr 2012; published 15 May 2012

angles disappears and the effective NA of the lens is drastically reduced from 1.3 to 1.2 (Fig. 12(d)). Such lenses should not be used for this purpose.

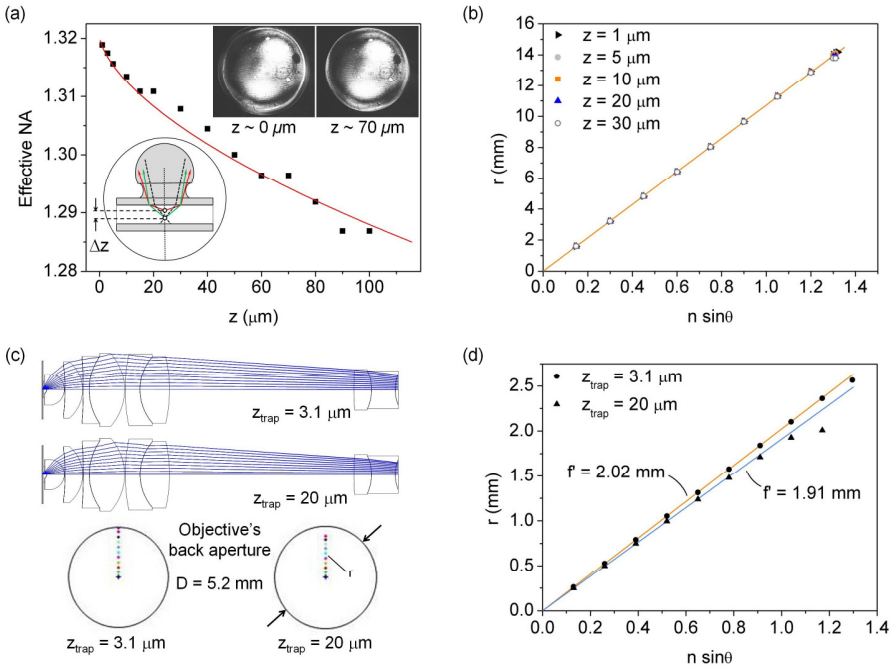


Fig. 12. Analysis of the requirement of a collecting lens of long focal length. (a) Experimental light patterns at the BFP of the condenser, for two axial positions of the trap, and plot showing the dependence of the effective numerical aperture of the collecting lens with the axial distance. An increasing, but still small, fraction of the light travelling at large angles is lost. (b) Aplanatism of the condenser lens for increasing cover-glass-to-sample distance, the differences are barely noticeable. (c) A computer simulation of an oil-immersion objective with a focal length $f' = 2$ mm, used as a substitute condenser and (d) degree of fulfillment of the Abbe sine condition. This lens is more sensitive to axial changes in the sample position because of its shorter focal length.

Finally, experimental data show that a PSD is a critical requisite. Other kinds of photodiodes, such as QPDs, are often used in BFPI. They do not, however, provide the true position of the centroid of the light pattern at the BFP of the condenser lens, which induces errors in the measurement of the total beam momentum, and as a consequence produces incorrect force values. For example, we think that the relatively high dispersion of the data in Ref [18]. is largely due to their using a QPD, as they did employ a high-NA condenser and the experiment involved small modifications of the sample properties. We have similarly observed a larger data dispersion in the relationship between $\kappa$ and $\beta$ when replacing the PSD by a QPD, as shown in Fig. 13. In the experiment shown, a microsphere was trapped and dragged by the surrounding fluid as the whole microchamber was moved with a piezoelectric stage. The photodetector signal was recorded and plotted against the hydrodynamic force applied on the trapped particle given by Stokes' equation, $F = 6\pi\eta a v$, where $\eta$ is the medium viscosity at the operating temperature and $a$ and $v(t) = 2\pi f x_0 \cdot cos(2\pi f t)$ correspond to the radius and the velocity of the bead, respectively. The latter was determined from the velocity of the piezoelectric stage, which was driven with a sinusoidal voltage at frequency $f << f_c$, the corner frequency of the system. We found that small changes in sample properties, for example, a slight increase in the sphere diameter (from 1.16 $\mu$m to 3.06 $\mu$m), had a clear impact on instrument calibration (Fig. 13(a)). In contrast, such an effect was not observed when the QPD was replaced by a PSD, as shown in Fig. 13(b). Furthermore, we found a clear discrepancy between the value of $\alpha$ computed from the theory in Ref [17], which assumes a QPD at the BFP, and those in Table 1

#167413 - $15.00 USD Received 26 Apr 2012; accepted 27 Apr 2012; published 15 May 2012

($\alpha$ = 42 pN/V). QPDs are more sensitive than PSDs. However, unless needed to measure position alone, their use should be avoided.

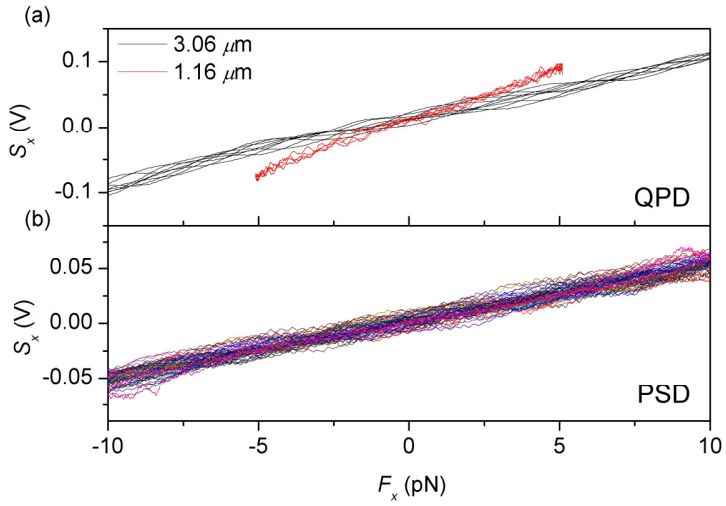


Fig. 13. QPD vs. PSD. (a) A QPD produces outputs that are sensitive to the size of the sample as opposed to (b) a PSD, whose outputs are proportional to the centroid of the light distribution, and thus faithfully represent the net momentum flux when placed at the BFP.

**Acknowledgments**

We are indebted to the company IZASA (Barcelona, Spain) for kindly lending us duplicates of our microscope objectives. We thank Christopher Evans and Prof. E. Martín-Badosa for the careful reading of the manuscript, and J. Mas for fruitful discussions. This work was funded by the Spanish Ministry of Education and Science, under grants FIS2007-65880 and FIS2010-16104, as well as by the Agency for Assessing and Marketing Research Results (AVCRI) of the University of Barcelona. A. Farré is the recipient of a doctoral research grant from the Generalitat de Catalunya.

#167413 - $15.00 USD Received 26 Apr 2012; accepted 27 Apr 2012; published 15 May 2012

# Stretching single DNA molecules to demonstrate high-force capabilities of holographic optical tweezers

Arnau Farré, Astrid van der Horst, Gerhard A. Blab, Benjamin P. B. Downing, and Nancy R. Forde

Journal of Biophotonics
Vol. 3, 224-233 (2010)

J. Biophoton. **3**, No. 4, 224–233 (2010) / **DOI** 10.1002/jbio.200900107

Journal of BIOPHOTONICS

FULL ARTICLE

# Stretching single DNA molecules to demonstrate high-force capabilities of holographic optical tweezers

*Arnau Farré*[1,2,†], *Astrid van der Horst*[1,3,†], *Gerhard A. Blab*[1], *Benjamin P. B. Downing*[1], *and Nancy R. Forde*[*,1]

[1] Department of Physics, Simon Fraser University, 8888 University Drive, Burnaby, British Columbia, V5A 1S6, Canada
[2] Optical Trapping Lab – Grup de Biofotònica, Departament de Física Aplicada i Òptica, Universitat de Barcelona, Martí i Franquès 1, Barcelona 08028, Spain
[3] Currently at the Department of Physics and Astronomy, VU University, De Boelelaan 1081, 1081 HV Amsterdam, The Netherlands

Received 23 December 2009, revised 28 January 2010, accepted 29 January 2010
Published online 16 February 2010

**Key words:** holographic optical tweezers, DNA, force measurement

**Supporting information** for this article is available free of charge under http://dx.doi.org/10.1002/jbio.200900107

The well calibrated force-extension behaviour of single double-stranded DNA molecules was used as a standard to investigate the performance of phase-only holographic optical tweezers at high forces. Specifically, the characteristic overstretch transition at 65 pN was found to appear where expected, demonstrating (1) that holographic optical trap calibration using thermal fluctuation methods is valid to high forces; (2) that the holographic optical traps are harmonic out to >250 nm of 2.1 μm particle displacement; and (3) that temporal modulations in traps induced by the spatial light modulator (SLM) do not affect the ability of optical traps to hold and steer particles against high forces. These studies demonstrate a new high-force capability for holographic optical traps achievable by SLM technologies.

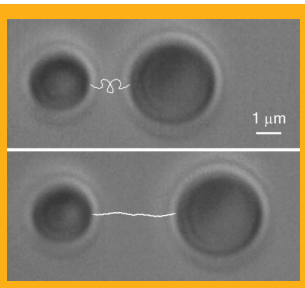


Superposed schematic of a DNA molecule stretched between microspheres held in two holographic optical traps.

## 1. Introduction

Holographic optical tweezers (HOT) is a technique in which the phase of a trapping laser beam is modulated, for example to generate multiple, steerable trapping foci in a sample chamber. The ability of HOTs to independently manipulate multiple trapped particles in three dimensions in real time has led to their application in a broad range of fields including micropatterning, optical sorting and, more recently, cell biology [1–3]. For the most part, these applications have taken advantage of the ability of optical traps to hold and manipulate particles, but have not made use of their force-measuring capabilities. This is due in large part to uncertainties in the shape of optical traps generated by the discrete phase modulation using spatial light modulators [4, 5], whether the traps can be considered as static when located at

* Corresponding author: e-mail: nforde@sfu.ca, Phone: 778-782-3161, Fax: 778-782-3592
† These authors contributed equally to this work.

a fixed position within a sample chamber [6, 7], changes in trap stiffness as optical traps are steered within a sample [6, 8], and the maximum forces attainable with this technique [3, 9]. All these questions must be addressed before HOTs find wide acceptance in quantitative force-measuring applications.

Previously, we demonstrated that HOT traps could be positioned with nanometre resolution, and furthermore showed that trap stiffness remained constant within 5% when traps were steered over distances of >20 μm within a sample chamber [6]. These results provided promising evidence that the technique could be used for force-measuring applications [3]. An additional requirement for this application is that HOT traps be capable of exerting high forces on trapped particles and of maintaining particles in the traps as their positions are updated. To date, most applications of this technique have used weak traps for manipulation rather than stiff traps for force measurement. Two recent papers have applied high forces to particles trapped in HOT, estimating that these exceeded 60 pN, however, in both cases, the high forces were calculated by assuming that the trap stiffness obtained at low forces (<2 pN) was valid in the high-force range [3, 9]. The harmonic range of an optical potential depends on many instrument-dependent parameters and on particle size and refractive index. Even for a conventional, non-holographic optical trap, the potential can become anharmonic for relatively small displacements from the trap centre (<100 nm) [10], suggesting that care must be taken when extending trap stiffness calibrations obtained from thermally sampled positions to high forces.

The most common method used to probe the optical potential experienced by a trapped particle is the application of a known drag force on the particle, either by moving the trapping chamber (and entrained fluid) at known speed [8, 9, 11], or by applying known flow speeds to the solution within the chamber [12]. For application to stiff optical traps, the former method requires a stage that can be translated at controlled high speeds, while the second requires controllable flow. Both methods require knowledge of the bead size, which has some uncertainty even for well calibrated commercial samples [13].

We demonstrate here an alternative approach, namely using the well-calibrated force-extension behaviour of DNA, to probe whether the harmonic potential of holographic optical traps extends to forces greater than 65 pN. The elasticity of double-stranded DNA (dsDNA) has been well established from single-molecule stretching experiments [14]. The force-extension curve is highly nonlinear, conforming at low forces to the entropic worm-like chain model of polymer elasticity and exhibiting a plateau at a force of 65 pN. In this so-called overstretch plateau, the molecular contour length increases by 70% as the two strands of DNA melt [15]. Observation of a plateau at 65 pN is a clear signature of a single, torsionally unconstrained dsDNA. The use of DNA as a metrology standard has previously been demonstrated in the low-force regime [16]. Here, we use the overstretch plateau as a force standard to demonstrate the capabilities of HOT for high-force measurements. We compare results of DNA measurements made with our conventional, single-beam optical tweezers instrument to the HOT measurements. We show that our HOT instrument can hold particles in stiff, harmonic traps in the presence of >65 pN of force applied through DNA tension, and that these particles stay trapped in the presence of high tension while trap positions are updated. These results further demonstrate the potential of this technique for high-force measurements.

## 2. Experimental

### *2.1 Holographic optical tweezers set-up*

Most DNA stretching measurements were conducted using our holographic optical tweezers instrument described previously and shown schematically in Figure 1 [6]. It uses a Holo-Eye HEO 1080P LCOS phase-only spatial light modulator (SLM) to spatially

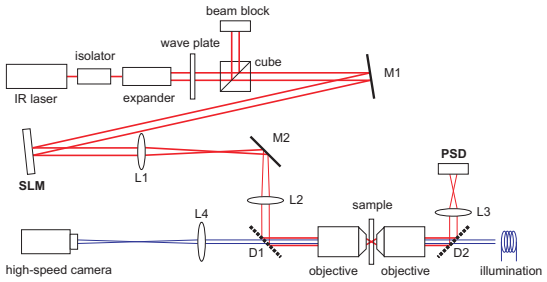


**Figure 1** (online color at: www.biophotonics-journal.org) Schematic of the holographic tweezers setup. An infrared laser beam is expanded, after which a half-lambda zero-order wave plate in combination with a polarizing beam splitter cube provides manual control over the power directed to a spatial light modulator (SLM). The SLM modulates the wavefront of the laser beam and the lenses L1 and L2 image the SLM onto the back focal plane of a high-numerical aperture objective lens, which focuses the light to create one or more optical traps. A second identical objective lens captures the light, which is imaged onto a position-sensitive diode (PSD) for trap calibration. The counterpropagating visible light, passing through the dichroic mirrors D1 and D2, is directed to the high-speed camera for particle tracking. See text for details.

Journal of
BIOPHOTONICS



modulate the phase of our 1064 nm trapping laser (Spectra Physics J20-BL-106C), with $2\pi$ phase modulation at each pixel. Phase patterns (kinoforms) are generated in LabVIEW using gratings-and-lenses calculations [17] with aberration corrections [18]. The light is focused by a high-numerical-aperture water-immersion objective lens (Olympus UplanApo/IR, 60×, 1.2 NA) into our sample chamber. A position-sensitive photodiode (PSD; OSI Optoelectronics, DL-10) is used for high-bandwidth measurements only to calibrate the trap stiffness of a single trapped particle [6], and is used because it has a much higher bandwidth than our camera. Images of the trapped particles were recorded at 368 frames/second using a high-speed camera (PCO, 1200 HS). Particle positions were determined from these images at high spatial resolution using correlation analysis [6]. In principle, these positions from our high-speed camera could be used to calibrate optical traps, however, for high trap stiffnesses such as used here, camera integration times must be properly taken into account ([19] and A. van der Horst et al., manuscript in preparation).

Figure 2 depicts the experimental geometry in our sample chamber. An end-labelled DNA molecule was stretched between two polystyrene microspheres, which were coated to specifically bind the ends of the DNA (Sections 2.3 and 2.4). Two different sizes of particles were used to distinguish between the labels. One HOT trap was kept stationary while the second was steered to different positions to stretch the DNA. The kinoforms for these positions were precalculated and sent to the SLM as an image stack, so that we reproducibly obtained identical trap separations for the same or different DNA molecules. Trap 1 was located at $(x, y) = (14.3\ \mu m, 8.9\ \mu m)$ with respect to the zero-order spot in the focal plane, while trap 2 was moved stepwise in the range from (17.5 μm, 8.9 μm) to ( 25.8 μm, 8.9 μm). Trap locations were chosen to avoid ghost traps in the vicinity of the DNA, and to sample more densely the steeper parts of the expected force-extension ($F - z$) curve (35.4 nm steps) while taking larger steps (177 nm) in the flatter parts of the curve. The HOT traps resided at each position for 0.3 seconds (110 image frames on our high-speed camera). At the end of a stretching experiment, when the attachment of the DNA to a particle broke [20], we released the bead in trap 2, after which the trap stiffness for the particle in trap 1, $\kappa_1$, was determined from power spectral analysis of its PSD position data [6]. A typical value for these experiments was $\kappa_1 = 250$ pN/μm. In principle, forces could also be measured using trap 2. However, the change in position of this trap for each DNA extension would result in increased uncertainty in particle offset from the trap centre and trap stiffness (Section 3.2), so only trap 1 was used for force measurements.

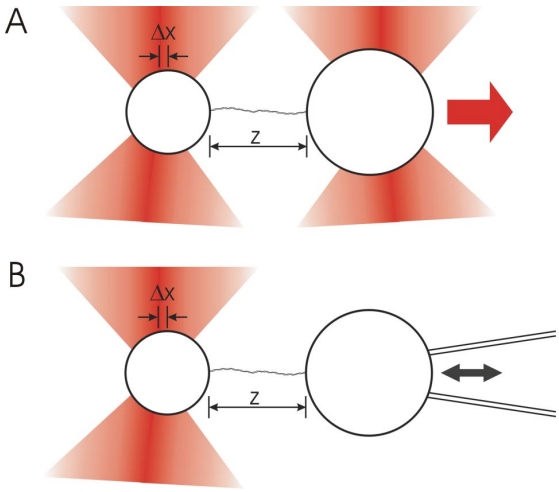


**Figure 2** (online color at: www.biophotonics-journal.org) **A.** Schematic of DNA stretching in our HOT instrument. A 2.10-μm-diameter antidigoxigenin-coated polystyrene sphere is trapped in the left, stationary HOT trap (trap 1), while a 3.17-μm-diameter streptavidin-coated polystyrene sphere is displaced stepwise to the right as this HOT trap (trap 2) is steered. An 11.7-kbp-long dsDNA molecule is modified at its ends with biotin and digoxigenin, respectively, which tether the DNA molecule specifically between the microspheres. The force applied to stretch the DNA is determined from the bead displacement from the stationary trap (trap 1), while the extension of the DNA is found from the separation between particles. **B.** Schematic of DNA stretching in our single-beam OT instrument. Here, the optical trap is stationary and the DNA is stretched by moving the micropipette.

## 2.2 *Single-beam optical tweezers set-up*

We used our separate single-beam optical tweezers instrument, described in more detail previously [21, 22], for control measurements to stretch DNA (Figure 2b). Similar to the HOT setup, it uses water-immersion objectives and a position-sensitive photodiode to produce and calibrate an optical trap, in this case from an 835 nm, 200 mW diode laser. DNA was stretched between an optically trapped bead and a second bead held on the tip of a micropipette by suction. The micropipette was mounted in the sample chamber, which was translated in the plane perpendicular to the optical axis by a nanometre-precision two-axis piezoelectric stage (Mad City Labs, Nano H-50). DNA stretching experiments were performed using the same polystyrene microspheres and DNA samples as in the HOT experiments. Images of the particles were recorded and saved at 10 Hz using a CCD camera (Flea, Point

 

Grey Research) and their positions were determined by correlation analysis.

## 2.3 DNA preparation and labelling

Double-stranded DNA molecules used in our experiments were obtained by digestion of plasmid pPIA2-6 [23] with restriction endonucleases EagI (New England Biolabs) and EcoRI (Invitrogen). The purified 11.7 kilobasepair (kbp) fragment was labelled using Klenow exo- DNA polymerase (Fermentas) and a mixture of dATP, dGTP, biotin-dCTP (Invitrogen) and digoxigenin-dUTP (Roche), each at 33 μM, resulting in dsDNA with two biotin groups at one end and two digoxigenin groups at the other.

## 2.4 Bead preparation and testing

Streptavidin (Molecular Probes) was crosslinked to carboxyl functionalized 3.17-μm diameter polystyrene microspheres (Spherotech) using EDC (Fluka Analytical). 2.10 μm diameter polystyrene microspheres, covalently coated with protein G (Spherotech), were allowed to react with anti-digoxigenin (Roche), whose Fc region binds to protein G. This interaction was then stabilized by crosslinking with DMP (Sigma-Aldrich). Before a stretching experiment, DNA was incubated for an hour at room temperature with the anti-digoxigenin beads, letting the antibody-antigen interaction coat the beads in DNA. The DNA concentration was approximately 0.1 nM during incubation, with a ratio of no more than 100 DNA molecules per bead. The beads were then incubated with 10 mg/ml BSA for 20 minutes to block non-specific binding, and finally washed to remove unbound DNA and BSA.

We have developed an assay for DNA binding to our anti-digoxigenin-coated microspheres, and tested it on a 2.1 kbp DNA fragment labelled using a protocol similar to that described in Section 2.3. Anti-digoxigenin beads and labelled DNA were incubated as described above. Unbound DNA was removed through repeated washing steps. The beads were then incubated for one hour on a mixer at room temperature with streptavidin alkaline phosphatase (Promega), which can bind to biotin on the free end of the DNA molecules. Free streptavidin alkaline phosphatase was washed away. The beads were then incubated with pNPP (Sigma-Aldrich), whose hydrolysis is catalysed by alkaline phosphatase to produce a yellow substrate with a strong absorbance peak at 405 nm. By ensuring pNPP was in excess and the incubation time was sufficiently short, the absorbance at 405 nm was proportional to the quantity of streptavidin alkaline phosphatase present, and so to the number of biotinylated DNA molecules. We normalized the optical density at 405 nm by the bead concentration to obtain a value proportional to the average number of DNA molecules bound per bead. Bead concentration was determined for each sample by measuring the intensity of 532 nm laser light it scattered at 90°, and comparing this to a calibration curve produced from samples of known concentration.

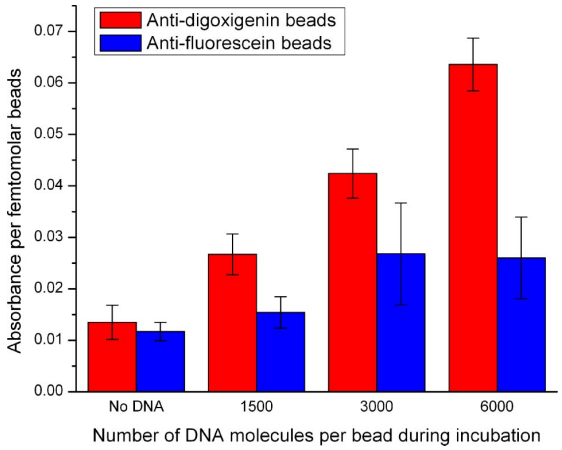


**Figure 3** (online color at: www.biophotonics-journal.org) Results of pNPP quantification of DNA binding to beads. Beads were incubated with labelled DNA at the indicated ratios, then quantified. DNA bound specifically to anti-digoxigenin coated beads and non-specifically to the anti-fluorescein coated control beads. The finite signal when no DNA was present indicated non-specific binding of streptavidin-alkaline phosphatase to the beads. Error bars show the standard deviation of 3 separate trials.

By using this assay, we confirmed that digoxigenin-labelled DNA was successfully bound to the anti-digoxigenin beads and had accessible biotins (Figure 3). Signal increased with DNA concentration, and was greater for specifically bound DNA (incubated with anti-digoxigenin beads) compared with non-specifically adsorbed DNA (incubated with anti-fluorescein coated beads). Due to the significant level of background signal in the absence of DNA, the assay works best for large numbers of bound DNA molecules (here, approximately 10 times the number per bead used in the single-molecule experiments), so is best suited to experiments testing whether or not bead and DNA labelling is effective.

## 2.5 Force-extension measurements of DNA

Experiments were performed in the middle of home-made multistream flow cells that consisted of two

Journal of
BIOPHOTONICS



microscope cover slips sandwiching a fluid channel created by excising a Y-shaped physical channel from the centre of a Nescofilm spacer (NESCO; chamber volume 10–20 μl). Holes drilled in one of the coverslips permitted fluid flow through two inlets and an outlet; the two inlet channels allowed us to use streptavidin and DNA-coated anti-digoxigenin microspheres simultaneously without mixing [24]. Before every experiment, both the chamber and the beads were washed with 10 mg/ml bovine serum albumin (BSA) to prevent non-specific interactions between the beads and glass surfaces. Experiments were conducted in a buffer solution (150 mM NaCl, 10 mM Tris and 1 mM EDTA, pH 8.0) in which the overstretch transition of dsDNA is expected to occur at 65 pN [25].

At the beginning of an experiment, the flow cell was positioned such that the traps were close to the interface between streams and only one type of beads was present in the field of view. After trapping one of the microspheres with a holographic trap, the chamber was moved up-/downwards, past the interface, to trap the other type of bead in a second holographic trap. Finally, the flow was stopped and the sample chamber repositioned so that the two trapped beads were in a region free of other beads. The two trapped microspheres were brought in proximity to enable the formation of the biotin-streptavidin interaction. (The 2- and 3-μm particles used in these experiments facilitated close approach of the two bead surfaces while maintaining a relatively large separation between the traps.) Tethers were detected by the tension-induced displacement of particles from the trap centres. In the HOT instrument, many tethers lasted only tens of seconds, much shorter lifetimes than in the single-beam optical tweezers instrument. This lifetime shortening was due to the higher power 1064 nm laser and could be improved by adding an oxygen scavenging system (PCA/PCD) to the sample [20].

Tethered DNA molecules were stretched stepwise using predetermined kinoforms, as described above. Camera images were analysed to obtain the positions of the particles and the offset of the particle from trap 1 as a function of time. Unless otherwise specified, the end-to-end extension of DNA, $z(t)$, was determined in each image using the positions of each particle relative to its initial position $(x_1(t), x_2(t))$, plus a fixed offset $x_0$: $z(t) = x_2(t) - x_1(t) + x_0$. The force applied to the bead in trap 1 (equal in magnitude to the tension in the DNA) was determined from $F_1(t) = -\kappa_1 x_1(t) + F_0$. The force and displacement offsets, constant for a given tether, are necessary because our correlation algorithm provides the position of each particle relative to its position in an initial reference template image, not an absolute position measurement [6].

Force-extension curves of DNA molecules were fit with the inextensible worm-like chain (WLC) model of entropic elasticity [26, 27]:

$$F(z) = \frac{k_B T}{L_p}\left[\frac{1}{4\left(1-\frac{z}{L_c}\right)^2} + \frac{z}{L_c} - \frac{1}{4}\right]. \quad (1)$$

$L_c$ is the contour length of the DNA (in our case 3.96 μm), $L_p$ is its persistence length, $k_B$ is Boltzmann's constant and $T$ is the absolute temperature. $L_p$ and the offsets $x_0$ and $F_0$ are the fitting parameters used for each experimental force-extension curve. There is a strong interdependence among these three parameters, particularly evident when fitting a limited number of $F$-$z$ data points as from our HOT measurements. Thus, an estimate of $x_0$ and $F_0$ was first obtained by setting $L_p = 53$ nm; using these values as initial guesses for a least-squares fit, $x_0$, $F_0$ and $L_p$ were allowed to vary to best fit the available data. DNA's force-extension behaviour is known to deviate from the inextensible WLC model at high forces [28], and so fits reported here were performed to data points below 5 pN.

For determinations of the residuals between the experimental HOT $F - z$ data and a WLC fit, only $x_0$ and $F_0$ were allowed to vary in fitting each curve, while $L_c = 3.96$ μm and $L_p = 45$ nm were held fixed. (This value of $L_p$ was used for consistency with the average value found for this sequence of DNA in our single-beam optical tweezers instrument.) The point of this analysis was to quantify observed modulations, and thus it was important to compare the measurements to the same model, even if this did not represent the best fit for each curve that would have been obtained by allowing $L_p$ to vary.

## 3. Results and discussion

### 3.1 Stretching DNA to high force

Supplementary Movie 1 shows a DNA stretching experiment with three stretches and relaxations. Still images from such an experiment are shown as the figure in the abstract to this article (with a schematic of a tethered DNA molecule superposed for illustrative purposes). Figure 4 shows a plot of each bead's position as a function of time as a DNA molecule is stretched, with the tether breaking at the end of this experiment. The regions of different slope are due to the difference in step sizes chosen for sampling different regions of the force-extension curve. As trap 2 is steered and the DNA stretched, the gradual displacement of particle 1 from the stationary trap is

 

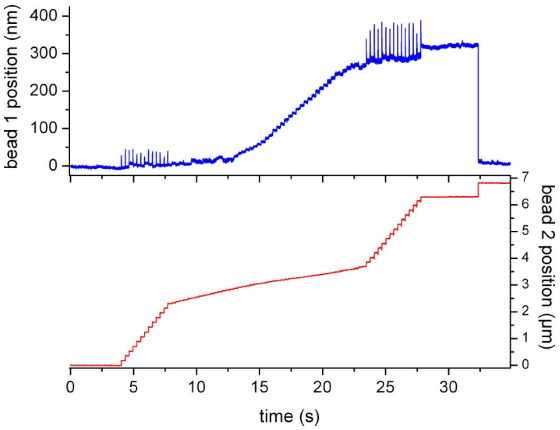


**Figure 4** (online color at: www.biophotonics-journal.org) Bead positions vs. time as obtained from high-speed camera images for the bead in trap 1 (top) and the bead in trap 2 (bottom), from a representative DNA stretching experiment. The different position scales arise because trap 2 is being steered.

clear (10–22 s), indicating increasing applied force, as is its approximately constant displacement during the overstretch transition (22–30 s). An additional feature is also apparent in these data: beads displace substantially during the update of a trap position (seen by the spikes in the trace of particle 1; particle 2 experiences displacements of similar magnitude, not seen because of the scaling in Figure 4). This effect has been noted previously for HOT traps [29] and is discussed more, below. In our experiments, particle excursions were greater for larger steps of trap 2, so could be minimized by using smaller step sizes, if desired. To ensure these dynamics were excluded from our analysis, the average particle positions for each kinoform were determined using only the central 60% of the data at each extension (66 data points).

The average positions of the trapped particles, as determined from video tracking, were used to determine the end-to-end extension of the DNA, $z$, and the force, $F$, required to attain this extension, as described in the Methods Section. A representative force-extension curve of DNA, recorded in our HOT instrument, is shown in Figure 5. This shows the expected WLC response at low forces, followed by the characteristic overstretch transition at 65 pN. The appearance of the plateau at 65 pN demonstrates that the calibrated trap stiffness from the power spectrum of thermally induced motion is valid to forces of at least 65 pN. For these experiments with a trap stiffness of $\kappa_1 = 250$ pN/μm, our results demonstrate that 2.10-μm-diameter particles in stiff HOT traps experience a harmonic potential out to displacements of at least 260 nm.

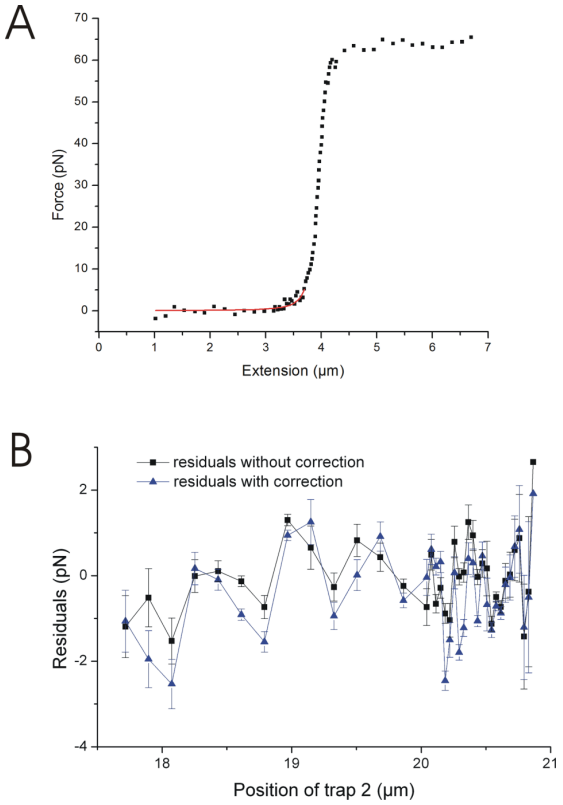


**Figure 5** (online color at: www.biophotonics-journal.org) **A.** Representative force-extension curve of DNA, showing characteristic overstretch transition at 65 pN. Overlaid on the black data points is a WLC fit with $L_p = 45$ nm. The small number of data points involved in the fit below 5 pN results in large uncertainties of fitting parameters. If more information about this low-force region were desired, trap 2 could be stepped in smaller increments. **B.** Force residuals from WLC fits to $F$-$z$ data from 4 different molecules (7 curves) showing systematic deviation from expected values (black squares). The positions here correspond to the region <5 pN in plot a. Data points represent the mean values and error bars the standard errors of the means. Lines are a guide to the eye. Using a corrected position of trap 1, determined for each position of trap 2, the force residuals are altered but still display systematic modulations (blue triangles).

The spikes in Figure 4 correspond to updates of the position of trap 2. It is remarkable that the trapped particles are not lost during this refreshing of the SLM, particularly because of the significant tension in the DNA. Previous work showed that HOT traps can be repositioned in step sizes of a bead radius without losing the trapped particle, even in the presence of external flow [29]. The maximal forces exerted in that work were approximately 2 pN. Here, our results show that the trap position

Journal of
BIOPHOTONICS



can be changed in 177 nm steps and, for our system, the particles are retained in the traps even in the presence of 65 pN of force exerted through the DNA. Additionally, these results demonstrate that the 300 Hz trap modulations introduced by our SLM [6, 7] do not affect the ability of the HOT traps to maintain particles in the presence of high external force.

### 3.2 *Apparent force modulations*

Force-extension curves measured for DNA in our HOT instrument exhibit apparent force modulations (Figure 5), most clearly seen in the flatter portions of the curves. These appear to be systematic, as seen by the non-zero average force residuals between WLC fits and measured $F - z$ data. The modulations are not due to the DNA or beads used in these experiments. Figure 6 shows an example of a force-extension curve recorded for DNA from the same sample, immobilized using beads from the same preparation, stretched in our single-beam optical tweezers instrument. It is clear that this measurement shows the expected WLC behaviour at low forces, and furthermore, exhibits the overstretch plateau at 65 pN, as expected. Thus, the modulations observed in the HOT measurements are specific to that instrument.

We sought to account for these small, yet systematic, modulations by examining our assumptions of a stationary trap 1 and of constant trap 1 stiffness.

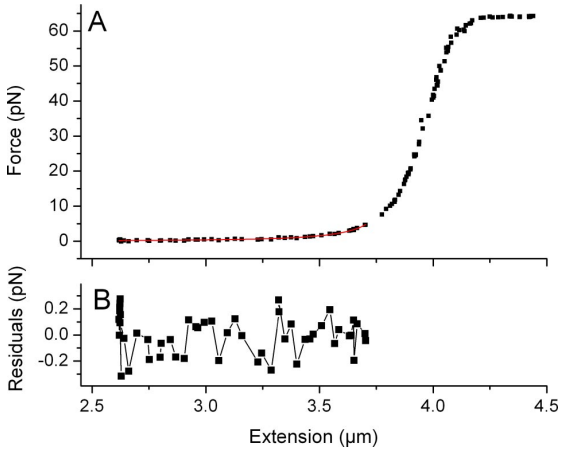


**Figure 6** (online color at: www.biophotonics-journal.org) **A.** Representative force-extension curve of DNA recorded in our single-beam optical tweezers instrument, showing the WLC fit to the data ($L_p = 48$ nm). **B.** Residuals of force from this WLC fit, which are much smaller than for the HOT stretching data. Lines are a guide to the eye.

If either of these values changed during a stretching experiment, we would miscalculate the true force, since forces are determined from $F_1(t) = -\kappa_1 \, \Delta x_1(t)$.

Close examination of Figure 4 reveals discontinuous changes in the position of trap 1 throughout the experiment, an effect particularly perceptible in the flatter portions of the curve. To determine the extent of this movement, we performed separate experiments using the same kinoforms, in which a 2.10 μm particle was trapped in trap 1. An "empty" trap 2 was then stepped alternately between its maximum separation from trap 1 and intermediate positions, to minimize contributions of drift to these measurements [6], and the mean position of the bead in trap 1 at each position of trap 2 was determined from image analysis. As seen in Figure 7, deviations of these mean positions from the overall average position are small (<6 nm) but reproducible. They are apparent in both $x$ and $y$ directions, although the deviations in the direction perpendicular to trap steering are considerably smaller than in the parallel direction. Using the "corrected" trap 1 positions for each kinoforms (Figure 7), we recalculated the forces in our DNA measurements. While slightly changing the $F$-$z$ curve, a systematic deviation in force residuals of the same order as before correction remained (Figure 5b).

We also investigated whether the apparent modulations in force arose from significant changes in trap stiffness in trap 1 as trap 2 was steered. Based on our previous work, this was not expected, but the

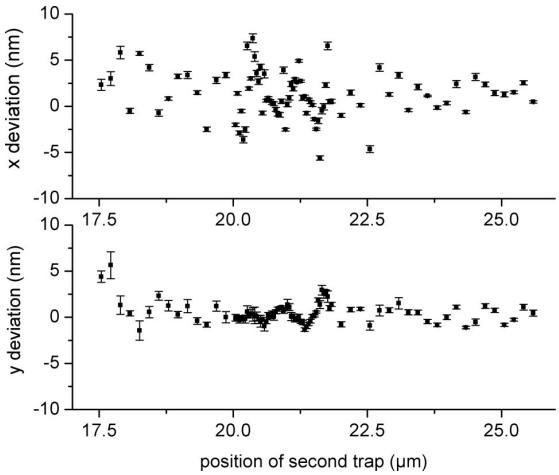


**Figure 7** The position of the particle in trap 1 versus the $x$ position of trap 2. Plotted are the deviations of the mean positions from the overall average position for particle 1 in both $x$ (top) and $y$ (bottom) directions. The error bars indicate the standard deviation ($N = 8$). Systematic deviations in both directions from the mean position are observed, even though trap 2 is steered only in the $x$ direction.

 

positions used here brought the particles closer to each other than we had previously studied [6]. We performed power spectrum measurements of a 2.10 μm particle held in trap 1 with positions of trap 2 corresponding to the maximum and minimum positions of trap 1 measured in Figure 7 (20.4 μm and 21.6 μm, respectively). The calibrated stiffness values differed by only 2% (data not shown), an insignificant change.

It is possible that the modulations arise from out-of-plane motion of particle 1: the correlation algorithm we use is designed to track particle positions in the ($x$, $y$) plane only. Out-of-plane motion, along the optic axis, could result in perceived motion in the ($x$, $y$) plane, resulting in a measured apparent displacement of the trapped particle. In these measurements, with DNA stretched in the $x$ direction, out-of-plane motion would arise from the shift of the traps along the optic axis. This should be accounted for by correcting the position of trap 1 (Figure 7). Furthermore, if the DNA were being stretched increasingly out of the ($x$, $y$) plane, the $z$-offset of a bead should change monotonically with increasing trap separation, not in an oscillatory fashion. This monotonic axial displacement was observed for some tethers, as seen in Supplementary Movie 1, though was generally most apparent immediately before losing the particle from the trap.

The most likely source of the observed modulations is interference between the two holographic traps [A. Farré et al., manuscript in preparation]. Work with two non-holographic optical traps found that even with orthogonally polarized beams, a 2% cross-talk between beams existed, giving rise to changes in intensity and light distribution within the two traps [13]. This resulted in modulations in trap positions on the order of 1 nm for traps separated by >500 nm, which increased to 5 nm as the traps approached closer. Presumably, such interference effects would be more evident with both traps having the same polarization, as in our case of phase-modulated HOT traps created with the same SLM. It is therefore somewhat surprising, although pleasantly so, that the modulations we observe here are only on the order of ∼6 nm, and were only on the order of <2 nm for previous work with traps separated by distances of ∼9 μm [6].

## 4. Conclusions

These studies have conclusively shown that calibrated high forces (>65 pN) are attainable with SLM-based holographic optical tweezers. In our setup, this demonstrates that HOT traps are harmonic out to displacements of >250 nm for 2.10 μm trapped particles. Furthermore, even though high forces are exerted on the trapped particles through DNA tension, particles are not lost from the HOT traps as trapping kinoforms are updated on the SLM.

The maximal laser power, and hence trap stiffness, are limited by the damage threshold of the SLM. The trap stiffness ($\kappa \sim 250$ pN/μm) we have used here is a factor of three higher than previous maximum stiffnesses reported for HOT traps [3, 6]. In principle, for single-molecule stretching experiments, two traps of different stiffness could be created, providing one trap of higher stiffness than we have used (and thereby increasing the maximum force obtainable within the harmonic region), but this was unnecessary for the present work.

We observed small (<2 pN) but systematic modulations in apparent force applied to the DNA as a function of particle separation. This is likely due to optical interference between holographic traps, which can result in changes of the equilibrium position of particles by ∼5 nm, but is not manifest as changes in trap stiffness. While these modulations are undesired, they are small when compared with force and length scales for measurements of soft biomaterials [30] and thus should not prove problematic for application of this technique to quantitative high-force measurements.

**Acknowledgements** We thank Andrew Wieczorek for assistance developing the pNPP assay. This work is supported by a Discovery Grant from the Natural Sciences and Engineering Research Council of Canada (NSERC), funding from the Canada Foundation for Innovation (CFI) and from the Human Frontier Science Program (HFSP). AF is sponsored by a doctoral research fellowship from the Generalitat de Catalunya (grant FI). BPBD thanks NSERC and the Michael Smith Foundation for Health Research (MSFHR) for fellowship support. NRF is a Cottrell Scholar of the Research Corporation and an MSFHR Scholar.

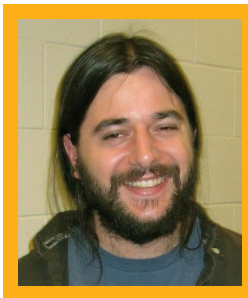

**Arnau Farré** obtained his B.Sc. in Physics from the Universitat de Barcelona (Spain) in 2007 and his M.Sc. in Biophysics from the same university in 2008. He is currently a Ph.D. student in the field of optical tweezers and biological applications in the Optical Trapping Lab – Grup de Biofotònica at the Universitat de Barcelona (UB). During the first semester of 2009, Mr. Farré worked in the Department of Physics at Simon Fraser University, where he carried out the present work.

Journal of
BIOPHOTONICS



**Astrid van der Horst** did her Ph.D. research on optical trapping both in the Bio-Assembly and Organization group of Marileen Dogterom at the FOM-Institute for Atomic and Molecular Physics (AMOLF) in Amsterdam and in the Soft Condensed Matter group of Alfons van Blaaderen at Utrecht University, the Netherlands. She was a postdoctoral researcher at Simon Fraser University from 2006–2009 and currently holds a 3-year postdoctoral fellowship from the Foundation for Fundamental Research on Matter (FOM) at the VU University in Amsterdam.

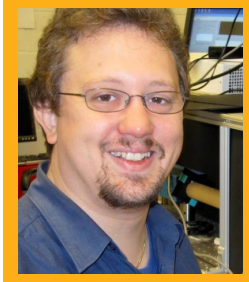

**Gerhard Blab** obtained his Dipl.-Ing. in Biophysics from the Johannes Kepler University in Linz, Austria and his Ph.D. in Physics from Leiden University in the Netherlands. He currently works as a postdoctoral researcher at Simon Fraser University.

**Benjamin Downing** obtained his B.Sc. in Physics from Dalhousie University. He is currently an M.Sc. student in the Department of Physics at Simon Fraser University.

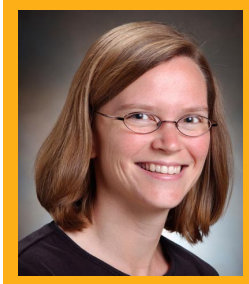

**Nancy Forde** obtained her B.Sc. in Chemical Physics from the University of Toronto, her Ph.D. in Chemistry from the University of Chicago, and was a postdoctoral researcher and HHMI associate with Carlos Bustamante at UC Berkeley. She has been a faculty member in the Department of Physics at Simon Fraser University since 2004, where she leads an interdisciplinary biophysics research group.

## References

[1] K. Dholakia, P. Reece, and M. Gu, Chem. Soc. Rev. **37**, 42 (2008).
[2] D. G. Grier, Nature **424**, 810 (2003).
[3] C. O. Mejean, A. W. Schaefer, E. A. Millman, P. Forscher, and E. R. Dufresne, Opt. Express **17**, 6209 (2009).
[4] G. Sinclair, J. Leach, P. Jordan, G. Gibson, E. Yao, Z. Laczik, M. Padgett, and J. Courtial, Opt. Express **12**, 1665 (2004).
[5] J. Xia and H. Yin, Opt. Eng. **48**, 020502 (2009).
[6] A. van der Horst and N. R. Forde, Opt. Express **16**, 20987 (2008).
[7] A. van der Horst, B. P. B. Downing, and N. R. Forde, in Optical Trapping Applications (Optical Society of America, Washington, DC, 2009), p. OMB3.
[8] F. Belloni, S. Monneret, F. Monduc, and M. Scordia, Opt. Express **16**, 9011 (2008).
[9] L. Ikin, D. M. Carberry, G. M. Gibson, M. J. Padgett, and M. J. Miles, New J. Phys., 023012 (2009).
[10] W. J. Greenleaf, M. T. Woodside, E. A. Abbondanzieri, and S. M. Block, Phys. Rev. Lett. **95**, 208102 (2005).
[11] K. C. Neuman and S. M. Block, Rev. Sci. Instrum. **75**, 2787 (2004).
[12] G. J. L. Wuite, R. J. Davenport, A. Rappaport, and C. Bustamante, Biophys. J. **79**, 1155 (2000).
[13] C. Bustamante, Y. R. Chemla, and J. R. Moffitt, Cold Spring Harbor Protocols **2009**, doi:10.1101/pdb.ip73 (2009).
[14] C. Bustamante, Z. Bryant, and S. B. Smith, Nature **421**, 423 (2003).
[15] J. van Mameren, P. Gross, G. Farge, P. Hooijman, M. Modesti, M. Falkenberg, G. J. L. Wuite, and E. J. G. Peterman, Proc. Nat. Acad. Sci. USA **106**, 18231 (2009).
[16] J. P. Rickgauer, D. N. Fuller, and D. E. Smith, Biophys. J. **91**, 4253 (2006).
[17] D. R. Burnham and D. McGloin, Opt. Express **14**, 4175 (2006).
[18] K. D. Wulff, D. G. Cole, R. L. Clark, R. DiLeonardo, J. Leach, J. Cooper, G. Gibson, and M. J. Padgett, Opt. Express **14**, 4169 (2006).
[19] W. P. Wong and K. Halvorsen, Opt. Express **14**, 12517 (2006).
[20] M. P. Landry, P. M. McCall, Z. Qi, and Y. R. Chemla, Biophys. J. **97**, 2128 (2009).
[21] Y. Deng, J. Bechhoefer, and N. R. Forde, J. Opt. A: Pure. Appl. Opt. **8**, S256 (2007).
[22] B. P. B. Downing, A. van der Horst, M. Miao, F. W. Keeley, and N. R. Forde, in Optical Trapping Applications (Optical Society of America, Washington, DC, 2009), p. OTuA3.
[23] R. J. Davenport, G. J. L. Wuite, R. Landick, and C. Bustamante, Science **287**, 2497 (2000).
[24] L. R. Brewer and P. R. Bianco, Nat. Meth. **5**, 517 (2008).
[25] S. B. Smith, Y. J. Cui, and C. Bustamante, Science **271**, 795 (1996).

 

[26] C. Bustamante, J. F. Marko, E. D. Siggia, and S. Smith, Science **265**, 1599 (1994).
[27] J. F. Marko and E. D. Siggia, Macromol. **28**, 8759 (1995).
[28] C. Bouchiat, M. D. Wang, J. F. Allemand, T. Strick, S. M. Block, and V. Croquette, Biophys. J. **76**, 409 (1999).
[29] E. Eriksson, S. Keen, J. Leach, M. Goksör, and M. J. Padgett, Opt. Express **15**, 18268 (2007).
[30] G. Lenormand, S. Henon, A. Richert, J. Simeon, and F. Gallet, Biophys. J. **81**, 43 (2001).

# Positional stability of holographic optical traps

Arnau Farré, Marjan Shayegan, Carol López-Quesada, Gerhard A. Blab, Mario Montes-Usategui, Nancy R. Forde, and Estela Martín-Badosa

Optics Express
Vol. 19, 21370-21384 (2011)

# Positional stability of holographic optical traps

**Arnau Farré,[1] Marjan Shayegan,[2] Carol López-Quesada,[1] Gerhard A. Blab,[3,4] Mario Montes-Usategui,[1] Nancy R. Forde,[3] Estela Martín-Badosa[1,*]**

[1]*Optical Trapping Lab – Grup de Biofotònica, Departament de Física Aplicada i Òptica, Universitat de Barcelona, Martí i Franquès, 1 08028 Barcelona, Spain*

[2]*Department of Chemistry, Simon Fraser University, 8888 University Drive, Burnaby, British Columbia, V5A 1S6, Canada*

[3]*Department of Physics, Simon Fraser University, 8888 University Drive, Burnaby, British Columbia, V5A 1S6, Canada*

[4]*Current address: Molecular Biophysics, Universiteit Utrecht, Postbus 80000, 3508 TA Utrecht, The Netherlands*

**estela.martinb@ub.edu*

**Abstract:** The potential of digital holography for complex manipulation of micron-sized particles with optical tweezers has been clearly demonstrated. By contrast, its use in quantitative experiments has been rather limited, partly due to fluctuations introduced by the spatial light modulator (SLM) that displays the kinoforms. This is an important issue when high temporal or spatial stability is a concern. We have investigated the performance of both an analog-addressed and a digitally-addressed SLM, measuring the phase fluctuations of the modulated beam and evaluating the resulting positional stability of a holographic trap. We show that, despite imparting a more unstable modulation to the wavefront, our digitally-addressed SLM generates optical traps in the sample plane stable enough for most applications. We further show that traps produced by the analog-addressed SLM exhibit a superior pointing stability, better than 1 nm, which is comparable to that of non-holographic tweezers. These results suggest a means to implement precision force measurement experiments with holographic optical tweezers (HOTs).



**OCIS codes**: (140.7010) Laser trapping; (170.4520) Optical confinement and manipulation; (230.6120) Spatial light modulators; (350.4855) Optical tweezers.

## References and links

1. Y. Hayasaki, M. Itoh, T. Yatagai, and N. Nishida, "Nonmechanical optical manipulation of microparticle using spatial light modulator," Opt. Rev. **6**(1), 24–27 (1999).
2. D. G. Grier, "A revolution in optical manipulation," Nature **424**(6950), 810–816 (2003).
3. A. Jesacher, S. Fürhapter, S. Bernet, and M. Ritsch-Marte, "Size selective trapping with optical "cogwheel" tweezers," Opt. Express **12**(17), 4129–4135 (2004).
4. T. Čižmár, M. Mazilu, and K. Dholakia, "In situ wavefront correction and its application to micromanipulation," Nat. Photonics **4**(6), 388–394 (2010).
5. K. Dholakia and T. Cizmar, "Shaping the future of manipulation," Nat. Photonics **5**(6), 335–342 (2011).
6. E. R. Dufresne and D. G. Grier, "Optical tweezer array and optical substrates created with diffractive optics," Rev. Sci. Instrum. **69**(5), 1974–1977 (1998).
7. J. E. Curtis, B. A. Koss, and D. G. Grier, "Dynamic holographic optical tweezers," Opt. Commun. **207**(1-6), 169–175 (2002).
8. R. Di Leonardo, F. Ianni, and G. Ruocco, "Computer generation of optimal holograms for optical trap arrays," Opt. Express **15**(4), 1913–1922 (2007).
9. P. Yeh and C. Gu, *Optics of Liquid Crystal Displays* (John Wiley & Sons Inc., 2009).
10. M. Reicherter, T. Haist, E. U. Wagemann, and H. J. Tiziani, "Optical particle trapping with computer-generated holograms written on a liquid-crystal display," Opt. Lett. **24**(9), 608–610 (1999).
11. A. van der Horst and N. R. Forde, "Calibration of dynamic holographic optical tweezers for force measurements on biomaterials," Opt. Express **16**(25), 20987–21003 (2008).
12. A. van der Horst, B. P. B. Downing, and N. R. Forde, "Position and intensity modulations in holographic optical traps created by a liquid crystal spatial light modulator," in *Optical Trapping Applications*, Vol. 1 of 2009 OSA Technical Digest (CD) (Optical Society of America, 2009), paper OMB3.

#151453 - $15.00 USD Received 21 Jul 2011; revised 17 Sep 2011; accepted 17 Sep 2011; published 13 Oct 2011

13. C. O. Mejean, A. W. Schaefer, E. A. Millman, P. Forscher, and E. R. Dufresne, "Multiplexed force measurements on live cells with holographic optical tweezers," Opt. Express **17**(8), 6209–6217 (2009).
14. A. Farré, A. van der Horst, G. A. Blab, B. P. B. Downing, and N. R. Forde, "Stretching single DNA molecules to demonstrate high-force capabilities of holographic optical tweezers," J. Biophotonics **3**(4), 224–233 (2010).
15. L. T. McLane, K. M. Carroll, J. Scrimgeour, M. D. Bedoya, A. Kramer, and J. E. Curtis, "Force measurements with a translating holographic optical trap," Proc. SPIE **7762**, 77621J, 77621J-10 (2010).
16. J. R. Moffitt, Y. R. Chemla, S. B. Smith, and C. Bustamante, "Recent advances in optical tweezers," Annu. Rev. Biochem. **77**(1), 205–228 (2008).
17. S. Serati and J. Harriman, "Spatial light modulator considerations for beam control in optical manipulation applications," Proc. SPIE **6326**, 63262W, 63262W-11 (2006).
18. A. Hermerschmidt, S. Osten, S. Krüger, and T. Blümel, "Wave front generation using a phase-only modulating liquid-crystal-based micro-display with HDTV resolution," Proc. SPIE **6584**, 65840E, 65840E-10 (2007).
19. J. R. Moore, N. Collings, W. A. Crossland, A. B. Davey, M. Evans, A. M. Jeziorska, M. Komarcevic, R. J. Parker, T. D. Wilkinson, and H. Xu, "The silicon backplane design for an LCOS polarization-insensitive phase hologram SLM," IEEE Photon. Technol. Lett. **20**(1), 60–62 (2008).
20. A. Lizana, A. Márquez, L. Lobato, Y. Rodange, I. Moreno, C. Iemmi, and J. Campos, "The minimum Euclidean distance principle applied to improve the modulation diffraction efficiency in digitally controlled spatial light modulators," Opt. Express **18**(10), 10581–10593 (2010).
21. E. Eriksson, S. Keen, J. Leach, M. Goksör, and M. J. Padgett, "The effect of external forces on discrete motion within holographic optical tweezers," Opt. Express **15**(26), 18268–18274 (2007).
22. M. Persson, D. Engström, A. Frank, J. Backsten, J. Bengtsson, and M. Goksör, "Minimizing intensity fluctuations in dynamic holographic optical tweezers by restricted phase change," Opt. Express **18**(11), 11250–11263 (2010).
23. D. J. McKnight, "Continuous view of dc-balanced images on a ferroelectric liquid-crystal spatial light modulator," Opt. Lett. **19**(18), 1471–1473 (1994).
24. A. Farré, C. López-Quesada, J. Andilla, E. Martín-Badosa, and M. Montes-Usategui, "Holographic optical manipulation of motor-driven membranous structures in living NG-108 cells," Opt. Eng. **49**(8), 085801 (2010).
25. I. Moreno, A. Lizana, A. Márquez, C. Iemmi, E. Fernández, J. Campos, and M. J. Yzuel, "Time fluctuations of the phase modulation in a liquid crystal on silicon display: characterization and effects in diffractive optics," Opt. Express **16**(21), 16711–16722 (2008).
26. F. Li, N. Mukohzaka, N. Yoshida, Y. Igasaki, H. Toyoda, T. Inoue, Y. Kobayashi, and T. Hara, "Phase modulation characteristics analysis of optically-addressed parallel-aligned nematic liquid crystal phase-only spatial light modulator combined with a liquid crystal display," Opt. Rev. **5**(3), 174–178 (1998).
27. Hamamatsu Photonics K. K., LCOS-SLM X10468 series -LC driving system- 2010.
28. K. Berg-Sørensen, L. Oddershede, E.-L. Florin, and H. Flyvbjerg, "Unintended filtering in a typical photodiode detection system for optical tweezers," J. Appl. Phys. **93**(6), 3167–3176 (2003).
29. S. F. Tolić-Nørrelykke, E. Schäffer, J. Howard, F. S. Pavone, F. Jülicher, and H. Flyvbjerg, "Calibration of optical tweezers with positional detection in the back focal plane," Rev. Sci. Instrum. **77**(10), 103101 (2006).
30. A. van der Horst and N. R. Forde, "Power spectral analysis for optical trap stiffness calibration from high-speed camera position detection with limited bandwidth," Opt. Express **18**(8), 7670–7677 (2010).
31. E. A. Abbondanzieri, W. J. Greenleaf, J. W. Shaevitz, R. Landick, and S. M. Block, "Direct observation of base-pair stepping by RNA polymerase," Nature **438**(7067), 460–465 (2005).
32. L. Nugent-Glandorf and T. T. Perkins, "Measuring 0.1-nm motion in 1 ms in an optical microscope with differential back-focal-plane detection," Opt. Lett. **29**(22), 2611–2613 (2004).
33. Y. Deng, J. Bechhoefer, and N. R. Forde, "Brownian motion in a modulated optical trap," J. Opt. A, Pure Appl. Opt. **9**(8), S256–S263 (2007).
34. K. Berg-Sørensen and H. Flyvbjerg, "Power spectrum analysis for optical tweezers," Rev. Sci. Instrum. **75**(3), 594–612 (2004).

## 1. Introduction

Since proposed in the late 1990s [1], the capabilities of holographic technology to precisely modulate the light of an optical trap in real time have awoken the interest of the optical trapping community. Holographic optical tweezers (HOTs) provide a powerful means to dynamically generate exotic beam shapes or complex 3D patterns of light foci for a wide variety of manipulation experiments [2–5].

The use of diffractive elements to split a laser beam into arrays of traps was first implemented by Dufresne and Grier [6]. A desired pattern of traps was obtained by placing a fixed, computer-generated hologram at a conjugate plane of the objective's entrance pupil. An improvement of this basic idea quickly followed with the introduction of a spatial light modulator (SLM) into the beam path. A phase kinoform on the liquid crystal (LC) display could be updated at video rate, which translated into real-time control of several traps

#151453 - $15.00 USD Received 21 Jul 2011; revised 17 Sep 2011; accepted 17 Sep 2011; published 13 Oct 2011

independently [7]. Different strategies to compute these kinoforms at high rates have been reported and a wide choice of algorithms that optimize several performance metrics is currently available [5,8].

Parallel nematic liquid crystal SLMs provide a simple way to modulate light, since they allow a precise phase modulation of the incident beam without changing its amplitude [9]. The molecules of the liquid crystal tilt in response to an applied voltage, so the extraordinary refractive index of the material and therefore the phase of the beam can be controlled at each pixel. Independent voltages are sent to the display in the form of a two-dimensional gray-level mask [9], which contains Fourier transform information of the desired pattern of traps [10].

The dynamic modulation of the light provided by the SLM can however introduce undesired temporal fluctuations in both the phase and the intensity of the beam, and can ultimately degrade the trap performance [11,12]. Although holographic traps have been used for force measurements [13–15], their use could arguably compromise the reliability of quantitative experiments when accuracy and stability are key [16].

The phase of the reflected beam in a phase-only SLM is controlled solely by the orientation of the LC molecules, whose response is, in turn, dependent on the applied voltage and on the viscosity and elasticity of the liquid crystal mixture [17]. If the voltage is modulated quickly enough, the LC molecules sense only its average value, whereas modulations slower than the relaxation time of the LC (determined by its viscosity and elasticity) are followed by the molecules, resulting in a time-dependent phase flicker [17–20].

Unfortunately, SLMs typically require the application of a time-varying voltage to operate. One timescale involves the refresh frequency of the kinoform displayed on the LC (generally at video rate), which makes the display turn off for a short period of time and back on [21,22]. More importantly, because charge accumulation on the LC walls occurs with DC voltages, degrading device performance [23], the applied voltage must change sign (typically at hundreds of Hertz within each refresh period). This modulation can lead to modulation of the phase, with differences in LC response depending on whether the modulator is digitally or analog-addressed [19].

In analog-addressed SLMs, the molecules are subjected only to the charge-balancing switching of the driving voltage. In this case, the amplitude of the signal, the parameter that controls the tilt angle of the LC molecules, can take on continuous values within an operating voltage range. By contrast, digitally-addressed SLMs are binary in nature, and require a more complex mechanism to modify the signal amplitude, which considerably increases the fluctuations inside the LC cell [19]. Digital backplanes provide exclusively two different voltage levels and any intermediate value must be achieved through pulse-width modulation (PWM). In PWM a combination of square waves of varying duration is used within each refresh period to obtain a mean voltage equivalent to the analog value required by the LC to provide the desired phase change.

Here, we provide evidence that the use of digital technology for driving the SLM can result in lower stability of the phase, and ultimately in a lower trap pointing stability than analog addressing. However, even in this case, the use of appropriate addressing schemes can reduce the spatial instability of holographic tweezers to acceptable levels.

Finally and most importantly, we show that the resulting stability of holographic traps generated by analog-addressed SLMs is comparable to conventional, non-holographic tweezers. This suggests the capability of holographic traps for precision force measurements and their potential application to important new fields of research.

## 2. Experimental setup

We carried out two sets of experiments to study the time-dependent stability of laser beams modulated by SLMs: we first analyzed the stability of the phase delay introduced by the modulators, and, then, we measured the influence of this on the trap position, through the analysis of the motion of holographically trapped particles.

#151453 - $15.00 USD Received 21 Jul 2011; revised 17 Sep 2011; accepted 17 Sep 2011; published 13 Oct 2011

The experiments were conducted using two different holographic optical tweezers setups, one at Simon Fraser University (Canada) and the other at the University of Barcelona (Spain) [11,24]. Infrared (1064 nm) lasers (J20-BL-106C Spectra Physics and YLM-5 IPG Photonics) and liquid-crystal-on-silicon (LCoS) phase-only SLMs (HEO 1080P Holoeye and X10468-03 Hamamatsu) were used. The Holoeye device is a digitally-addressed SLM whereas the Hamamatsu modulator uses analog addressing circuitry.

We have compared the results from three different SLM settings. The Holoeye SLM offers the possibility of selecting several programmable addressing schemes, which differ in their addressing frequencies and in the number of available gray levels (phase levels). Therefore, in addition to the measurements with the analog Hamamatsu SLM (256 gray levels), we studied two different digital addressing sequences of the HoloEye SLM, denoted by the manufacturer as 5-5 (192 gray levels) and 0-6 (64 gray levels), respectively [18]. Here, the first digit indicates the number of equally weighted bitplanes and the second digit indicates the number of binary elements in the addressing sequence.

### *2.1 Phase measurements*

There exist several alternatives for measuring the phase delay introduced by an SLM onto a laser beam [25]. We have used a straightforward method (see Appendix 1) that is appropriate for pure phase SLMs [26].

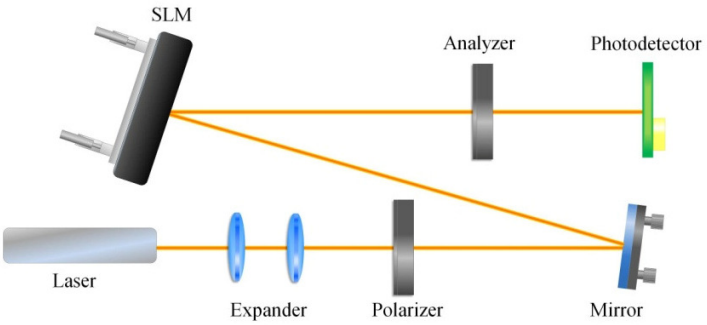


Fig. 1. Setup for phase measurements. Two polarizers at 45° and –45° with respect to the LC alignment direction are inserted before and after the SLM, respectively, and the intensity as read by the photodetector provides information on the phase fluctuations.

The setup is depicted in Fig. 1. Two polarizers at 45° and –45° with respect to the LC alignment direction were inserted before and after the SLM, respectively. The intensity, $I$, of the reflected light after the analyzer is related to the phase delay $\phi$ introduced by the modulator to the beam according to [26]:

$$I(\phi) = I_{offset} + I_0 \sin^2\left(\frac{\phi}{2}\right). \qquad (1)$$

Here, $I_{offset}$ and $I_0$ represent the minimum and amplitude of intensity modulations, respectively. A photodetector (QPD, QP154-Q-HVSD, Pacific Silicon Sensors; or PSD PDP90A, Thorlabs) was used to record the temporal fluctuation of this intensity at 15 kHz. The signal was measured for different constant gray levels, that is, for different phase delays imprinted on the SLM. (The mean phase delay introduced by a given gray level is given by the so-called "gamma curve" used for each SLM setting, discussed in Appendix 1). The measured intensities were used to determine the phase as a function of time via Eq. (1). Power spectra of the intensity were calculated, each as an average of 40 independent 1-second measurements.

#151453 - $15.00 USD Received 21 Jul 2011; revised 17 Sep 2011; accepted 17 Sep 2011; published 13 Oct 2011

*2.2 Bead position measurements*

Positional changes of the holographic traps were indirectly inferred from an analysis of the motion of trapped beads. As the information provided by back-focal-plane interferometry proved to be inconsistent (see Results and Discussion) we utilized high-speed camera tracking. Thus a CMOS camera (PCO, 1200 hs, 1280x1024 pixels, acquisition rate 2500 frames/sec) and a fast back-illuminated Electron Multiplying CCD camera (EM-CCD, Ixon-860, Andor Technologies, 128x128 pixels, acquisition rate ~1.2 kHz) were used to measure the fluctuations in position of a 2 μm diameter polystyrene bead held in a holographic trap.

A single holographic trap was generated offset by tens of microns in both $x$ and $y$ directions from the zero-order optical center. We used in the two setups the same kinoform, a phase ramp with deliberately different spatial frequencies in the two directions. Differences in position modulations in the $x$ and $y$ directions were found when using both SLMs. We focus our analysis on modulations in the $x$ direction, which were found to be larger, and discuss this further below.

## 3. Results and Discussion

We first analyzed the temporal stability of the phase of the modulated beam. This quantity is of fundamental importance to trap performance since it controls the trap position.

Examination of the phase versus time plots shows fluctuations for both analog- and digitally-addressed SLMs, with clearly larger modulations for the latter device (Fig. 2, left column). The amplitude of the flicker depends on the imposed gray level (phase delay), with the maximum amplitude of phase modulations occurring at a different phase value for each SLM and setting (Holoeye: gray level = 192, phase delay = 1.7π for 5-5 and gray level = 224, phase delay = 1.75π for 0-6; Hamamatsu: gray level = 64, phase delay = 1.2π), and flickering by as much as 0.31π and 0.16π for the 5-5 and the 0-6 settings, respectively, and $5 \cdot 10^{-4}\pi$ for the Hamamatsu. The larger phase fluctuations observed in our digitally-addressed modulator suggest that holographic traps generated with this SLM will suffer from a lower position stability. However, a large amplitude of phase modulations will not in and of itself cause modulations of trap position (Fig. 3a). Rather, it is the variation in amplitude (Fig. 3b) and/or temporal phase of the modulations among different gray levels that ultimately determines the spatial stability of the optical traps.

For a deeper analysis of temporal stability, we examined the signals with the largest amplitude of phase modulation for each SLM. We computed the power spectrum of the measured $I(\phi)$ signal to obtain information about the frequency dependence of the phase noise introduced by the modulator (Fig. 2, right column). For the analog-addressed device, the SLM introduces peaks at 240 Hz and 480 Hz (Fig. 2(a)), which, according to the manufacturer, correspond to the addressing frequencies of the SLM electronics [27]. For comparison, we included in this plot the spectrum of the laser alone. Its characteristic flat spectrum is affected by the noise introduced by the detector at higher frequencies (~6 kHz), and by the transparency of the silicon photodiode, which acts as a band-pass filter with $f_{3dB}$ = 6.7 kHz (close to that found by others [28]).

#151453 - $15.00 USD Received 21 Jul 2011; revised 17 Sep 2011; accepted 17 Sep 2011; published 13 Oct 2011

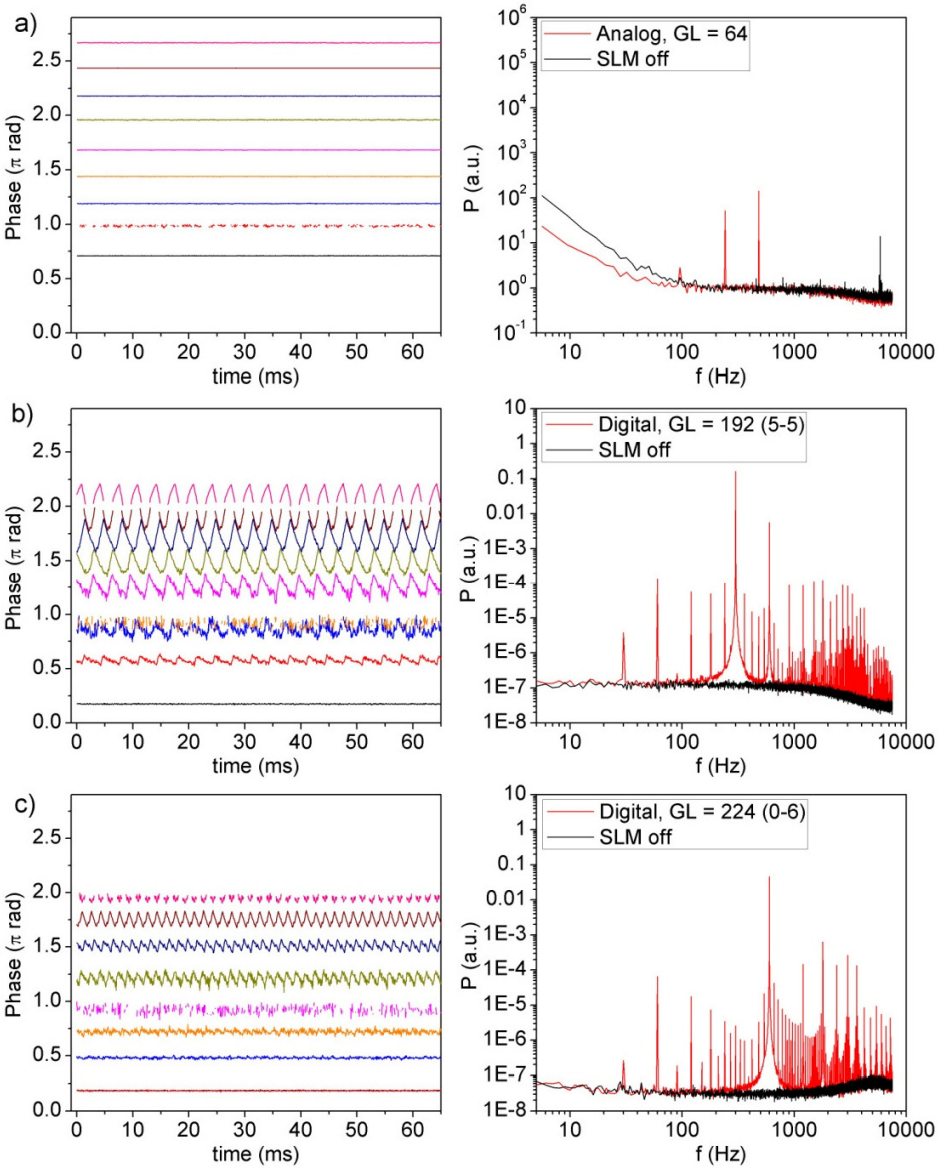


Fig. 2. Left column: phase variation as a function of time for (a) the analog-addressed SLM, (b) the 5-5 setting of the digitally-addressed SLM and (c) the 0-6 setting of the digitally-addressed SLM. In each plot, different curves correspond to different gray levels: 0 (bottom), 32, 64, 96, 128, 160, 192, 224 and 255 (top). Missing data points are due to the fact that Eq. (1) is fit to mean intensity values; therefore, measured intensities greater than ($I_{offset}$ + $I_0$) or less than $I_{offset}$ (resulting from phase delays of π and 2π, respectively) cannot be converted to phase delays. Right column: for each SLM setting, a power spectrum of the trace with the largest phase modulation shows the frequency dependence of $I(\phi)$ modulation.

Discrete frequency peaks also appear at the addressing frequency when using the digitally-addressed SLM ($f_0$ = 300 Hz for the 5-5 setting, and $f_0$ = 600 Hz for the 0-6 setting). In this case, however, the amplitude of the noise is considerably larger and, in addition to the

#151453 - $15.00 USD Received 21 Jul 2011; revised 17 Sep 2011; accepted 17 Sep 2011; published 13 Oct 2011

addressing frequency, oscillations also appear at 60 Hz, due to the display refresh, and overtones of both fundamental modes.

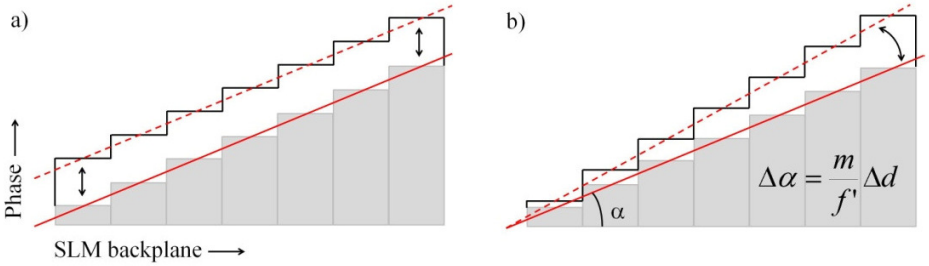


Fig. 3. (a) Phase modulations of equal amplitude that are synchronous will not change the phase gradient, maintaining the spatial frequency of the kinoform. In contrast, phase modulations that are asynchronous and/or (b) differ in amplitude can alter the phase gradient. In this schematic example, temporal variation of the angle $\alpha$ leads to a modulation of the trap position $d$, where $f'$ is the objective's focal length and $m$ is the magnification of the telescope used to image the SLM onto the objective's entrance pupil.

The large number of peaks at higher frequencies for the digitally-addressed SLM is associated with the pulse-width modulation of the driving voltage amplitude. In PWM, the time spent at each of the two voltages of the supplied digital signal is modulated to generate intermediate time-averaged voltages. Dwell times in each state are fractions of the address cycle time $1/f_0$ and give rise to higher frequency peaks in the power spectrum. The dominant timescale, however, is that of the fundamental mode, where modulation is slowest. At higher frequencies, the viscosity of the LC results in smaller amplitudes of LC molecule reorientation in response to voltage changes, and this gives rise to lower noise. This same effect makes the 0-6 setting, driven at a higher addressing frequency, more stable compared to the 5-5 setting (or to the 22-6 setting with $f_0$ = 120 Hz, as observed in [11]).

We next assessed how these phase fluctuations translated into trap position instabilities and how the latter depended on the SLM electronics and settings. In principle, trap positions can be measured directly by monitoring the back-reflection of laser foci from the coverslip of the trapping chamber. We previously used this method to characterize the position modulations of holographically created traps, but modulations in intensity and shape of the foci can reduce the accuracy of high-resolution tracking algorithms [12]. Instead, here we studied the motion of trapped particles as probes for the spatial and temporal modulations of these holographically created traps.

As shown in [29], any periodic perturbation dragging a trapped particle appears in the distinctive Lorentzian shape of the power spectrum as a single peak at the oscillation frequency. In particular, the perturbation introduced by the modulator shows up as multiple spikes at the addressing frequency and overtones [11]. The height of these peaks is intimately connected with the amplitude of the trap motion (see Appendix 2), thus providing a means to quantify the pointing stability.

In conventional optical tweezers, these stability measurements would be performed using back-focal-plane interferometry (BFPI) for position detection. The technique is popular due to its high temporal and spatial resolution for position tracking. However, previous results using HOTs [11] had warned us that the amplitude of the bead oscillation obtained from the height of power spectrum peaks may differ significantly from the direct observation of motion with a high-speed camera. The problem is related to the presence of other traps which can interfere, in and out of phase, with the light scattered by the trapped particle at the back focal plane of the collecting lens [12].

In order to prevent undesired interference, here we used a pinhole at a plane conjugate to the sample to eliminate spurious light entering the trapping chamber from zero and higher

#151453 - $15.00 USD Received 21 Jul 2011; revised 17 Sep 2011; accepted 17 Sep 2011; published 13 Oct 2011

diffraction orders. Despite this filtering, there are inconsistencies in our results, in which peaks appear in the BFPI power spectra that are not observed with high-speed camera tracking (both techniques with similar resolution) and the magnitudes of peak heights in the $x$ and $y$ directions are dependent on the presence of the pinhole. Furthermore, the height of the peaks at $f_0$ increased for increasing laser powers, indicating a larger relative motion of the trapped particle (see below), which is incongruous with the resulting stiffening of the trap.

In BFPI, deflection is normalized by intensity to give displacement, so modulations in intensity may manifest as measured changes in position. Furthermore, any slight temporal delay between acquisition of the deflection and intensity readings may result in convolution of the temporal fluctuations in these independent values, and may be a possible explanation for the failure of BFPI to capture correctly the position modulations of the holographic optical trap, as seen by comparison with high-speed camera imaging.

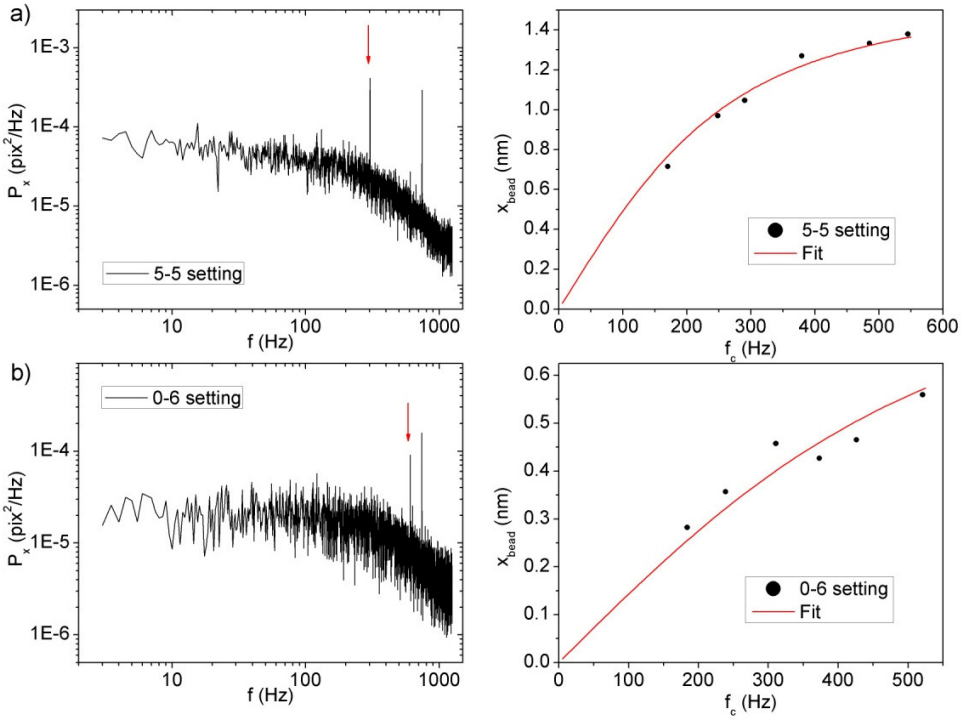


Fig. 4. Left column: power spectra of trapped bead position for different digitally-addressed SLM settings: (a) 5-5 and (b) 0-6. The SLM peak appears at $f_0$ = 300 Hz and $f_0$ = 600 Hz, respectively (red arrows). The peak at 742 Hz is caused by a fan in the high-speed camera. Right column: the amplitude of the oscillation obtained from the peak height is plotted for traps with different corner frequencies. The fit of Eq. (3) to the experimental results gives the trap motion, $x_0$.

Instead of BFPI, we therefore used high-speed cameras to provide a direct observation of trapped particle motion. We first present the results for the digitally-addressed SLM. A typical spectrum of a holographically trapped bead is shown in Fig. 4 for each addressing scheme (5-5 and 0-6). Peaks at 300 Hz and 600 Hz, respectively, appear as clear signatures of beam modulation. The spectra frequently exhibit only one peak, at the fundamental mode of the addressing frequency $f_0$, indicating that, despite all the noise observed in the phase plots (Fig. 2), the particle's motion is ultimately dominated by a pure sinusoidal modulation: $x_{trap}(t) = x_0 \sin(2\pi f_0 t)$.

The power spectrum of the bead's position in the purely sinusoidal case is [29]:

#151453 - $15.00 USD Received 21 Jul 2011; revised 17 Sep 2011; accepted 17 Sep 2011; published 13 Oct 2011

$$P = \frac{D/\pi^2}{f^2 + f_c^2} + \frac{x_{bead}^2}{2}\delta(f - f_0), \tag{2}$$

where $D$ is the bead's diffusion constant, $f_c$ is the trap roll-off frequency (proportional to trap stiffness), $\delta(f)$ is the Dirac delta function, and the amplitude of the bead oscillation, $x_{bead}$, is given by (see Appendix 2):

$$x_{bead} = \frac{x_0}{\sqrt{1 + f_0^2/f_c^2}}. \tag{3}$$

This equation shows that the response of the trapped particle is dependent upon the strength of the optical potential. Only when the laser power overcomes the viscous forces imposed by the surrounding fluid does the particle start to follow the trap, and phase fluctuations turn into position fluctuations. Moreover, the existence of a closed mathematical relation between the trap strength and the bead motion provides a means to verify that the cause underlying the appearance of noise in the power spectra is from actual trap movements, and is also a way to determine the trap oscillation amplitude, $x_0$.

The height of the peak at $f_0$ in each power spectrum was used to obtain an experimental measurement of $x_{bead}$ (Appendix 2):

$$x_{bead} = \sqrt{2(P_{Peak} - P_{therm})\cdot\Delta f}, \tag{4}$$

where $P_{peak}$ and $P_{therm}$ are as defined in Appendix 2. Each data point in Figs. 4(a) and 4(b), right column, is derived from one power spectrum, which is in turn the average of 40 measurements. The experiments were repeated to obtain $x_{bead}$ for traps with different corner frequencies, which were controlled by means of the laser power. The results are fit by Eq. (3) to obtain the value of $x_0$, as illustrated in Fig. 4. The value for the 5-5 setting, $x_0$ = 1.6 ± 0.3 nm, is in agreement with previous results [12], while for the 0-6 setting, we determined a smaller oscillation, $x_0$ = 0.8 ± 0.1 nm, consistent with the improvement seen in the phase measurements. Moreover, the good fit supports the model that the physical mechanism by which peaks show up in the spectra is indeed a physical oscillation of the trap. The error in $x_0$ corresponds to the standard deviation of $x_0$ values determined in this manner from measurements on three different beads.

The flicker of the analog-addressed modulator was, by contrast, barely detectable and therefore more difficult to quantify (Fig. 5(a)). Only for large laser powers did peaks appear in the power spectra, and even then, the perturbations were small. In order to assess the system resolution and, therefore, our capability to extract reliable results from these sensitive measurements, we introduced a controlled oscillation as a benchmark.

A piezo stage was used to drive these particle oscillations at a designated frequency, $f_{piezo}$ = 30Hz, and amplitude, $x_{piezo}$ = 20 nm. Simultaneously, the trapped bead was dragged by the fluctuating trap at 480 Hz. Figures 5(a) and 5(b) show two examples of power spectra determined from camera measurements, in which the SLM peak and the piezostage oscillation appear, respectively. In general, however, the two contributions do not appear simultaneously. The SLM effect is present only at high laser powers, when the elasticity of the trap is sufficiently high to drag along the particle, whereas the piezo oscillation becomes visible at low powers when the viscous drag from the fluid motion overcomes the optical force from the laser.

Measurements were carried out for different roll-off frequencies (Fig. 5(c)). The reliability of the results was ensured by measuring the amplitude of the particle motion due to the surrounding fluid in every experiment with two complementary techniques: BFPI and high-speed camera tracking. In this case, BFPI did provide satisfactory results since no fluctuations in the intensity altered the measurement. In addition, since trap calibration can be more

#151453 - $15.00 USD Received 21 Jul 2011; revised 17 Sep 2011; accepted 17 Sep 2011; published 13 Oct 2011

complicated with the high-speed camera [30], we used BFPI to accurately estimate the roll-off frequency.

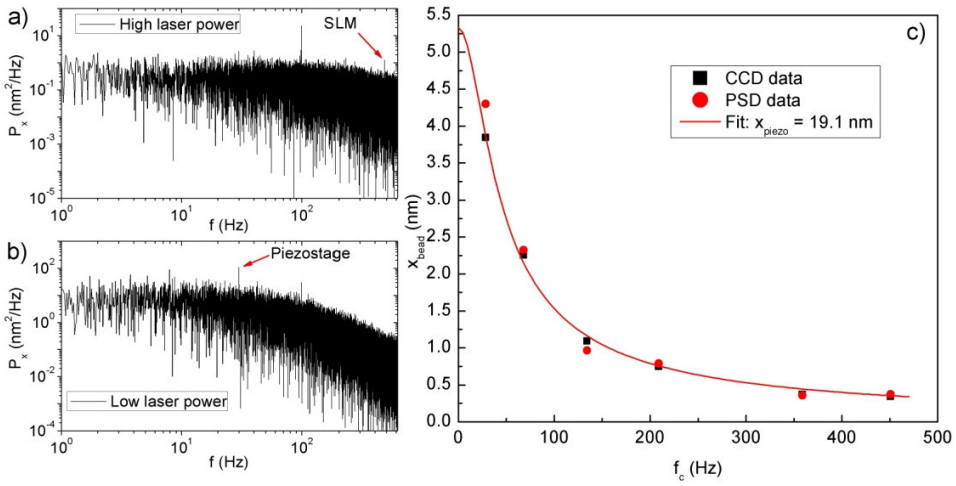


Fig. 5. Power spectra of a 2µm trapped bead determined using a high-speed camera for (a) high and (b) low laser powers, under the simultaneous action of two oscillations: the laser phase fluctuation and a piezostage movement. The peak at 100 Hz is parasitic electronic noise from the room illumination. (c) The amplitude of the piezostage oscillation obtained from the 30 Hz peak from camera data is plotted against the trap roll-off frequency determined from BFPI. The red line is a fit using Eq. (5).

The data and fit shown in Fig. 5(c) correspond to the expected result [29]:

$$x_{bead} = \frac{T \cdot x_{piezo}}{\sqrt{1+\left(f_c / f_{piezo}\right)^2}}, \tag{5}$$

where $T = 0.27935$ is the value of the piezo stage electronics transfer function at $f_{piezo} = 30$ Hz (the real amplitude of the bead motion was $20 \cdot T = 5.6$ nm). The fitting of the results with Eq. (5) gives us a measure of the amplitude of the piezo oscillation ($x_{piezo}$ ~19.1 nm) that matches the nominal value ($x_{piezo} = 20$ nm).

As a final step, using Eqs. (3) and (4), we determined the amplitude of the SLM-induced trap fluctuation from the peaks at 480 Hz in the same data. Because the amplitude of this motion is so small, control experiments using the piezo stage to induce a range of bead displacements (from ~4 nm to 0.3 nm) were performed in order to evaluate our position resolution.

The result for the analog-addressed SLM ($x_0 = 0.4 \pm 0.1$ nm) seems to be constant for different trap positions in the sample plane. This value is comparable to the position stability observed in the most stable non-holographic tweezers (with external optics also in air) [31,32], which indicates that, here, the trap stability is not compromised by the presence of beam modulations.

Interestingly, we found significant differences in position stability along the $x$ and $y$ axes for both modulators. For the 5-5 setting of the digital-addressed SLM, we estimate $2y_0 = 0.9$ nm, while for the 0-6 setting, no peak is detectable in the power spectrum at $f_0 = 600$ Hz, even at the highest laser powers, suggesting that sub-nanometer stability is attainable in the $y$ direction. Similarly, no peaks appeared in the $y$ direction with the analog-addressed device. Because the kinoform used here was asymmetric, we wondered if the increased stability in $y$ was related to the smaller displacement of the holographic trap from the zero order (*i.e.*, to a

#151453 - $15.00 USD Received 21 Jul 2011; revised 17 Sep 2011; accepted 17 Sep 2011; published 13 Oct 2011

shallower phase gradient in $y$ than in $x$). To test this hypothesis, we repeated these experiments using a "flipped" kinoform, in which the $x$ and $y$ phase gradients were swapped. Although here the phase gradient along $y$ was steeper, the spatial modulations of the trap remained larger in the $x$ direction.

Here, we have focused on characterizing the position instability along the less stable direction, because ultimately, it is the overall movement of the trap that is relevant for precision measurements. By examining only one axis, one might obtain the impression that the digitally-addressed SLM provides exceptionally stable pointing stability, while this is true only in one direction.

**Table 1. Experimental results for holographic trap position instability along the less stable axis, for the different addressing schemes used here.**

| | Hamamatsu | Holoeye 0-6 | Holoeye 5-5 | Holoeye 22-6 (from [11]) |
|---|---|---|---|---|
| Modulation frequency $f_0$ (Hz) | 480 | 600 | 300 | 120 |
| Total trap displacement (nm) ( = $2x_0$) | 0.8 ± 0.2 | 1.6 ± 0.2 | 3.2 ± 0.6 | >5 |

The values for the trap position instability for both modulators and the different settings analyzed herein are summarized in Table 1. These correspond to pointing instabilities of 0.4 μrad (Holoeye 5-5), 0.23 μrad (Holoeye 0-6) and 0.06 μrad (Hamamatsu). The performance of the analog SLM is similar to that of the most stable non-holographic optical traps, where pointing stabilities of 0.05 μrad have been achieved [32]. These results, jointly with the temporal behavior of the phase, show that: 1) pointing instabilities come from the modulated LC driving voltage; 2) these fluctuations are larger for our digitally-addressed SLM, which uses pulse-width modulation to adapt the binary applied voltages to small incremental changes in phase; 3) for SLMs with digital electronics, the effect of the flickering decreases with an increase in addressing frequency [17]; and 4) analog-addressed modulators provide similar stability to non-holographic tweezers [31,32].

Additionally, we find that the light intensity in a trap created by both the digitally- and the analog-addressed SLMs is modulated in time, as seen by a peak at $f_0$ in the power spectrum of intensity modulations from a trapped particle recorded using BFPI (data not shown and [11,12]). The influence of these modulations on force measurements has not been thoroughly investigated, though it has been demonstrated that the use of a time-averaged intensity provides correct force values [14]. Furthermore, because intensity fluctuations do not give rise to peaks in position variance at the modulation frequency [33], the analysis producing the results presented in Table 1 should be unaffected by modulations in trap intensity.

Our digitally-addressed SLM does exhibit less stability than the analog-addressed SLM, but the large phase fluctuations observed surprisingly do not give rise to equivalent instabilities of the trap position. Although still unknown, the reason for this lower than expected position modulation may lie in the somewhat synchronous modulations across gray levels that occur with this digital addressing scheme, giving a predominant effect more like Fig. 3(a) than Fig. 3(b). In any case, we have observed that improvements can be achieved by selecting among available digital addressing schemes (each corresponding to a different addressing rate). It is possible to reduce the amplitude and alter the frequency of the SLM-induced flicker [11,18,20]. Shorter sequences give rise to higher addressing frequencies, which improves the trap performance. We have previously shown an improvement in performance by changing from 22 to 6 (120 Hz addressing) to 5-5 (300 Hz addressing) [11,12], and here, we have found further improvement in the temporal stability by using the 0-6 setting (600 Hz addressing). These findings are consistent with the fact that a shorter temporal sequence permits a higher repetition rate in a frame period and therefore, less relaxation of the liquid crystals between addressing pulses. However, the shorter sequence significantly reduces the number of accessible gray levels from 192 (5-5) to 64 (0-6), which

#151453 - $15.00 USD Received 21 Jul 2011; revised 17 Sep 2011; accepted 17 Sep 2011; published 13 Oct 2011

can have a strong effect on the efficiency of diffraction into the desired first-order beam, particularly at larger steering angles [11]. In addition, due to the design of the modulator's addressing scheme, the 0-6 setting has the disadvantage of not being able to modulate 1064 nm light by a full $2\pi$ (see Appendix 1).

The reduction of the phase flickering for increasing addressing frequencies in the digitally-addressed SLM suggests that a further improvement of the trap position stability might be possible with SLMs based on alternative technologies permitting higher addressing rates [17]. All these various considerations should be taken into account when designing experiments requiring precision positioning with HOTs.

## 4. Conclusions

Analog-addressed SLMs provide a high stability to the modified laser beam when generating holographic optical traps. Measurements of the phase of the modulated beam allowed us to explain the fluctuations observed in the power spectra of holographically trapped beads. The oscillations of the electronic signal sent to the LC are the root cause of these instabilities. With digitally-addressed modulators these fluctuations can dominate the motion of the trapped sample depending on the addressing frequency of the electronics, whereas in the analog-addressed devices, the oscillations are notably reduced, so they do not introduce visible effects on the stability of the trap. Digitally-addressed SLMs offer, in general, reasonable performance, which can be further improved with higher speed addressing [17]. Analog-addressed SLMs, on the other hand, can provide stability comparable to that of non-holographic traps. With the added benefit of real-time positioning of independent traps in three dimensions, a feature not possible in conventional multi-trap optical tweezers instruments, our results demonstrate the advantages to using HOTs for precise quantitative experiments for a wide range of applications.

## Appendix 1

For a phase-only SLM, phase modulation can be extracted from intensity readings and does not require an interferometric or diffraction-based measurement. For incoming light linearly polarized at 45° degrees with respect to the extraordinary axis of the SLM nematic liquid crystal molecules, only the extraordinary component of the electric field is modulated by the SLM, while the ordinary component is unaltered. At the exit, light is thus elliptically polarized, with the degree of ellipticity depending on the phase shift $\phi$ introduced in the modulated component. It follows that the intensity after a second polarizer with its transmission axis at −45° has the expression of Eq. (1). A minimum intensity ($I_{min} = I_{offset}$) is read out when no delay is introduced by the SLM (when the SLM is off or when $\delta = 2m\pi, m \in Z$), as light will emerge linearly polarized with the same orientation as the incoming light (taking into account a double reflection by the mirror before the SLM and the backplane mirror behind the LC cell) and thus will be blocked by the crossed analyzer. On the contrary, a delay $\delta = (2m+1)\pi, m \in Z$ will rotate the polarization by 90°, and the intensity after the analyzer will be maximum ($I_{max} = I_{offset} + I_0$).

#151453 - $15.00 USD Received 21 Jul 2011; revised 17 Sep 2011; accepted 17 Sep 2011; published 13 Oct 2011

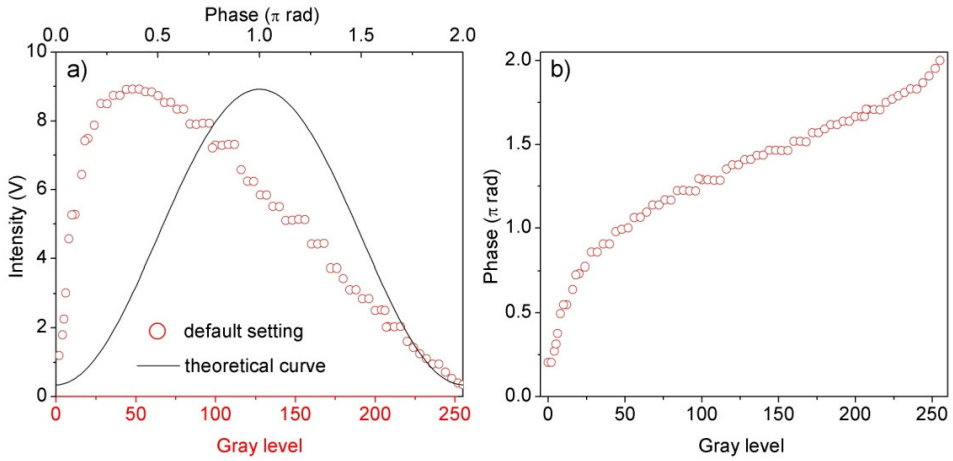


Fig. 6. Determination of the default gamma curve for the Holoeye SLM in the 0-6 addressing scheme. (a) Mean intensity measured for different constant gray levels (red circles) and sine squared theoretical curve from Eq. (1) (black line) after determination of $I_0$ and $I_{offset}$ from the experimental data. The divergence between these curves shows that gray level and phase delay are not linearly related in this default setting. (b) The default gamma curve, extracted from part (a), gives a nonlinear relation between phase and gray level, not the desired outcome.

We do not have, however, direct control over $\phi$ but over the gray level, which is used by the SLM to generate such a phase delay through the applied voltage signal according to the addressing scheme. Unfortunately, there is often a non-linear relationship between phase and gray level [9], so the phase – gray-level curve (the so-called gamma curve) needs to be determined and linearized by properly modifying the internal look-up-table (LUT) of the SLM controller. This LUT is provided by some manufacturers to ensure a linear response of the SLM with gray levels. For other SLMs (such as the Holoeye SLM used here), a gamma curve that provides a linear relationship between phase and gray levels is not provided, and, because it can vary with addressing mode and wavelength of operation, it must be determined by the end user. We now outline how to optimize the gamma curve when trying to determine phase modulation from intensity measurements through Eq. (1).

The mean intensity for each gray level (as measured by the photodetector) is represented by a red circle in Fig. 6(a), when using the Holoeye SLM in the 0-6 addressing mode with the default 0-6 gamma curve. We clearly see that the sine squared response predicted by Eq. (1) is deformed by the nonlinear relationship between the gray level and the phase. Nonetheless, the maximum intensity, $I_{max}$, still corresponds to linear polarization parallel to the analyzer ($\pi$ phase shift), while $I_{min}$ corresponds to a crossed linear polarization (zero or $2\pi$ phase shift). The intermediate intensities correspond to elliptically polarized light given by intermediate phase shifts according to Eq. (1), where $I_{offset} = I_{min}$ and $I_0 = I_{max} - I_{min}$ . Thus, if we plot how intensity changes with phase (black line in Fig. 6(a)), we can determine the phase shift $\phi$ that occurred for each gray level by means of its intensity $I$, through:

$$\phi = 2 \cdot \sin^{-1} \sqrt{\frac{I - I_{offset}}{I_0}}. \qquad (6)$$

Figure 6(b) shows the dependence of the phase with the gray level deduced from this adjustment. We can clearly see a non-linear behavior and that for this addressing setting the phase shift extends only from ~$0.2\pi$ το $2\pi$. (For the 5-5 addressing scheme, the default gamma curve provides a much more linear gray scale - phase relation over a $2\pi$ range for 1064 nm light.)

#151453 - $15.00 USD Received 21 Jul 2011; revised 17 Sep 2011; accepted 17 Sep 2011; published 13 Oct 2011

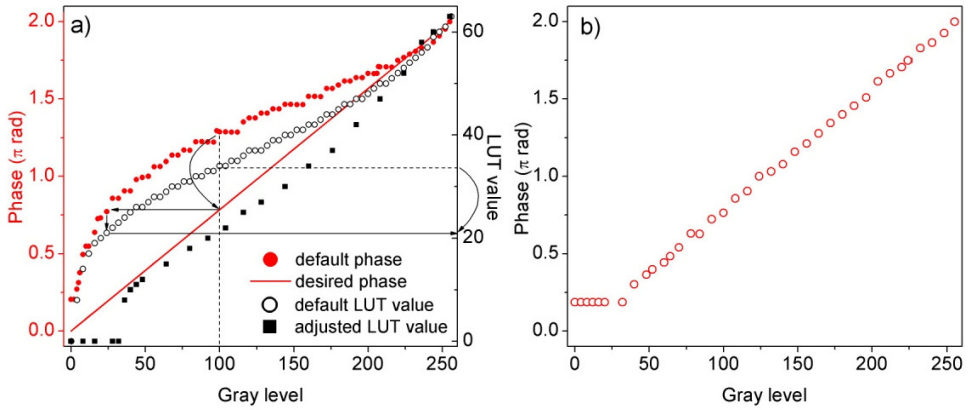


Fig. 7. (a). In order to change the old phase values (filled red circles, left axis) to the desired phase values (red line, left axis), the default LUT value assigned to each gray level (open black circles, right axis) needs to be changed. The filled black squares (right axis) correspond to the new LUT values after adjustment. (b). Resulting phase vs. gray level plot for 0-6, demonstrating the correct linear relation between these two parameters. Note, however, that this setting does not provide a full 2π phase modulation for 1064 nm light.

To obtain a linear relationship between phase and gray level, for each gray level, the correct LUT value must be assigned such that the desired phase delay is generated at the SLM. For instance, as shown in Fig. 7(a) for a gray level of 100, in order to change the corresponding phase delay from 1.28π (default) to 0.78π (desired), we must modify the LUT value for this gray level from 34 to 21. By performing the measurements at small increments of gray scale, we are able to provide new LUT values that lead to a linear gamma curve (Fig. 7(b)). This modified, improved gamma curve was used for all 0-6 measurements reported in this work.

## Appendix 2

The amplitude of the particle oscillation in Eq. (3) can be readily derived from the equation of motion governing the dynamics of the system in the absence of thermal noise:

$$m\ddot{x}(t) + \gamma\dot{x}(t) + k\left(x(t) - x_{trap}(t)\right) = 0, \tag{7}$$

where $x(t)$ is the particle's position at time $t$, $m$ is the particle mass, $\gamma$ is the viscous drag coefficient, $k$ is the harmonic trap stiffness, and the trap motion is described by a pure sine with frequency $f_0$ : $x_{trap}(t) = x_0 \sin(2\pi f_0 t)$ . At the timescales of the measurements presented here, the viscosity of the fluid typically overdamps the inertial forces of the particles in it [34], which translates into a small Reynolds number ($Re$<<1). This guarantees that the first term in Eq. (7) vanishes, so the final expression is simplified to:

$$\gamma\dot{x}(t) + kx(t) = kx_{trap}(t). \tag{8}$$

The general solution is obtained as a combination of two terms: a transient component with a characteristic exponential decay, and a stationary solution given by sinusoidal motion with frequency $f_0$. The decay time in the former term, $\tau \equiv 2\pi\gamma/k$ , takes values on the order of milliseconds, meaning that this contribution becomes relevant at several kHz (negligible for the timescales analyzed in the power spectra presented here). Thus, the final solution to Eq. (8) is given by the stationary term, where the amplitude corresponds to Eq. (3):

#151453 - $15.00 USD Received 21 Jul 2011; revised 17 Sep 2011; accepted 17 Sep 2011; published 13 Oct 2011

$$x(t) = x_{bead}\sin\left(2\pi f_0 t + \phi\right) = \frac{x_0}{\sqrt{1+{}^{f_0^2}\!/_{f_c^2}}}\sin\left(2\pi f_0 t - \arctan\left(\frac{f_0}{f_c}\right)\right). \quad (9)$$

Here, $f_c$ is the roll-off frequency, given by $f_c = k/2\pi\gamma$ (=1/$\tau$). As explained in Section 3, the value of $x_{bead}$ was experimentally obtained from the height of the peaks in the power spectra. Eq. (4) was used for this purpose. We followed a similar approach to that in [29] to obtain this formula.

The temporal Fourier transform of Eq. (9) is given by:

$$\tilde{x}(f) = x_{bead}e^{i\phi}\,\frac{\delta(f+f_0)-\delta(f-f_0)}{2i}, \quad (10)$$

where $\delta(f)$ is the Dirac delta function. Then, the one-sided power spectrum associated with the oscillation corresponds to a delta function at frequency $f_0$:

$$P(f) = \frac{2\left|\tilde{x}(f)\right|^2}{T_{msr}} = \frac{x_{bead}^2}{2}\delta(f-f_0). \quad (11)$$

Here, $T_{msr}$ is the measurement time for each power spectrum. The integral under the curve is given by $x_{bead}^2/2$, which can be connected to the experimental measurement obtained from the area under the peak, $A$, as follows:

$$A = \left(P_{peak} - P_{therm}\right)\Delta f = \frac{x_{bead}^2}{2}. \quad (12)$$

The peak height $P_{peak}$ is integrated above the thermal noise background $P_{therm}$ (determined by a Lorentzian fit to the power spectrum) and the frequency spacing is $\Delta f = 1/T_{msr}$. From this last equation one obtains Eq. (4).

**Acknowledgements**

Astrid van der Horst initiated investigations of HOT stability at SFU. This work has been partly funded by the Spanish Ministry of Education and Science (FIS2007-65880 and FIS2010-16104; EM-B), by the Natural Sciences and Engineering Research Council of Canada (NSERC; NRF) and by a grant from the Human Frontier Science Program (RGP-2007; NRF). AF acknowledges an FI grant from the Generalitat de Catalunya.

#151453 - $15.00 USD Received 21 Jul 2011; revised 17 Sep 2011; accepted 17 Sep 2011; published 13 Oct 2011

# References


[1] A. Ashkin, *"Acceleration and trapping of particles by radiation pressure,"* Phys. Rev. Lett. 24, 156-159 (1970). 2

[2] A. Ashkin and J. M. Dziedzic, *"Radiation pressure on a free liquid surface,"* Phys. Rev. Lett. 30, 139-142 (1973). 2

[3] J. P. Gordon, *"Radiation forces and momenta in dielectric media,"* Phys. Rev. A 8, 14-21 (1973). 2, 7

[4] A. Ashkin, J. M. Dziedzic, J. E. Bjorkholm, and S. Chu, *"Observation of a single-beam gradient force optical trap for dielectric particles,"* Opt. Lett. 11, 288-290 (1986). 2, 3, 7

[5] A. Ashkin, J. M. Dziedzic, and T. Yamane, *"Optical trapping and manipulation of single cells using infrared laser beams,"* Nature 330, 769-771 (1987). 2, 4

[6] A. Ashkin and J. M. Dziedzic, *"Optical levitation by radiation pressure,"* Appl. Phys. Lett. 19, 283-285 (1971). 3

[7] A. Ashkin, *"Trapping of atoms by resonance radiation pressure,"* Phys. Rev. Lett. 40, 729-732 (1978). 4

[8] R. D. Vale, T. S. Reese, and M. P. Sheetz, *"Identification of a novel force-generating protein, kinesin, involved in microtubule-based motility,"* Cell 42, 39-50 (1985). 5

[9] A. Ashkin, *"Forces of a single-beam gradient laser trap on a dielectric sphere in the ray optics regime,"* Biophys. J. 61, 569-582 (1992). 5, 7

[10] K. Svoboda and S. M. Block, *"Biological applications of optical forces,"* Annu. Rev. Biophys. Biomol. Struct. 23, 247-285 (1994). 5

[11] S. C. Kuo and M. P. Sheetz, *"Force of single kinesin molecules measured with optical tweezers,"* Science 260, 232-234 (1993). 5, 8, 11

[12] K. Svoboda, C. F. Schmidt, B. J. Schnapp, and S. M. Block, *"Direct observation of kinesin stepping by optical trapping interferometry,"* Nature 365, 721-727 (1993). 5, 9, 10, 12

[13] T. A. Nieminen, V. L. Y. Loke, A. B. Stilgoe, G. Knner, A. M. Braczyk, N. R. Heckenberg, and H. Rubinsztein-Dunlop, *"Optical tweezers computational toolbox,"* J. Opt. A: Pure Appl. Opt. 9, S196-S203 (2007). 7

## REFERENCES


[14] Y. Harada and T. Asakura, *"Radiation forces on a dielectric sphere in the Rayleigh scattering regime,"* Opt. Commun. 124, 529-541 (1996). 7

[15] M. J. Lang and S. M. Block, *"Resource Letter: LBOT-1: Laser-based optical tweezers,"* Am. J. Phys. 71, 201-215 (2003). 8

[16] J. T. Finer, R. M. Simmons, and J. A. Spudich, *"Single myosin molecule mechanics: piconewton forces and nanometre steps,"* Nature 368, 113-119 (1994). 8, 20

[17] S. Kamimura and R. Kamiya, *"High-frequency vibration in flagellar axonemes with amplitudes reflecting the size of tubulin,"* J. Cell Biol. 116, 1443-1454 (1992). 8

[18] W. Denk and W. W. Webb, *"Optical measurement of picometer displacements of transparent microscopic objects,"* Appl. Opt. 29, 2382-2391 (1990). 9

[19] L. P. Ghislain and W. W. Webb, *"Scanning-force microscope based on an optical trap,"* Opt. Lett. 18, 1678-1680 (1993). 9, 15, 19

[20] L. P. Ghislain, N. A. Switz, and W. W. Webb, *"Measurement of small forces using an optical trap,"* Rev. Sci. Instrum. 65, 2762-2768 (1994). 9

[21] K. Visscher, S. P. Gross, and S. M. Block, *"Construction of multiple-beam optical traps with nanometer-resolution position sensing,"* IEEE J. Select. Top. Quant. Electron. 2, 1066-1076 (1996). 10, 20

[22] F. Gittes and C. F. Schmidt, *"Interference model for back-focal-plane displacement detection in optical tweezers,"* Opt. Lett. 23, 7-9 (1998). 10, 20, 21, 26

[23] A. Pralle, M. Prummer, E.- L. Florin, E. H. K. Stelzer, and J. K. H. Hrber, *Three-dimensional high-resolution particle tracking for optical tweezers by forward scattered light,* Microsc. Res. Tech. 44, 378-386 (1999). 10, 26

[24] A. Rohrbach and E. H. K. Stelzer, *"Three-dimensional position detection of optically trapped dielectric particles,"* J. Appl. Phys. 91, 5474-5488 (2002). 10

[25] A. Rohrbach, H. Kress, and E. H. K. Stelzer, *"Three-dimensional tracking of small spheres in focused laser beams: influence of the detection angular aperture,"* Opt. Lett. 28, 411-413 (2003). 10

[26] S. Perrone, G. Volpe, and D. Petrov, *"10-fold detection range increase in quadrant-photodiode position sensing for photonic force microscope,"* Rev. Sci. Instrum. 79, 106101 (2008). 10

[27] E. Schäffer, S. F. Nrrelykke, and J. Howard, *"Surface forces and drag coefficients of microsphere near a plane surface measured with optical tweezers,"* Langmuir 23, 3654-3665 (2007). 11

[28] S. M. Block, D. F. Blair, and H. C. Berg, *"Compliance of bacterial flagella measured with optical tweezers,"* Nature 338, 514-518 (1989). 11, 25

[29] A. Ashkin, K. Schutze, J. M. Dziedzic, U. Euteneuer and M. Schliwa, *"Force generation of organelle transport measured in vivo by an infrared laser trap,"* Nature 348, 346-348 (1990). 11, 25

[30] A. van der Horst and N. R. Forde, *"Power spectral analysis for optical trap stiffness calibration from high-speed camera position detection with limited bandwidth,"* Opt. Express 18, 76707677 (2010). 14, 21

[31] K. Berg-Sørensen and H. Flyvbjerg, *"Power spectrum analysis for optical tweezers,"* Rev. Sci. Instrum. 75, 594-612 (2004). 14

[32] K. Berg-Sørensen, L. Oddershede, E.- L. Florin, and H. Flyvbjerg, *"Unintended filtering in a typical photodiode detection system for optical tweezers,"* J. Appl. Phys. 93, 3167-3176 (2003). 14

[33] D. Selmeczi, S. Tolić-Nørrelykke, E. Schäffer, P. H. Hagedorn, S. Mosler, K. Berg-Sørensen, N. B. Larsen, and H. Flyvbjerg, *Brownian motion after Einstein: some new applications and new experiments,"* Lect. Notes Phys. 711, 181-199 (2007). 15

[34] E. L. Florin, A. Pralle, E. H. K. Stelzer, J. K. H. Hörber, *"Photonic force microscope calibration by thermal noise analysis,"* Appl. Phys. A 66, S75-S78 (1998). 15

[35] F. Czerwinski, A. C. Richardson, and L. B. Oddershede, *"Quantifying noise in optical tweezers by Allan variance,"* Opt. Express 17, 13255-13269 (2009). 15

[36] S. F. Tolic-Nørrelykke, E. Schäffer, J. Howard, F. S. Pavone, F. Jülicher and H. Flyvbjerg, *"Calibration of optical tweezers with positional detection in the back focal plane,"* Rev. Sci. Instrum. 77, 103101 (2006). 17

[37] A. Buosciolo, G. Pesce, and A. Sasso, *New calibration method for position detector for simultaneous measurements of force constants and local viscosity in optical tweezers,"* Opt. Commun. 230, 357-368 (2004). 17

[38] M. Fischer and K. Berg-Sorensen, *"Calibration of trapping force and response function of optical tweezers in viscoelastic media,"* J. Opt. A: Pure Appl. Opt. 9, S239-S250 (2007). 17

[39] M. Fischer, A. C. Richardson, S. N. S. Reihani, L. B. Oddershede and K. Berg-Srensen, *"Active-passive calibration of optical tweezers in viscoelastic media,"* Rev. Sci. Instrum. 81, 015103 (2010). 17

[40] S. B. Smith, Y. Cui, and C. Bustamante, *"Overstretching B-DNA: the elastic response of individual double-stranded and single-stranded DNA molecules,"* Science 271, 795-798 (1996). 19

[41] S. B. Smith, *"Stretch transitions observed in single biopolymer molecules (DNA or protein) using laser tweezers,"* Doctoral Thesis, University of Twente, The Netherlands (1998). 19

[42] S. B. Smith, Y. Cui, and C. Bustamante, *"Optical-trap force transducer that operates by direct measurement of light momentum,"* Methods Enzymol. 361, 134-162 (2003). 19, 23, 25

## REFERENCES


[43] C. J. Bustamante and S. B. Smith, *"Light-force sensor and method for measuring axial optical-trap forces from changes in light momentum along an optic axis,"* US Patent No.7133132 (2006). 19

[44] K. C. Neuman and S. M. Block, *"Optical trapping,"* Rev. Sci. Instrum. 75, 2787-2809 (2004). 20

[45] J. R. Moffitt, Y. R. Chemla, S. B. Smith, and C. Bustamante, *"Recent advances in optical tweezers,"* Annu. Rev. Biochem. 77, 205228 (2008). 21

[46] H. Misawa, K. Sasaki, M. Koshioka, N. Kitamura, and H. Masuhara, *"Multibeam laser manipulation and fixation of microparticles,"* Appl. Phys. Lett. 60, 310-312 (1992). 20

[47] K. Visscher, G. J. Brakenhoff, and J. J. Krol, *"Micromanipulation by multiple optical traps created by a single fast scanning trap integrated with the bilateral confocal scanning laser microscope,"* Cytometry 14, 105-114 (1993). 20, 21

[48] Y. Hayasaki, M. Itoh, T. Yatagai, and N. Nishida, *"Nonmechanical optical manipulation of microparticle using spatial light modulator,"* Opt. Rev. 6, 2427 (1999). 21

[49] E. R. Dufresne and D. G. Grier, *"Optical tweezer array and optical substrates created with diffractive optics,"* Rev. Sci. Instrum. 69, 19741977 (1998). 21

[50] C. O. Mejean, A. W. Schaefer, E. A. Millman, P. Forscher, and E. R. Dufresne, *"Multiplexed force measurements on live cells with holographic optical tweezers,"* Opt. Express 17, 62096217 (2009). 21

[51] M. Reicherter, S. Zwick, T. Haist, C. Kohler, H. Tiziani, and W. Osten, *Fast digital hologram generation and adaptive force measurements in liquid-crystal-display-based holographic tweezers,"* Appl. Opt. 45, 888-896 (2006).

[52] F. Belloni, S. Monneret, F. Monduc, and M. Scordia, *"Multiple holographic optical tweezers parallel calibration with optical potential well characterization,"* Opt. Express 16, 9011-9020 (2008). 21

[53] A. van der Horst and N. R. Forde, *"Calibration of dynamic holographic optical tweezers for force measurements on biomaterials,"* Opt. Express 16, 2098721003 (2008). 21, 25, 29

[54] C. H. J. Schmitz, J. P. Spatz, and J. E. Curtis, *"High-precision steering of multiple holographic optical traps,"* Opt. Express 13, 86788685 (2005). 21

[55] M. Persson, D. Engström, A. Frank, J. Backsten, J. Bengtsson, and M. Goksör, *"Minimizing intensity fluctuations in dynamic holographic optical tweezers by restricted phase change,"* Opt. Express 18, 11250 11263 (2010). 21

[56] R. Di Leonardo, F. Ianni, and G. Ruocco, *"Computer generation of optimal holograms for optical trap arrays,"* Opt. Express 15, 19131922 (2007). 21

[57] M. Montes-Usategui, E. Pleguezuelos, J. Andilla, and E. Martín-Badosa, *"Fast generation of holographic optical tweezers by random mask encoding of Fourier components,"* Opt. Express 14, 2101-2107 (2006). 21

[58] S. Bianchi and R. Di Leonardo, *"Real-time optical micro-manipulation using optimized holograms generated on the GPU,"* Comp. Phys. Comm. 181, 1444-1448 (2010). 21

[59] E. Eriksson, S. Keen, J. Leach, M. Goksör, and M. J. Padgett, *"The effect of external forces on discrete motion within holographic optical tweezers,"* Opt. Express 15, 1826818274 (2007). 29